Materials Science and Engineering, R16 (1996) 97–159

R Reports: *A Review Journal*

Interfacial interaction between low-energy surfaces

Manoj K. Chaudhury

Department of Chemical Engineering, Lehigh University, Bethlehem, PA 18015, USA

Received 31 March 1995; accepted in final form 16 April 1995

Abstract

This review is concerned primarily with the correlation between the interfacial interactions and the constitutive properties of low-energy organic surfaces. It starts with a discussion on the estimation of the surface free energy of organic solids from contact angles, followed by a review of the surface energetics and adhesion. The experimental measurements of surface free energy, in most cases, are themselves dependent upon the specific models of interfacial energetics and therefore are indirect. A direct method of estimating adhesion and surface free energy is based on contact mechanics, which measures the deformation produced on contacting elastic semispheres under the influence of surface forces and external loads. Since the equilibrium is described by the balance of the elastic and surface forces of the system, the load-deformation data can be translated directly to estimate the adhesion and surface free energies. In most cases however, the contact deformations obtained from the loading and unloading cycles exhibit hysteresis, which are sensitive to the structure and chemical compositions of the interfaces. For non-hysteretic systems, the surface free energies obtained from these contact deformations compare well with the values obtained from contact angles. The application of this method to the studies of dispersion and hydrogen-bonding interaction is reviewed.

Keywords: Surface interactions; Interfacial interactions; Adhesion; Hysteresis; Contact deformation; Friction

1. Introduction

Wetting, adhesion, friction, crystal growth and many other materials phenomena are owing to the physico-chemical processes occurring within length scales of surfaces and interfaces of a few angstroms. Even when the bulk processes dominate a material function, e.g. the rheological adhesion of a pressure-sensitive adhesive, its extensive behavior is often limited by the processes occurring at interfaces. The ongoing attempts of the material scientists to tie together the hierarchy of interfacial phenomena on some common grounds are based on two fundamental properties of interfaces: energetics of interactions and dynamics. Thus it is believed that the adhesion of two different solid surfaces can be predicted from their ability to induce spontaneous spreading of high surface tension liquids, because both the processes are governed by interfacial forces. The friction behavior of solid surfaces, on the other hand, is controlled by the interfacial dynamics, which has some features that are common to the sliding behavior of a liquid drop on a solid surface.

Hysteresis is a common occurrence with almost all types of practical interfacial phenomena. For example, the contact angle formed by a liquid on a solid surface depends on whether the drop is growing or decreasing in size. The contact angle of the withdrawing drop is normally lower than that of a growing drop, implying a higher adhesion tension in the former case. Similarly, the forces necessary to separate two surfaces is normally much greater than the forces by which the two surfaces come into contact in the first place. For studies aimed at measuring the thermodynamic properties of surfaces and interfaces, it is highly desirable to use model systems that exhibit negligible hysteresis. In this regard, several carefully prepared organic surfaces have shown great promise. Practical interfacial phenomena are however hardly governed by equilibrium thermodynamic properties. While they provide the necessary driving force for a change to occur, most interfacial phenomena are characterized

SSDI 0927-796X(95)00185-9

by dynamics. The dynamic behavior results from the metastable thermodynamic states. The energy barriers separating the metastable states are often so much higher than the vibration energy of the system that the interface never attains the globally minimum energy state within any realistic time. The energy barrier may also be of similar magnitude of some characteristic vibration energy of the system, in which case an observable time-dependent progression towards the minimum energy state can take place with a concomitant dissipation of interfacial energy.

In describing a real interfacial phenomenon, be it dewetting of a liquid from a solid surface or the separation of two solids, it is equally important to study the non-equilibrium interfacial processes, such as the processes that fall within the realm of equilibrium thermodynamics.

Surface chemists have traditionally focused upon such questions as: how the bonds are formed at an interface; what are the corresponding changes in the energy and how they correlate with the chemical constitution of surfaces. By contrast, engineering of the surfaces and interfaces to control their hysteretic behavior has received much less attention. Early studies of Dettre and Johnson, Neumann and Good as well as Timmons and Zisman delineating the dependence of hysteresis on surface roughness, heterogeneity and intermolecular digitation are useful in this regard; but more work is needed before we can use these understandings to further engineering practices. Here lies an important challenge to the future of interfacial engineering.

In this review, we attempt to summarize some of the essential details of the interfacial interactions at both microscopic and macroscopic levels. Since most of the fundamental research in this regard has been carried out with organic polymer surfaces, they will be the focus of our review.

Wetting has traditionally been the standard method of analysing the energetics of solid surfaces. The review thus starts with a discussion of the theory of interfacial interactions in connection to wetting and contact angle, placing a special emphasis on the Langmuir's principle of independent surface action. This principle provides a useful method to predict the behavior of complex organic systems in terms of their subunit properties.

The theory of interfacial interaction is divided to treat non-specific (van der Waals) and specific (donor–acceptor) interactions separately. In discussing these specific interactions, we make a slight departure from our original theme, dealing with the organic surfaces and discuss some issues related to the donor–acceptor interactions at organic–inorganic interfaces, in order to illustrate their generalities.

Next, we discuss the recent developments in the methods of contact mechanics, which are capable of providing the surface thermodynamic properties of elastic solids in a direct and quantitative manner.

2. Theories of surface and interfacial interactions

2.1. Principle of independent surface action

A fundamental breakthrough in the research of low-energy surfaces resulted from Langmuir's [1–5] pioneering studies of organic thin films. Based on his studies of the organic films adsorbed onto high-energy surfaces, Langmuir developed several remarkable insights into the nature of intermolecular interactions across condensed phases. He realized, for example, that the interaction at surfaces is the result of the uncompensated fields emanating, primarily, from their outermost molecular layers. This finding led to the highly celebrated principle of independent surface action (ISA). ISA provides a convenient approximate method of investigating the surface and interfacial properties of complex organic surfaces. As an example, let us consider the case of hexane and hexyl alcohol, whose surface tensions are nearly the same, even though the alcohol forms hydrogen bonds and hexane does not.

Langmuir proposed that the hexyl alcohol is so oriented at the liquid surface that its hydrogen bonding group faces towards the liquid phase and its hydrocarbon group is exposed outward. The surface tension of the entire liquid is determined by the hydrocarbon portion of the alcohol, which is nearly the same as that of hexane. With the aid of the ISA principle, Langmuir proposed that the disymmetric molecules can be highly oriented at a surface and, in some cases, in a highly packed state.

Langmuir made other observations on the effect of the surface structure on the wettability of solids. He found that oil droplets can bead up and roll off a surface which consists of close-packed methyl groups. In order to rationalize this observation, Langmuir proposed that the surface energy of the methyl group must be lower than that of the methylene group, which is the major constituent of oil. Another important discovery of Langmuir is what is known as autophobicity. Certain liquids, such as cetyl alcohol, can easily roll off a high-energy surface such as glass. Langmuir proposed that the alcohol molecules are adsorbed onto the glass surface by forming hydrogen bonds and its methyl groups are exposed to the air. Since the surface energy of the methyl surface is lower than that of alcohol itself, the liquid drops do not wet the glass surface, which is another demonstration of ISA principle.

2.2. *Wettability and surface constitution*

Next to Langmuir, the most significant contribution to the research of organic surfaces was due to Zisman and coworkers [6–8]. Zisman and collaborators studied the wettabilities of several organic polymers with a wide variety of liquids (Fig. 1). They produced self-assembled films of alkyl and fluoroalkyl acids and amines on metal surfaces and found that the wettabilities of these surfaces follow a systematic trend with respect to the surface tensions of the probe liquids. When the cosine of the contact angles of the liquids are plotted against their surface tensions, a nearly linear plot is obtained (Fig. 2). This line, when extrapolated to the cos $\theta = 1$ axis, meets the axis at a point which was termed by Zisman as the critical surface tension of wetting "γ_c". γ_c is a measure of the surface free energy of the solid, which demarcates those liquids ($\gamma_{lv} < \gamma_c$) which spread on the solid surface as a thin continuous film from those ($\gamma_{lv} > \gamma_c$) which do not. γ_c is not however equal to the surface free energy γ_{sv}, because γ_{sl} need not be zero even when θ is zero. Zisman found that γ_c varies systematically with the chemical constitution of the solid substrate (see Table 1).

The advantage of this kind of correlation between γ_c and the constitutive properties of the surfaces is that the surface energy or wettability of a complex organic surface can be reasonably predicted if its chemical composition at the outermost layer can be estimated. For example, the surface free energy

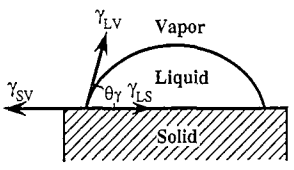

Fig. 1. A liquid drop on a solid surface. The mechanical equilibrium of a liquid drop on a solid surface is determined by the balance of the three surface tension forces acting at the liquid–solid–vapor contact line. The mechanical equilibrium is represented by the famous Young's [9] equation: $\gamma_{lv} \cos\theta = \gamma_{sv} - \gamma_{sl}$; where γ_{lv}, γ_{sv}, and γ_{sl} are the surface free energies (normally, the word "surface tension" is reserved for liquids. "Surface free energy" is used mainly for solids. Even though a surface tension force is also present on a solid surface, its effect is overshadowed by the elastic forces in the solid. Greenhill and McDonald [44] measured the tension of solids near the melting point. The fact that γ_{sl} acts like a force is evident in the capillary rise of liquids or the movement of liquids on a solid surface under the influence of the surface energy gradient of the solid [10]) of the liquid–vapor, solid–vapor and solid–liquid interfaces respectively. We will use the unit of surface tension (mN m^{-1}) for a liquid–vapor interface and surface free energy (mJ m^{-2}) for the liquid–solid and solid–vapor interfaces.

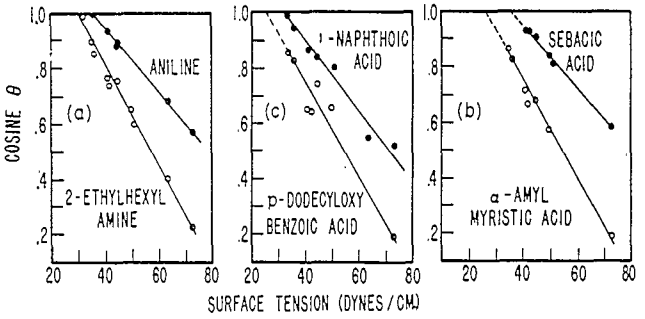

Fig. 2. Zisman's Plot. Wettability of various monolayers on platinum prepared by retraction from aqueous solution. (Here 1 dyne $cm^{-1} = 1$ mN m^{-1}.) Reprinted with permission from American Chemical Society (Ref. [8]), © 1964 American Chemical Society.

Table 1
Critical surface tension of wetting and surface composition

Polymer	Structural formula	γ_c (mJ m^{-2})
Poly(vinylidine chloride)	$-(CH_2CCl_2)_n-$	40
Poly(vinyl chloride)	$-(CH_2CHCl)_n-$	39
Polyethylene	$-(CH_2)_n-$	31
Poly(vinyl fluoride)	$-(CH_2CHF)_n$	28
Poly(vinylidine fluoride)	$-(CH_2CF_2)_n-$	25
Polytrifluoroethylene	$-(CF_2CHF)_n-$	22
Polytetrafluoroethylene	$-(CF_2)_n-$	18
$-CH_3$ (crystal)	$-CH_3$	22
$-CH_3$ (monolayer)	$-CH_3$	24
$-CF_3$ (monolayer)	$-CF_3$	6
Polystyrene	$-(CH_2CHC_6H_6)_n-$	33
Poly(methyl methacrylate)	$-(CH_2CH_3COOCCH_3)_n-$	39

of polydimethylsiloxanes, whose surface is primarily composed of methyl groups, is about 22 mJ m^{-2} — a value which could be guessed from the critical surface tension value of the methyl groups (22–24 mJ m^{-2}).

2.3. *Surface free energy and tailgroup properties*

Zisman and coworkers, like Langmuir, noticed that the surface free energy of the methyl group is significantly lower than that of the methylene group. The polarizability of the CH_3 group (1.9 Å^3) is larger than that of the CH_2 (1.3 Å^3) group, and on this basis the surface energy of a methyl surface should be slightly higher than that of the methylene surface, but the experimental results prove that the contrary to be true. Adam [11] proposed that the difference between the methyl and methylene groups lies in the way they are oriented at the surface. The carbon atom of the methyl group is much more shielded by the hydrogen atoms than that of the methylene group; this shielding reduces its surface energy more than that of the methylene group. The wettability of an olefin surface is similarly paradoxical. The $CH{=}CH_2$ group is more polarizable than the CH_3 and CH_2 groups, because of its double-bond character ($\alpha_{C-C} = 0.64$ Å^3, $\alpha_{C=C} = 1.66$ Å^3). Therefore, the surface energy of a surface composed of olefin groups should be higher than those of the methyl and methylene groups. Polyacetylene [12], which exposes a large amount of –C=C– groups at the surface, has indeed a high surface free energy (ca. 43 mJ m^{-2}). The surface energy of an olefin surface [13] (24 mJ m^{-2}), in a self-assembled monolayer is, however, only slightly higher than that of the methyl surface. An extension

of Adam's hypothesis suggests that the olefin groups of the monolayer film are so oriented that their outermost surface is composed of mainly hydrogen, so that its surface energy is comparable with that of a CH_3 surface. Recent studies of helium diffraction [14] and NEXAFS [15] aimed at estimating the structure of the tailgroup in the self-assembled monolayer however does not provide a direct support of Adam's notion of an ordered tailgroup. In the helium diffraction studies, although a certain degree of order in the tailgroup region is observed at very low temperatures, it is mostly disordered at room temperature. Our NEXAFS studies also indicate that the terminal vinyl group on a self-assembled monolayer is mostly disordered. Thus, exactly how the shielding of carbon atoms by hydrogen influences the surface free energy and its relationship to the tailgroup motion is not clearly understood and at present it remains an open question.

2.4. Molecular interpretation of surface free energy: surface free energy components

The surface free energy (γ_{sv}) of a solid [16] is defined as the change in the total surface free energy (G) per unit change in surface area (A) at constant temperature (T), pressure (P) and moles (n), i.e.

$$\gamma_{sv} = (\partial G/\partial A)_{T,P,n} \tag{1}$$

For liquids, the surface area can be changed under the above conditions. For solids however, surface area cannot, in general, be changed without affecting its chemical potential. Therefore, in changing the area, work needs to be done against the elastic forces in the solids. In a given experiment involving stretching of solid surfaces, it is often difficult to delineate the effects of bulk and surface mechanics.

Contact angles of non-swelling liquids on an ideally rigid solid provide a nearly ideal situation to examine the energetics of solid surfaces using Young's equation. The research carried out by Langmuir, Zisman and Adams stimulated other surface scientists [16–21] to investigate ways to determine directly the surface free energies of solids from contact angles. In his monumental collected works, Gibbs [22] commented that the surface free energies of solids cannot be derived from contact angles because there is virtually no way of estimating the interfacial free energy of solid and liquid. The major simplification of Young's equation was actually possible as a result of Dupré's [23] equation combining the work of adhesion at the solid–liquid interface with the surface and interfacial tensions of the solid–vapor, solid–liquid and solid–vapor interfaces.

$$W_{sl} = \gamma_{sv} + \gamma_{lv} - \gamma_{sl} \tag{2}$$

The Dupre equation amounts to a conservation of total energy in a reversible process of adhesion and cohesion of two phases. The combination of the Young and Dupre equation results in Eq. (3).

$$\gamma_{lv}(1 + \cos\theta) = W_{sl} \tag{3}$$

In this way, the two unknowns (γ_{sv} and γ_{sl}) of the original Young's equation can be reduced to only one, W_{sl}. The left-hand side of Eq. (3) is actually a deformation term; it may be viewed as the strain energy of the liquid drop per unit area. Unlike solids, the strain energy is contributed here by surface tension alone. The equality of the deformation energy to the work of adhesion describing the stability of a liquid drop is somewhat akin to the condition of the stability of crack in elastic solids. Eq. (3) still does not allow estimation of the surface free energy from the contact angle and one more simplification was necessary. The next major simplification of the Young–Dupre equation was due to Good and Girifalco [17], who proposed, analogous to the Berthelot [24] combining rule of intermolecular interaction, that the work of adhesion can be expressed as a geometric mean of the surface tensions of the pure components γ_{sv} and γ_{lv}:

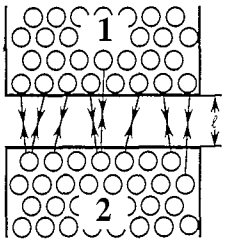

Fig. 3. Interaction energy between two semi-infinite parallel plates is calculated by pairwise summation of the the interaction energies of the atoms and molecules of the two materials.

$$W_{sl} = 2\Phi(\gamma_{sv}\gamma_{lv})^{0.5} \tag{4}$$

where Φ is a correction factor for intermolecular interaction. Φ is equal to unity if the intermolecular forces acting across the interface are alike, such is the case with a hydrocarbon liquid interacting with a hydrocarbon solid. Φ is less than unity when the intermolecular interactions that constitute cohesive and adhesive forces do not match, such as the case with a hydrogen-bonding liquid interacting with a pure hydrocarbon surface. Good and Girifalco expressed Φ in terms of the molecular level parameters of surfaces such as polarizability, ionization potential and dipole moments. These derivations were based on the pairwise additivity rule of intermolecular interactions which was introduced previously by Bradley [25], de Boer [26] and Hamaker [27].

Combination of the Good–Girifalco equation and the Young–Dupre equation results in a fundamental equation (Eq. (5)) of wettability that allows estimation of the surface free energy of the solid.

$$\gamma_{lv}(1+\cos\theta) = 2\Phi(\gamma_{sv}\gamma_{lv})^{0.5} \tag{5}$$

When the primary forces constituting the cohesive and adhesive interactions are of the dispersion type, $\Phi = 1$ and Eq. (5) reduces to $\gamma_{sv} = \gamma_{lv}(1+\cos\theta)^2/4$. According to this equation, $\cos\theta$ will be unity only when $\Phi^2\gamma_{sv}$ is equal to γ_{lv}. This is also a definition of Zisman's γ_c. Thus one obtains a relationship between γ_c and γ_{sv} as $\gamma_c = \Phi^2\gamma_{sv}$. The critical surface tension of wetting is equal to the surface free energy of a solid only when the interaction parameter Φ is equal to unity. Otherwise, the γ_c value from a typical Zisman's plot needs to be corrected by dividing it with Φ^2 in order to obtain the surface free energy of the solid.

The problem now is that the value of Φ is not known a priori; its computation depends upon the detailed knowledge of the chemical constitution of the solids and liquids as well as the model used to compute it. The early treatments of Good and Girifalco used pairwise additivity to compute interaction energies across condensed phases, and these treatments underwent several revisions in view of the later developments of the theories of intermolecular interactions across condensed phases (Fig. 3).

2.5. Microscopic approach to interfacial interaction

According to the pairwise additivity rule, the energy of interaction between two semi-infinite flat slabs is given by the following equation:

$$G_{12} = \int_{v_1} \mathrm{d}v_1 \int_{v_2} n_1 n_2 g_{12}\, \mathrm{d}v_2 \tag{6}$$

where $\mathrm{d}v_1$ and $\mathrm{d}v_2$ are the volume elements of bodies 1 and 2 with respective volumes v_1 and v_2, n_1 and n_2 are the number densities of the oscillators in bodies 1 and 2, and g_{12} is the interaction energy between two oscillators of bodies 1 and 2. The interaction energy between two flat slabs was calculated

rigorously by Good and Girifalco by considering the Debye, Keesom and London forces. Here we will give a heuristic derivation of the Good–Girifalco equation using McLachlan's [28] equation (see also Israelachvili [29]) according to which g_{12} can be expressed as:

$$g_{12} = -(6kT/R^6) \sum_{n=0}^{\infty}{}' \alpha_1(i\omega_n)\alpha_2(i\omega_n) \tag{7}$$

where $\alpha(i\omega_n)$ is the polarizability of the oscillator expressed along the complex frequency axis $i\omega_n$. With this expression for g_{12}, the overall interaction energy can be written as:

$$G_{12} = -A_{12}/(12\pi l^2) \tag{8}$$

where A_{12} is the Hamaker constant and l is the separation distance. A_{12} is given by:

$$A_{12} = 6\pi^2 n_1 n_2 kT \sum_{n=0}^{\infty}{}' \alpha_1(i\omega_n)\alpha_2(i\omega_n) \tag{9}$$

The polarizability appearing in the summation can be decomposed into two terms: one arising from the zero frequency (d.c. photon) interaction and the other from the higher frequency interaction:

$$\alpha_1(i\omega_n) = (\mu^2/3kT)/(1+\omega_n/\omega_{\text{rot}}) + \alpha_e(0)/[1+(\omega_n/\omega_e)^2] \tag{10}$$

where μ is the dipole moment, ω_{rot} is the rotational frequency of the dipole, $\alpha_e(0)$ is the electronic polarizability and ω_e is the electronic excitation frequency.

The zero frequency term of Eq. (9) can be written as:

$$A_{12}|_{n=0} = \pi^2 n_1 n_2 [(\mu^2\mu_2^2/3kT) + \{\mu_1^2\alpha_{e2}(0) + \mu_2^2\alpha_{e1}(0)\} + 3kT\alpha_{e1}(0)\alpha_{e2}(0)] \tag{11}$$

The first term of the above equation is due to the classical dipole–dipole interaction, the second term is due to a dipole-induced dipole, and the third term is due to the Casimir–Polder interaction [30] (The Casimir–Polder interaction is due to electrically neutral atoms or molecules in unexcited state. The original derivation of this force was given by Casimir and Polder in the context of the interaction of an unexcited oscillator with a metal [30]. The formula agrees with the calculations in quantum electrodynamics for the interaction of two atoms at large distances (Landau and Lifshitz, QE). Recently, this force was verified experimentally by studying the bending of a beam of sodium atoms by a metal surface.); it is quite small and can be neglected in comparison with the other terms. The higher frequency component of the Hamaker constant can be written as:

$$A_{12}|_{n>0} = (3/2)\pi^2 n_1 n_2 h\omega_{e1}\omega_{e2}\alpha_{e1}(0)\alpha_{e2}(0)/(\omega_{e1}+\omega_{e2}) \tag{12}$$

which corresponds to the classical London dispersion interaction.

The Good–Girifalco interaction parameter Φ between two surfaces is the ratio of the work of adhesion (which is equal to the free energy, G) to the geometric mean of their works of cohesion:

$$\Phi = W_{12}/(W_{11}W_{22})^{0.5} \tag{13}$$

In view of Eqs. (8) and (13), Φ can be expressed as:

$$\Phi = (\sqrt{l_1 l_2}/l_{12})(A_{12}/\sqrt{A_{11}A_{22}}) \tag{14}$$

where l_1, l_2 and l_{12} are the equilibrium van der Waals separation distances. Good and Hope [31] showed that the interfacial separation distance (l_{12}) of two surfaces can be expressed as the geometric mean of l_{11} and l_{22}, and thus Φ can be expressed as a function of the Hamaker constants (Eqs. (11) and (12)) alone. Good and Girifalco calculated the value of Φ from Eq. (14) for a number of materials

and found that these values lay between 0.5 and 1. The values approaching unity are for those materials that interact only by London dispersion forces. The problem of this approach of Good and Girifalco is that the chemical composition needs to be accurately known to compute ϕ; furthermore, its computation is highly model dependent. Fowkes provided a method of analysing the energetics of surfaces from contact angles which does not require detailed knowledge of the surface compositions of solids. Fowkes [18] considered that the total surface tension of a solid or a liquid can be decomposed into components corresponding to the specific types of intermolecular interactions.

$$\gamma = \gamma^d + \gamma^p + \gamma^i + \ldots \tag{15}$$

where d, p, and i stand for the dispersion, polar and induction interactions. A large number of terms can follow afterwards as indicated by the dots.

This division of the surface tension into components allowed the work of adhesion to be expressed as follows [19,20]:

$$W_{12} = 2\sqrt{(\gamma_1^d \gamma_2^d)} + 2\sqrt{(\gamma_1^p \gamma_2^p)} + 2\sqrt{(\gamma_1^i \gamma_2^i)} \tag{16}$$

In order to estimate the surface free energy components of a solid surface, contact angles of several liquids are measured, liquids whose surface tension components have already been determined. The surface tension components of the solid are determined by combining Eqs. (3) and (16) as follows:

$$\gamma_{lv}(1+\cos\theta) = 2\sqrt{(\gamma_s^d \gamma_l^d)} + 2\sqrt{(\gamma_s^p \gamma_l^p)} + 2\sqrt{(\gamma_s^i \gamma_l^i)} \tag{17}$$

The induction components of the surface free energies of solids and liquids are generally negligible in comparison with the other two terms. Thus, for all practical purposes, it is sufficient to account for the dispersion and polar terms only. This equation, proposed independently by Owens and Wendt [19] and Kaelble and Uy [20], had been widely used to estimate the surface free energies of low energy solids. Once the surface energy components are determined, the work of adhesion between two different solids may be estimated using Eq. (16). The division of the surface tension into dispersive and non-dispersive components is perhaps the greatest contribution of Fowkes to surface chemistry. In order to find the utility of this approach, let us consider the case of the water–alkane interface. The dispersive and the H-bonding components [18] of the surface tension of water are about 22 mN m^{-1} and 50 mN m^{-1} respectively. Since the surface tension of oil, which is contributed entirely by the dispersion forces, is very close to the dispersion component of the surface tension of water, and thus the dispersion interaction is almost totally compensated at the water–alkane interface. What remains is only the H-bonding component of the surface tension of water operating at the interface. Thus the interfacial tension of the water–oil interface is about 50 mN m^{-1}. The situation is somewhat different for the water–mercury interface. Since the dispersion component (200 mN m^{-1}) of the surface tension of mercury [18,32] is much higher than that of water, the dispersion interaction is uncompensated at the interface. The total dispersion component of the surface tension of the mercury–water interface according to Fowkes equation is $22+200-2(22\times200)^{0.5}=90$ mN m^{-1}. The metallic component of the surface tension of mercury is about 284 mN m^{-1}. Thus the total interfacial tension at the mercury–water interface is $284+50+90=424$ mN m^{-1}, which is only slightly smaller than the total surface tension (484 mN m^{-1}) of liquid mercury.

There are other approximate generalizations of the Young's equation. One is based on the harmonic-mean [21] combining rule of surface tension components:

$$\gamma_{lv}(1+\cos\theta) = 4\gamma_{lv}^d \gamma_{sv}^d/(\gamma_{lv}^d + \gamma_{sv}^d) + 4\gamma_{lv}^p \gamma_{sv}^p/(\gamma_{lv}^p + \gamma_{sv}^p) \tag{18}$$

Several objections can be raised with respect to either the geometric- or the harmonic-mean combining rules of surface interactions. First of all, the surface free energies (and components) are free energy functions; all attempts to derive a relationship between the work of adhesion and surface free energies are based on interaction models that ignore entropy. Fowkes, for example, had to assume that the surface free energy and surface enthalpy form a ratio that is nearly a universal constant. Several assumptions have been made in the computation of the interaction energies themselves. All initial theories of interfacial interactions assumed a pairwise additivity rule for intermolecular potential, which is strictly valid for rarified media. The problem is not too severe for higher frequency dispersion interactions. But for zero frequency interaction, such as dipole–dipole interactions, random orientations of dipoles cancel each other's field, which reduces the interaction energy substantially from the value calculated from the pairwise additivity rule. Although there is no exact theory that circumvents all these difficulties, an improved understanding into the nature of the van der Waals interaction between condensed phases has been made possible through the introduction of Lifshitz's theory.

2.6. Macroscopic theory of Lifshitz

Lifshitz [33] used a macroscopic model, where the interaction energy between two surfaces is calculated from the Fourier transform of the normal component of the electromagnetic stress tensor. The relevant frequencies are determined from the boundary conditions that satisfy Maxwell's equations. In a simplified form, the Hamakar constant of interaction at short distances can be expressed according to Lifshitz's theory as follows:

$$A_{12} = 1.5kT \sum_{n=0}^{\infty}{}' \sum_{j=1}^{\infty} (\{[(\epsilon_1(i\omega_n) - 1)/(\epsilon_1(i\omega_n) + 1][(\epsilon_2(i\omega_n) - 1)/(\epsilon_2(i\omega_n) + 1)]\})^j / j^3 \quad (19)$$

Here, $\epsilon_m(i\omega_n)$ is the dielectric susceptibility of the material m ($m \epsilon \{1,2\}$) expressed along the complex frequency axis $i\omega_n$.

Lifshitz's theory of interaction provides a convenient protocol to calculate the interaction energy between condensed phases in terms of the dielectric susceptibilities of the materials which are continuum properties. Since the continuum properties are used, the theory is valid for large separation distance. For separation distances comparable with the molecular sizes, as is the case with wetting and adhesion, the theory is not strictly applicable because the molecular graininess modulates [34] the dielectric profile. Furthermore, the molecular symmetry present in the bulk is broken at the surface resulting in an uncompensated electrostatic field, which is not considered in the Lifshitz's formalism. The need to consider the fine structure of solid surfaces was exemplified in the experiments of Silberzan and Leger [35], who conducted wettability studies on mixed silane monolayers comprising of methyl and olefin groups. In order to account for the wettability of these surfaces, it was necessary to consider the monolayer as a stratified medium. The overall energetics of wetting was computed by summing up the contributions on a layer by layer basis.

Although the continuum approach of Lifshitz does not rigorously apply to wetting and adhesion problems, the required corrections are of second order for dispersion forces.

Fowkes [18,41], Israelachvili [29], Hough and White [36] as well as van Oss et al. [37,38] calculated the Hamaker constants of a number of non-polar liquids and solids, and found that the dispersion component of the surface tension and Hamaker constants form a ratio which is approximately constant for a number of different materials (Table 2). This empirical correlation provides an approximate means of calculating the surface tensions of liquids from Hamaker constants and vice versa. For hydrogen-bonding liquids, as one would expect, this approach leads only to the dispersion component

Table 2
Hamaker constant and surface tension. Reprinted with permission from *Chem. Rev.* (Ref. [37]). © 1988 American Chemical Society

Material	Temp. (°C)	A (Hamaker constant) ($\times 10^{20}$) (J)	γ^d (mJ m^{-2})	A/γ^d ($\times 10^{21}$) (m^2)
Helium	−271.5	0.0535	0.353	1.51
Hydrogen	−255	0.511	2.31	2.21
Nitrogen	−183	1.42	6.6	2.15
Argon	−188	2.33	13.2	1.76
Hexane	25	3.91	18.4	2.12
Heptane	25	4.03	20.14	2.00
Octane	25	4.11	21.8	1.88
Decane	25	4.25	23.9	1.78
Dodecane	25	4.35	25.4	1.71
Tetradecane	25	4.38	26.6	1.64
Hexadecane	25	4.43	27.7	1.60
Poly(tetrafluoroethylene)	25	3.8	19	2.00
Water	25	4.62	21.8	2.12
Methanol	25	3.94	18.5	2.12
Ethanol	25	4.39	20.1	2.18
Chloroform	25	5.34	27.1	1.96
Benzene	25	4.66	28.9	1.60
Chlorine	−50	5.4	29.2	1.80
Carbon disulfide	25	5.07	32.3	1.56
Glycerol	25	6.7	34	1.97
Polystyrene	25	6.58	38	1.73
Poly(methyl methacrylate)	25	7.11	40	1.77
Mercury	25	33	200	1.65

of the surface tension; the rest of the surface tension is contributed by the H-bonding or other structural interactions.

2.7. *Surface tensions and dipole moments*

Lifshitz's theory has been used to estimate just how much of the interfacial interactions of the polar liquids is contributed by the dipolar interactions. For example, using the pairwise additivity criterion, the dipolar component of the surface tension of water is estimated to be about 2.5 times larger than the dispersion interaction term. The zero frequency term of the Lifshitz's equation, which is contributed by the dipolar interactions, predicts that this term is almost negligible in comparison with the higher frequency-dispersion interactions. The ratio of the zero frequency term to the sum of higher frequency terms gives the ratio of γ^p to γ^d. For a single component, Eq. (19) can be approximated as:

$$A_{11} = 1.5kT \sum_{n=0}^{\infty}{}' [(\epsilon_1(i\omega_n) - 1)/(\epsilon_1(i\omega_n) + 1)]^2 \tag{20}$$

The ratio γ^p/γ^d for a single component is then given by

$$\gamma^p/\gamma^d = [(\epsilon_1(0) - 1)/(\epsilon_1(0) + 1)]^2/2 \sum_{n=1}^{\infty} [(\epsilon_1(i\omega_n) - 1)/(\epsilon_1(i\omega_n) + 1)]^2 \tag{21}$$

Table 3
Interfacial tension and dipole moments

Compound	Contacting phase	μ (Debye)	γ (mN m^{-1})
Water	Air	1.85	72.8
Chloroform	Air	1.01	27.13
Ethanol	Air	1.7	22.4
Acetonitrile	Air	3.4	29.3
Benzene	Air	0	28.9
Toluene	Air	0.4	28.5
Benzene	Water	0	35
Heptane	Water	0	50.2
Nitrobenzene	Water	3.9	25.7
Ethanol	Water	1.7	0 (dissolves)

Eq. 21 was evaluated numerically for water, using the methods of Ninham and Parsegian [39] and of Krupp [40]. The result was the value 0.07, which is significantly lower than the value 2.43 obtained by the pairwise additivity approximation. According to the calculation based on Lifshitz theory, γ^p of water should be about 1.4 mJ m^{-2}, which is significantly lower than the commonly accepted value of 51 mJ m^{-2}. The Lifshitz's calculation agrees with the contention of Fowkes [41], according to which, γ^p of water is negligible because the conflicting dipolar fields cancel each other. Since Fowkes, it has now become a popular fashion to ignore dipolar forces for surface interactions completely; but it should be borne in mind that the dipoles generally have certain degree of orientation at the air–solid or solid–solid interfaces, and thus have uncompensated electrostatic fields, the effect of which may not be negligible. For liquids however, no simple correlation between surface (or interfacial) tension and molecular dipolar moments can be found (see Table 3).

Most current theories treat the interfacial forces as composed of two major components. One component, known as the LW (Lifshitz–van der Waals) component of the interaction, is composed of the dispersion forces with a small contribution from the orientational and induction terms. The LW component of the interaction energy follows the same geometric mean combining rule as shown in Eq. (16). The non-dispersive component of the interfacial interaction arises from the electron donor–acceptor or acid–base interactions. These donor–acceptor interactions will be reviewed in Section 2.12, but before that we review here some other factors which contribute to the surface and interfacial tensions of polymers. These factors are related to strain energy due to chain folding, anisotropic polarizability and chain scission.

2.8. *Effect of chain folding in surface tension*

The previous discussion of surface and interfacial tension is based upon the consideration that an uncompensated electrodynamic field acts at the surface. On some surfaces of polymer crystals, however, chains fold, which contributes to the surface and interfacial free energy in terms of strain energy. Another contribution of interfacial free energy comes from the anisotropy of the interface; parallel chains interact more strongly than the unoriented chains. These effects are manifested clearly in the melting and crystallization of polymer crystals.

Hoffman et al. [42] measured the interfacial tension between solid–liquid interfaces in polyethylene from the kinetics of crystal melts. The melting temperatures of small crystals and also the rate of homogeneous crystallization are affected by the interfacial tensions of the crystals and melt. This

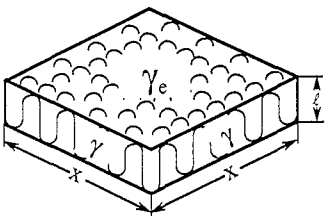

Fig. 4. Idealized diagram of a polyethylene crystal. The fold face of the crystal has a surface free energy of γ_e. The surface free energy of the side is γ [42]. Adapted with permission from Plenum Publishing Corporation.

is so because the heat of fusion of small particles have a component that is dependent on the surface excess free energy.

The melting points of a polyethylene crystal (Fig. 4) is given by Eq. (22).

$$T_m = T_m^\circ[1 - 2\gamma_e/(\Delta h_f)l] \tag{22}$$

where T_m is the observed melting point for a thin platelet, T_m° is the melting point of an infinite crystal and Δh_f is the heat of fusion per unit volume of the crystal.

The rate of homogeneous nucleation as a function of surface free energy is expressed as follows:

$$I = I_0 \exp[-U^*/R(T - T_\infty)] \exp[-30.2\gamma^2\gamma_e(T_m^0)^2/(\Delta h_f)^2(\Delta T)^2 f^2 kT] \tag{23}$$

where T_∞ is a hypothetical temperature at which all motions associated with viscous flow ceases; it is related to the glass transition temperature of the polymer. U^* is the activation energy associated with the chain motion.

From the experiments of crystal melting and rate of homogeneous nucleation, the values of γ and γ_e are found to be about 93 mJ m^{-2} and 14 mJ m^{-2} respectively. Both the values are high considering the fact that these are values of interfacial tensions against melts. From the arguments based on uncompensated fields, the interfacial tension in these cases should only be about 1–2 mJ m^{-2}. Hoffman et al. argued that the surface energy of the fold face is so high because it contains a component arising from the strain energy of chain folding. The difference comes from the work of chain folding on going from the trans to the gauche conformation in the folded zone. The required (4.24–5.06 kcal $mole^{-1}$) free energy change due to chain fold compares well with the theoretical estimate (4 kcal $mole^{-1}$).

The rather high interfacial tension obtained at the lateral surface of the crystal was explained by Fowkes [43]. Fowkes considered the fact that the energy of interaction of parallel hydrocarbon chains is higher than that of randomly oriented chains, because of the strong polarizability of the carbon–carbon backbone. Based on the anisotropic nature of bond polarizability, Fowkes estimated that the surface free energy of the parallel chains should be 70% higher than that of the non-oriented chains. The surface tension of liquid hydrocarbon, in the range of infinite molecular weight is about 35 mJ m^{-2}. So the surface tension of solid hydrocarbon with all chains parallel to each other should be in the range of 59 mJ m^{-2}. This view of Fowkes has been corroborated by the findings of Greenhill and McDonald [44].

The method used by Greenhill and McDonald to determine the surface tension of solid paraffin is based upon the assumption that solids act as viscous liquids near their melting points. In this method, the mechanical stress produced on a crystal is measured at different strain rates and is extrapolated to zero strain rate. The stress, in order to give a zero strain rate, must balance the surface tensional force along the circumference of the crystal. Thus the negative intercept at the strain rate axis obtained from the linear extrapolation of the strain rates versus stress gives the surface tension of the material. The value of the surface tension of solid paraffin obtained using this method is about 66 mJ m^{-2} at 29.5

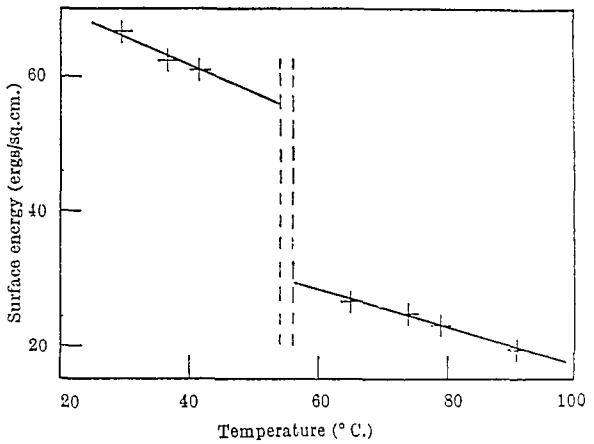

Fig. 5. Surface free energy of paraffin wax shows a clear discontinuity close to the melting point. Reprinted with permission from *Nature* (Ref. [44]). © 1953 Macmillan Magazines Ltd.

°C, and 60 mJ m^{-2} at 40 °C (Fig. 5). These values agrees with the value (59 mJ m^{-2}) proposed by Fowkes. (Here, 1 erg $cm^{-2} = 1$ mJ m^{-2}.)

2.9. *Surface free energy of glassy polymers from crazing*

Another component of the surface tension of a polymer, which becomes significant in fracture, arises from the scission of polymer chains. The importance of the van der Waals surface energy and that arising from chain scission in the processes of the fracture of glassy polymers has been reviewed by Kramer and Berger [45]. In the fracture of glassy polymers, before regular cracks appear, planar crack-like defects are formed, which consist of many fine (5–20 nm diameter) fibrils. Both the fibril formation within the craze and the magnitude of crazing stress were described by a Taylor meniscus instability process. The surface tension (γ) of the void resulting from the formation of craze microfibrils can be related to the fibril spacing D_o and the tensile stress (S) of the craze interface by the following equation:

$$D_o = 8\gamma/\beta S \tag{24}$$

where β is a constant proportionality factor between the average hydrostatic stress (σ_o) and the tensile stress at the craze interface.

The authors considered two different molecular mechanisms for the formation of the void surface: one resulting from the disentanglement of the polymer chain, in which case, the craze surface tension (γ) should be the van der Waals surface tension (γ) of the polymer (≈ 40 mJ m^{-2}); the other resulting from the chain scission. Craze surface tension due to chain scission is a sum of the van der Waals surface energy (γ_{vw}) and a term originating from the chain scission.

$$\gamma = \gamma_{VW} + (1/4)ndU \tag{25}$$

where n is the density of network strands, d is the root-mean-square end-to-end distance between junction points in the network and U is the polymer backbone bond energy. Since nd scales as $n^{1/2}$, increasing the strand density has a strong effect on the magnitude of craze surface tension. At temperatures close to the T_g, only disentanglement is expected, whereas at room temperature chain scission is expected. Kramer et al. tested this hypothesis by studying the formation of craze microfibril in a high molecular weight polystyrene ($M_w = 1\,800\,000$) using low-angle electron diffraction. From these measurements, they obtained values of $\gamma = D_o S/8$. At temperatures, lower than T_g, the value of γ is

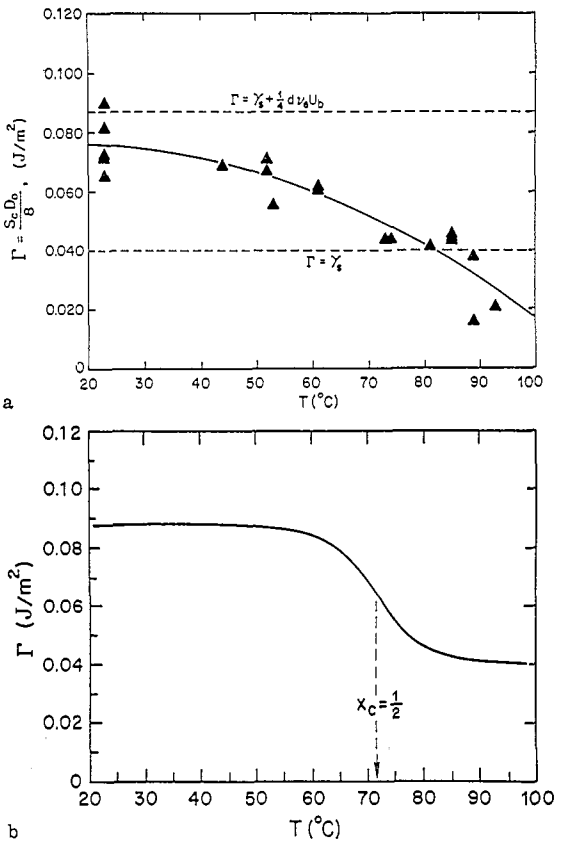

Fig. 6. Plots of $D_0S/8$ vs. temperature: experimental (a) and theoretical (b). Reprinted with permission from Springer-Verlag (Ref. [45]).

about 80 mJ m^{-2}; but as T_g is approached, γ converges to about 40 mJ m^{-2} (Fig. 6), corresponding to the value of the van der Waals surface energy of the polymer. The strand density of entangled polystyrene is about 3×10^{25} m^{-3}, the chain scission term is about 40 mJ m^{-2}. The estimated value of the craze surface tension of polystyrene (80 mJ m^{-2}) is similar to the experimental values.

2.10. Role of surface free energy in the adhesion under liquid media: stability of particle suspension

Neumann et al. [46] devised several methods to estimate the surface free energy of solids, which are based on adhesion under liquid media. The central theme of these methods is based on the following equation:

$$\Delta G_{132} = \gamma_{12} - \gamma_{13} - \gamma_{23} \tag{26}$$

where ΔG_{132} denotes the free energy of adhesion of two surfaces 1 and 2 in liquid 3. In principle, the free energy of adhesion can take any value from negative to positive, depending upon the relative magnitudes of the interfacial tensions of the three interfaces. When 1 and 2 denote the same particles, Eq. (26) reduces to

$$\Delta G_{131} = -2\gamma_{13} \tag{27}$$

In Neumann's studies, it has been assumed that the interfacial tension between a solid and liquid can only be positive or zero. If the interfacial tension is positive, the particles will coagulate spontaneously leading to an unstable suspension. This kind of situation arises for hydrophobic particles

suspended in a hydrophillic liquid, such as water. If, now, the surface tension of the liquid is slowly decreased by adding a low surface tension liquid to the first, a situation may arise when γ_{13} becomes zero. In that case, there is no driving force for the particles to adhere, and a stable suspension results. The surface tension of the liquid mixture at which this occurs was taken by Neumann et al. as the surface free energy of the particle [47]. They used this technique to determine the surface tensions of several polymer particles, including biological cells and bacterias.

2.11. Van der Waals repulsion between particles

Another interesting variation of the experiment described earlier is based on the van der Waals repulsion between particles. As predicted by the Lifshitz theory, the interaction between two dissimilar materials in a liquid can become repulsive. For van der Waals particles, this phenomenon may be viewed as follows.

Consider that the polarizability of particle 1 is smaller than that of the liquid, whereas that of particle 2 is higher than the liquid. The equivalent model is that particle 1 is in a negative polarizability state compared with the liquid, whereas particle 2 is in a positive polarizability state. The photon emitted by the first oscillator will then polarize particle 2 in such a way that the fluctuating and induced dipole moments will be in the same direction. This situation, which is just opposite to the interaction in vacuum, leads to a repulsion between the two particles. This effect is the underlying mechanism for the particle rejection in advancing solidification front. Suppose a zone of a solid is melted, and the molten front is slowly advanced from one end to the other of a solid bar. If there are particles present in the solid, and if the surface free energy of the particles is intermediate of the surface free energies of the solid and liquid zones, the particles will be rejected by the interface. Otherwise they will be engulfed. Neumann et al. [48] studied this phenomenon with a number of polymeric particles in naphthalene, and found that the particles are either rejected or engulfed by the solidification front (see Fig. 7 for experimental set up). Engulfment of the particles depends on the speed of solidification. The particles which are rejected at lower speed are engulfed at higher speeds due to hydrodynamic drag forces. At a critical velocity, the repulsive van der Waals force is equal to the hydrodynamic drag force. Using dimensional analysis, Neumann et al. developed the following equation:

$$\Delta G = 2.64 \times 10^5 \frac{\rho_L^{0.847} T^{0.280} k_p^{0.720}}{\mu^{0.127} (\rho_p C_p)^{0.441}} D^{0.407} V_c^{0.847} \tag{28}$$

where ρ_p is the particle density, ρ_L is the liquid matrix density, C_p is the heat capacity of the particle per unit mass, k_p is the thermal conductivity of the particle, μ is the viscosity of the liquid matrix, T is the melting temperature of the matrix material and D is the particle diameter. Eq. (28) provides a

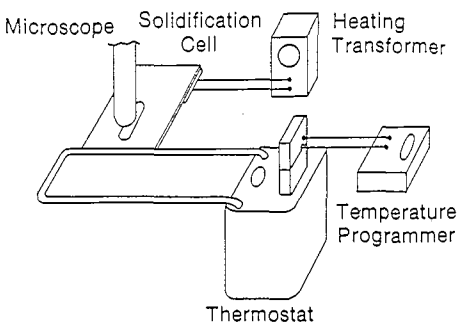

Fig. 7. A schematic diagram of the advancing solidification front apparatus [46]. Reprinted with permission from American Institute of Physics (Ref. [48]).

Table 4
Surface tension values of several polymers obtained from advancing solidification

Particle material	Surface free energy ($mJ\ m^{-2}$)
Acetal	44.3
Nylon-12	40.6
Nylon-6,12	34.0
PVC	32.7
PMMA	35.3

novel means to estimate the free energy of adhesion ΔG from the advancing solidification experiments. The free energy of adhesion can be further decomposed according to Eq. (29), which was used by Neumann to determine the surface free energies of several polymer particles (Table 4):

$$\Delta G = \gamma_{ps} - \gamma_{pl} - \gamma_{sl} \tag{29}$$

where γ_{ps}, γ_{pl} and γ_{sl} are the interfacial tensions of the particle–solid, particle–liquid and solid–liquid interfaces.

This technique was found to be applicable not only to various polymers but with biological cells at the interface of ice and water as well.

Neumann et al. assumed that the condition which leads to zero interfacial tension between solid and liquid also ensures that the surface tension of the solid is equal to that of the liquid. This however need not always be the case. Another implicit assumption is that the solid–liquid interfacial tension can only become zero or positive. Based on the acid–base argument (see below), one encounters the possibility of a negative interfacial tension. The interfacial tension between two surfaces can be written as follows:

$$\gamma_{12} = \gamma_{12}^{LW} + \gamma_{12}^{AB} \tag{30}$$

where LW and AB stand for the London–van der Waals and acid–base interactions respectively. One can further reduce the above equation as follows:

$$\gamma_{12} = (\sqrt{\gamma_1^{LW}} - \sqrt{\gamma_2^{LW}})^2 + (\gamma_1^{AB} + \gamma_2^{AB} - W_{12}^{AB}) \tag{31}$$

The LW component of the interfacial tension is always positive, whereas the AB component of the interaction can have a negative value. One obvious example of a negative γ_{ab} is that of an acid interacting with a base, neither of them being self-associative. In this case the AB component of the interfacial tension is negative. The sign of the total interfacial tension depends on the relative contribution of the LW and AB components.

2.12. Donor–acceptor interaction at surfaces

According to Fowkes [41], as well as Bolger and Michaels [49], the interaction between surfaces can be thought of consisting of two major components: dispersion forces and acid–base interactions. The first significant approach to the theory of acid–base interaction was due to Bronsted, who defined an acid as a proton donor and a base as a proton acceptor. In the Lewis concept of acid and base, acid is an acceptor of a lone pair of electron and a base is a donor of a lone pair of electron. In the Bronsted type of acid–base interaction, protons play the key role. In the Lewis concept, protons need not be present and this is therefore more general than Bronsted's definition.

A quantitative estimate of the Lewis acid–base interaction energy is obtained using Drago's formula. According to Drago et al. [50], the enthalpy (ΔH) of acid–base interactions can be estimated

Table 5
Drago's C and E parameters (kJ $mol^{-1/2}$)

Acid	C_A	E_A	Base	C_B	E_B
Chloroform	0.31	6.77	Ethylacetate	3.56	1.98
Phenol	0.90	8.85	Benzene	1.8	0.75
Water	0.67	5.01	Acetone	4.76	2.02
t-Butanol	0.61	4.17	Tetrahydrofuran	8.73	2.00
Boron trifluoride	6.30	16.3	Pyridine	13.09	2.39
Iodine	2.04	2.04	Triethylamine	22.67	2.02
Silica	8.98	2.33	Diethylsulfide	15.13	0.70
Rutile	11.6	2.09	PMMA	1.39	1.96

from certain parameters that express the basic (B) and acidic (A) properties of the two surfaces according to the following equation:

$$-\Delta H = C_A C_B + E_A E_B \tag{32}$$

where the constants C and E represent the covalent and electrostatic interactions (Table 5). Eq. (32) predicts the enthalpy of acid–base interaction for liquid mixtures with an accuracy of about 0.2 Kcal $mole^{-1}$.

Fowkes suggested that if the number of acid–base pairs at an interface is known, the free energy of the interfacial interaction can be obtained using the following formula:

$$\Delta G = n_{ab}\ \Delta H \tag{33}$$

In order to elaborate this idea let us take the case of the benzene–water interface. Normally, the interfacial tension between oil and water is about 51 mN m^{-1}. The interfacial tension (35 mN m^{-1}) at the benzene–water interface is about 16 mN m^{-1} lower than that of the oil–water interface, even though the surface tension of benzene (25 mN m^{-1}) is close to that of oil. The lower interfacial tension between benzene and water is due to the hydrogen bonding between the π electron of the benzene ring and the hydroxyl group of water. Fowkes suggested that this hydrogen bonding can be viewed as a subset of the acid–base interaction so that Drago's equation can be used to predict the enthalpy of interaction between benzene and water. This value is found to be about 5 kJ $moles^{-1}$. Assuming that benzene lies flat at the interface (so as to expose the π electrons to water), each molecule occupies an area of about 0.5 nm^2, and this gives the number of acid–base pairs to be 3.3 μmoles m^{-2}, corresponding to an enthalpy of interaction per unit area of 16.5 mJ m^{-2}. This value is in excellent agreement with the discrepancy of about 16 mJ m^{-2} between $\gamma_{\text{benzene–water}}$ and $\gamma_{\text{hydrocarbon–water}}$.

2.13. Negative interfacial tension

If we do a similar calculation for water–triethylamine, we find a value of ΔH_{12} as 34 kJ $mole^{-1}$. Using the area of triethylamine as 54.5 $Å^2$, we obtain the number of acid–base pairs to be about 3.04 μmoles m^{-2}. W_{12}^{ab} between the triethylamine–water interface is therefore 103 mJ m^{-2}. The total interfacial tension of a hypothetical interface of triethylamine and water turns out to be about -30 mJ m^{-2}. The possibility of a negative interfacial tension resulting from the acid–base interactions was postulated earlier by Chaudhury [38]. A negative interfacial tension however implies that the interface will disintegrate accompanied by chaotic and dissipative transport unless there are other mechanisms to stabilize the interface. Simultaneous existence of a negative interfacial tension and a positive cohesion pressure was alluded to by Ohki and Ohki [51] for the stability of biological lipid membranes.

2.14. Acid–base interaction in adsorption and adhesion

Drago et al. estimated the C and E parameters from the heat of solution. For powders and flat surfaces, heat of adsorption (ΔH) can be estimated from the temperature-dependent adsorption constants according to the following equation:

$$-\Delta H = -\Delta H_{ads} = RT_1T_2/(T_2-T_1)\ \ln\left(\frac{k(T_2)}{k(T_1)}\right) \tag{34}$$

where $k(T_2)$ and $k(T_1)$ are the adsorption constants at temperatures T_2 and T_1 respectively. These constants are generally determined from Langmuir's adsorption plots (Fig. 8) and using Eq. (32):

$$\frac{C}{\Gamma} = \frac{1}{\Gamma_m k(T)} + \frac{C}{\Gamma_m} \tag{35}$$

Where Γ is the surface concentration, Γ_m is the maximum value for Γ and C is the bulk concentration of the adsorbent.

If the heat of adsorption of liquids with known values of Drago's C and E parameters are estimated, the C and E values of solid surfaces can be found by solving Eq. (32). The value of Γ_m provides an estimate of the number of acid or base sites present on a solid substrate. Once these values are known, the acid–base component of the work of adhesion for two dissimilar materials can be estimated using Eqs. (32) and (33).

Fowkes also devised a method to determine the acid–base properties of flat solid surfaces using the contact angle. He measured the contact angles of a dispersive liquid mixed with a small amount of an acid or base on a solid surface. Using the Gibbs adsorption equation, the change of contact angle due to adsorption can be written as

$$\mathrm{d}(\gamma_l \cos\theta) = \mathrm{d}(\gamma_s - \gamma_{sl}) = \Gamma_i\, \mathrm{d}\mu_i \tag{36}$$

The surface excess quantity can be obtained as:

$$\Gamma_i = \mathrm{d}(\gamma_l \cos\theta)/\mathrm{d}\mu_i \tag{37}$$

From the surface excess quantities, the adsorption constants and the heat of adsorption can be determined using Eqs. (34) and (35).

This method of estimating acid–base parameters from contact angles has certain limitations as discussed below. Firstly, the method assumes that all the adsorption takes place at the solid–liquid interface. However, any strongly interacting species may diffuse on the solid–vapor interface by reactive diffusion (Holmes–Farley and Whitesides measured the contact angles of water on a derivatized polyethylene surface that contained titatrable fluorescent groups. Fluorescent quenching was

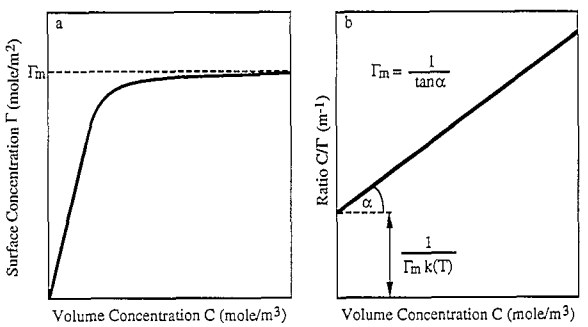

Fig. 8. A typical adsorption isotherm. Adapted with permission from Plenum Publishing Corporation (Ref. [41]).

observed in an annulus outside the liquid drop. The authors ascribed this quenching to the migration of protons at the solid–vapor interface.) and thus modify γ_s significantly. Thus strongly interacting solutes should be avoided. Secondly, it is necessary that the dispersion component of the surface tension of the liquids constituting the mixtures be very similar in order to minimize its influence on the overall adsorption energy.

Fowkes proposed that the adsorption of polymers from organic solvents onto inorganic surfaces is a process that involves dispersion forces and acid–base interactions. Because of the similarity of the polarizabilities of the liquids and polymers, the dispersion force contribution to adsorption is normally very small, and hence the acid–base interaction becomes the dominant contributor to adhesion. An example demonstrating the effect of the acid–base interaction in polymer adsorption is given in Fig. 9, which shows that the adsorption of a basic polymer, polymethylmethacrylate (PMMA), onto acidic silica is a maximum when the adsorption takes place from a neutral solvent. The adsorption decreases when the solvent competes with either the polymer or the substrate. Similar results are also found for the adsorption of an acidic polymer CPVC (chlorinated polyvinyl chloride) onto a basic substrate, calcium carbonate. These types of correlation between polymer adsorption and acid–base interaction led Fowkes to propose that the adhesion of polymers to inorganic surfaces is also contributed to by the acid–base interactions. In order to demonstrate this concept, Fowkes studied the adhesion of different polymers on acidic and basic glass surfaces. A cast film of PMMA adhered strongly to an acidic glass ($<0.1\%$ alkali metal oxides) and could not be peeled; whereas, it adhered weakly to a

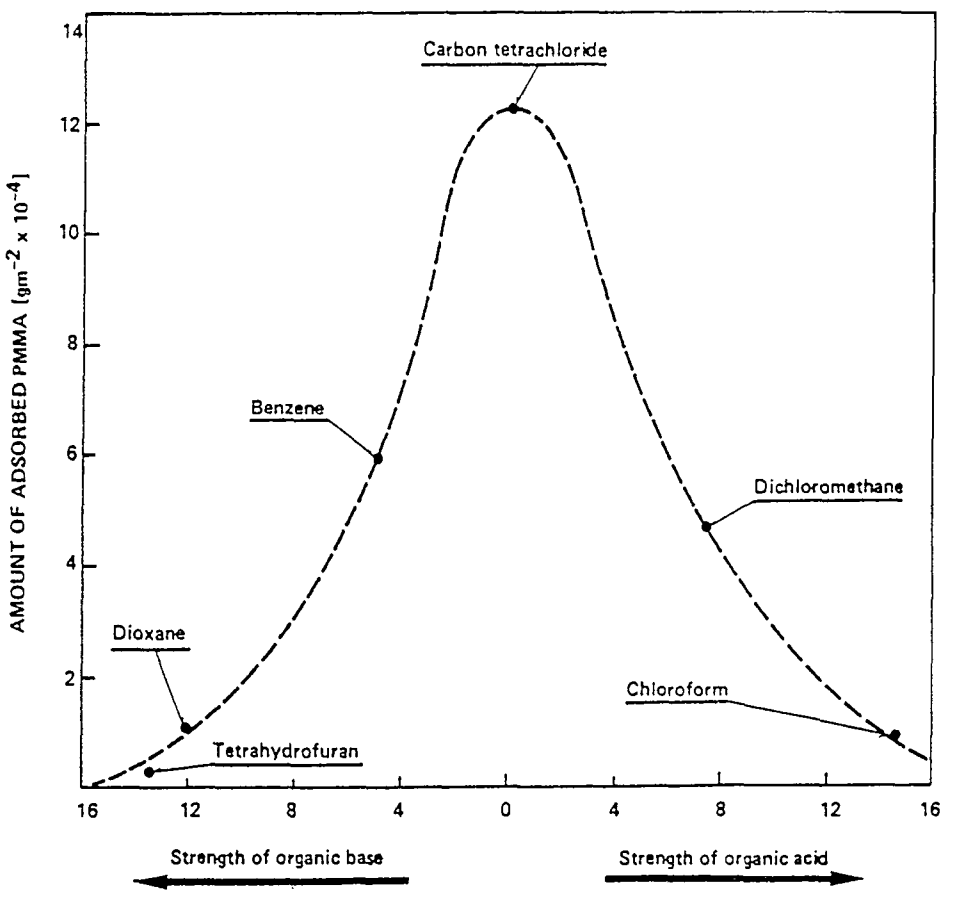

Fig. 9. Adsorption of PMMA onto silica from different solvents. Reprinted with permission from Plenum Publishing Corporation (Ref. [41]).

basic glass (20% sodium oxide) and could easily be peeled. If the basic glass was treated with hydrochloric acid, the surface was converted to silicic acid and PMMA adhered strongly to this substrate.

Several experiments involving structural and pressure-sensitive adhesives have provided abundant proof supporting the acid–base hypothesis of adhesion [52].

2.15. The role of acid–base interaction in the surface and interfacial free energy of polymethylmethacrylate

The success of the measurement of the surface free energy of solids from contact angles hinges upon the correct estimation of γ_{sl}. According to the Young's equation, the contact angle provides the value of the difference $\gamma_s - \gamma_{sl}$. We need another equation to solve for γ_s and γ_{sl}, which can be achieved approximately by measuring the surface tension of the liquid covered with a thin film of the insoluble monolayer of the polymer. The film has to be so thin that its elastic forces do not contribute to the measured surface tension. According to the principle of independent surface action, the total surface tension of the polymer-covered liquid surface is the sum of γ_s and γ_{sl}, which provides the conjugate condition to Young's equation for estimating γ_s and γ_{sl}. To illustrate this procedure, let us consider the PMMA–water interface. The surface tension of water coated with a thin layer [38] (ca. 10 Å) of PMMA is about 66.3 mN m^{-1}. According to the principle of independent surface action,

$$\gamma_s + \gamma_{sl} = 66.3 \text{ mN m}^{-1} \tag{38}$$

The contact angles of several liquids on such a thin film transferred onto a rigid substrate are shown in Table 6, and are compared with the contact angle values of bulk PMMA.

The similarity of the contact angles indicate that the surface properties of the thin film of PMMA are very similar to those of bulk PMMA. According to Young's equation, the difference $\gamma_s - \gamma_{sl}$ for PMMA and water is about 27.3 mJ m^{-2}. Therefore, according to Eq. (38), the values of γ_s and γ_{sl} turn out to be 46.7 mJ m^{-2} and 19.6 mJ m^{-2} respectively. The surface free energy of PMMA obtained from this method is slightly higher than the values estimated from contact angles (39–43 mJ m^{-2}).

Let us now see how the value of the interfacial free energy obtained above compares with the predictions of the dispersion interaction and acid–base theory. According to Fowkes, the interfacial tension can be expressed as follows:

$$\gamma_{sl} = \gamma_s + \gamma_l - 2\sqrt{(\gamma_s \gamma_l^{LW})} - W_{sl}^{ab} \tag{39}$$

Since PMMA is a base and is not self-associative, its total surface tension is contributed by the van der Waals interactions, i.e. $\gamma_s = \gamma_s^{LW}$. Thus Eq. (39) reduces to:

$$\gamma_{sl} = 56 - W_{sl}^{ab} \tag{40}$$

Table 6
Contact angles of various liquids on the surface of bulk PMMA and LB PMMA films

Liquid	Bulk PMMA	LB film of PMMA
Water	70	68
Glycerol	64	64
Formamide	53	53
Ethylene glycol	35	46
Methylene iodide	38	41

The enthalpy of the acid–base interaction [41] for PMMA and water, according to Eq. (32) is 8.27 kJ mole^{-1}. The significant unknown in converting ΔH to W_{sl} is the number of acid–base pairs at the PMMA–water interface. The number density of the repeat unit of methacrylate monomer in PMMA is about 5 μmoles cm^{-2}. If we use this value to approximate the number of acid–base pairs at the interface, we obtain a value of 41.5 mJ m^{-2} for W_{ab}, yielding the value of γ_{sl} as 14.5 mJ m^{-2}. This value of interfacial tension is slightly lower than the value (19.6 mJ m^{-2}) estimated from the surface tension and contact angle.

2.16. Modification of the acid–base behavior due to lateral interactions

Jensen [53] has recently made several valuable comments on Drago's method of estimating the acid–base interaction between solids; these are outlined below. Firstly, the method assumes that a molecule acts exclusively as an acid or a base. In reality, however, most molecules posses amphoteric acid–base characters. If one were to extend Drago's treatment to amphoteric surfaces one would need four empirical parameters. Thus the enthalpy of adduct formation for amphoteric surfaces needs to be represented by a four-term equation consisting of a total of eight parameters, which is not practical. Secondly, even though too much emphasis is placed on the implied meanings of E and C parameters representing electrostatic and covalent interactions, Jensen pointed out that there is no evidence that the terms are as they are used for. In modern molecular orbital theory, the results of which were prefigured by Small [54], the hydrogen-bond energy is represented as the product of two difference terms; the difference between values of a single parameter that characterizes the acid functionality for each of the two components and the corresponding difference for a single parameter for the basic functionality. Jensen pointed out that the separation of a Lewis acid–base interaction into electrostatic and covalent components is not necessary when an approximate choice of atomic orbital is made for the construction of a molecular orbital. Another question that arises is whether the surface manifestations of hydrogen bonding (or acid–base bonding) must correspond exactly to the bulk manifestations. For example, let us consider a solution of species that contains a hydroxyl group in a liquid polyether. From spectroscopic shifts in absorption frequencies and departures from the Raoult's law, it may be inferred that hydrogen bonding exists. Now, in interactions across an interface, it might be expected that whenever hydroxyl groups are present in one phase and ether groups in the other, hydrogen bonds will form. But this is not necessarily so. The protons of the hydroxyl groups may interact with the unshared pair of electrons of the other hydroxyl groups in the same phase, strongly enough that they are not available for Lewis neutralization across the interface. Fowkes noted that silicas containing a high concentration of hydroxyl groups are not as strongly hydrogen bonding as the silicas containing less-concentrated hydroxyl groups. This effect of lateral H-bonding to acid–base interactions has been elegantly studied by Whitesides and coworkers [55,56], who examined the acid–base reaction at surfaces by a method known as contact-angle titration.

2.17. Acid–base interaction in contact-angle titration

In these studies, the authors used well-defined surfaces of oxidized polyethylene, self-assembled monolayers of carboxylic acid functional alkane thiols adsorbed onto gold and carboxylic acid functional alkoxysiloxanes adsorbed onto silica. Because of their proximity, the carboxyl groups form strong hydrogen bonds laterally thereby stabilizing the proton. Normal pK_a values of carboxylic acid groups in solution range between 3 and 5. However the carboxylic acid surfaces display pK_a values in the range of 8–10. The higher the density of the carboxylic acid groups, the higher the shift of the pK_a values (Fig. 10). A similar but still stronger effect has recently been discovered by Whitesides et al.

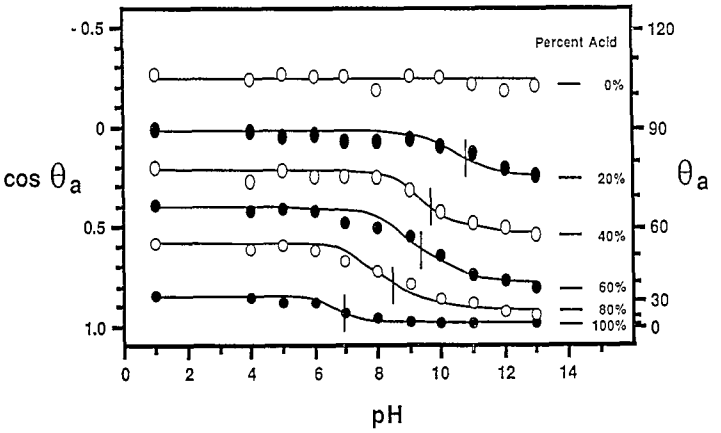

Fig. 10. Contact-angle titration of carboxylic acid surface. The surfaces were prepared by forming mixed monolayers of methyl and carboxylic acid functional alkyl siloxanes on silicon wafer. The pK_a (shown by vertical lines) of these surfaces shift to lower values as the concentration of carboxylic acid increases. This shift may be due to the lateral interactions of the carboxylic acid groups stabilizing the proton. Reprinted with permission from *Langmuir* (Ref. [55]). © 1989 American Chemical Society.

[57] for surfaces made up of boronic acid. For surfaces containing protonating groups such as amine [58], the pK_b values are shifted towards lower values indicating that the lateral hydrogen bonding prevents the basic groups from protonating.

When two condensed phases engage in acid–base interaction, one might ask: to what extent the single molecular acid–base parameters are applicable to estimate the interaction between condensed phases. In addition to the lateral Lewis neutralization as indicated earlier, the number of acid–base sites engaged in H-bonding can actually be reduced as a result of an electrical double layer that arises due to interfacial charge transfer. This point will be discussed in a later section (Section 2.21).

2.18. Other empirical methods of acid–base interactions

Chaudhury and co-workers [59] proposed an approximate method to estimate the acid–base interactions between surfaces of condensed phases. This treatment uses acid–base parameters that are defined for surfaces. For each surface two parameters are defined: Δ^+ and Δ^- standing for electron acceptor and electron donor surface parameters. Work of adhesion between two amphoteric surfaces is expressed as:

$$W^{ab}{}_{12} = \delta_1{}^+ \delta_2{}^- + \delta_1{}^- \delta_2{}^+ \tag{41}$$

The acid–base component of the surface tension is expressed as:

$$\gamma^{ab}{}_{11} = W^{ab}{}_{11}/2 = \delta_1{}^+ \delta_1{}^- \tag{42}$$

For example, the acid–base component of the work of adhesion of a liquid forming a finite contact angle on a solid is:

$$W^{ab}{}_{ls} = \gamma_l(1+\cos\,\theta) - 2(\gamma_l{}^{LW}\gamma_s{}^{LW})^{0.5} = \delta_1{}^+ \delta_2{}^- + \delta_1{}^- \delta_2{}^+ \tag{43}$$

Using water as a standard amphoteric liquid, the values of δ for several solids can be defined relative to water. Other amphoteric liquids, such as glycerol, formamide and ethylene glycols can also be used for this purpose. This method of dividing the surface and interfacial tension components has been useful in the semi-empirical analysis of contact angles of liquids on solid surfaces.

2.19. Bolger–Michaels method of estimating acid–base interactions

The methods of Drago and its extensions are mostly suitable for Lewis-type acid–base interactions. For acid–base interactions involving proton transfer, the method developed by Bolger and Michaels [49] is more suitable. Bolger and Michaels observed that a Bronsted-type acid–base interaction plays a very significant role in the adhesion of polymer coatings to metal oxides, and in particular to the hydrolytic stability of the resultant interface.

An oxide surface can form acid–base bonds with an organic compound via one of two routes:
Case A: surface interaction with an organic acid

$$-\mathrm{MOH} + \mathrm{HXR} \longrightarrow -\mathrm{MO}\overset{\mathrm{H}}{\ldots}\mathrm{HXR} \rightleftharpoons -\mathrm{MOH_2}^{+}\ldots\mathrm{XR}^{-} \tag{44}$$

$$\Delta_A (= \log k_A) = \mathrm{IEPS} - \mathrm{p}k_{A(A)} \tag{45}$$

Case B: surface interaction with an organic base

$$-\mathrm{MOH} + \mathrm{XR} \longrightarrow -\mathrm{MOH}\ldots\mathrm{XR} \rightleftharpoons -\mathrm{MO}^{-}\ldots\mathrm{HXR}^{+} \tag{46}$$

$$\Delta_B (= \log k_B) = \mathrm{p}k_{A(B)} - \mathrm{IEPS} \tag{47}$$

where k_A and k_B are the equilibrium constant of acid–base interaction, IEPS is the isoelectric point of the substrate's surface, $k_{A(A)}$ and $k_{A(B)}$ are the acidic and basic dissociation constants of the organic molecule. The free energy of the reaction is RT times the negative of Δ values. When Δ values are positive, the equilibrium lies towards the right of the schemes shown in Eqs. (44) and (46), i.e. acid–base bonding is preferred. However, very high values of Δ are not preferable because it means that the oxide surfaces will be attacked chemically and will corrode. Tables 7 and 8 show some examples of positive Δ values of interaction between organic molecules and oxide surfaces.

Table 7
Surface interaction with organic acids. Reprinted with permission from Plenum Publishing Corporation (Ref. [49])

Organic compound	$pK_{A(A)}$	Δ_A		
		SiO_2	Al_2O_3	MgO
Dodecyl sulfonic acid	−1	3	9	13
Trichloroacetic acid	0.7	1.3	7.3	11.3
Chloroacetic acid	2.4	−0.4	5.6	9.6
Phthalic acid	3.0	−1	5.0	9.0
Benzoic acid	4.2	−2.2	3.8	7.8
Adipic acid	4.4	−2.4	3.6	7.6
Acetic acid	4.7	−2.7	3.3	7.3
Hydrogen cyanide	6.7	−4.7	1.3	5.3
Phenol	9.9	−7.9	−1.9	2.1
Ethyl mercaptan	10.6	−8.6	−2.6	1.4
Water	15.7	−13.7	−7.7	−3.7
Ethanol	16	−14	−8	−4
Acetone	20	−18	−12	−8
Ethyl acetate	26	−24	−18	−14
Toluene	37	−35	−29	−25

Table 8
Surface interaction with organic bases. Reprinted with permission from Plenum Publishing Corporation (Ref. [49])

Organic compound	$pK_{A(A)}$	Δ_B		
		SiO_2	Al_2O_3	MgO
Trimethyl dodecyl ammonium hydroxide	12.5	10.5	4.5	0.5
Piperidine	11.2	9.2	3.2	−0.8
Ethylamine	10.6	8.6	2.6	−1.4
Triethylamine	10.6	8.6	2.6	−1.4
Ethylenediamine	10	8	2.0	−2
Ethanolamine	9.5	7.5	1.5	−2.5
Benzylamine	9.4	7.4	1.4	−2.6
Pyridine	5.3	3.3	−2.7	−6.7
Aniline	4.6	2.6	−3.4	−7.4
Urea	1.0	−1	−7	−11
Acetamide	−1	−3	−9	−13
Water	−1.7	−3	−9	−13
Tetrahydrofuran	−2.2	−4.2	−10.2	−14.2
Ethyl ether	−3.6	−5.6	−11.6	−15.6
t-Butanol	−3.6	−5.6	−11.6	−15.6
n-Butanol	−4.1	−6.1	−12.1	−16.1
Acetic acid	−6.1	−8.1	−14.1	−18.1
Phenol	−6.7	−8.7	−14.7	−18.1
Acetone	−7.2	−9.2	−15.2	−19.2
Benzoic acid	−7.2	−9.2	−15.2	−19.2

2.20. *Hard–soft acid–base principle*

For an excellent review of this subject see Lee [60]. An approach used for the studies of acid–base interaction between solids is based on the hard–soft acid–base (HSAB) principle expounded by Pearson [61]. Pearson classified acids and bases according to the hardness and softness of the inorganic compounds as follows.

1. Hardness implies the property of atoms that do not have easily excitable outer electrons and are not polarizable.
2. Softness implies atoms which have easily excitable outer electrons and are polarizable.
3. A hard base contains a donor atom of low polarizability and high electronegativity. It is associated with an empty orbital of high energy and hence is inaccessible.
4. A soft base contains a donor atom of high polarizability and low electronegativity.

The concepts of hardness and softness of molecules have been clarified in view of the recently developed density functional theory. A hard electrophile (or acid) has a high-energy lowest unoccupied molecular orbital (LUMO). A soft electrophile has a low-energy LUMO. A hard nucleophile (or base) and a soft nucleophile have low-energy and high-energy highest occupied molecular orbital (HOMO) respectively. According to Klopman and Hudson [62], the energy of interaction between a nucleophile and electrophile is expressed as:

$$\Delta E = -Q_{Nu}Q_{El}/(\epsilon R) + 2(C_{Nu}C_{El}\beta)^2/(E_{HOMO} - E_{LUMO}) \tag{48}$$

The first term is the Coulombic term and the second term is the frontier orbital term. Q_{Nu} and Q_{El} are the total charges of the nucleophile and electrophile respectively; C_{Nu} and C_{El} are the coefficients of the atomic orbital and β is the resonance integral; ϵ is the permittivity and R is the separation distance between the nucleophile and electrophile. It is stipulated that Drago's E parameters are related to the

first term of the right-hand side of Eq. (48), and the C parameters are related to the second term. On the basis of the above equation (see Lee [60]) the HSAB principle can be restated as follows.

1. A hard–hard interaction is the result of the dominance of the large Coulombic attraction as described by the first term of Eq. (48).
2. A soft–soft interaction is the result of a large orbital interaction between HOMO and LUMO.

The interfacial interaction between chromium and copper has recently been modelled by Cain et al. [63]. The modelling is based on a tight-binding extended Huckel method. Metals can be characterized by the band structure and the Fermi levels. Copper is considered more basic than chromium because it has more filled than empty orbitals. Thus for the Cr/Cu interaction, Cr becomes a Lewis acid and Cu becomes a Lewis base. Lee suggested that since all metals are classified as soft, a metal–metal interaction can be directly derived from the soft acid–soft base interaction, which is predominantly controlled by the frontier orbital. He discussed other types of HSAB interactions involving metal–semiconductor and metal–polymer interfaces. Most semiconductors are soft bases and they can readily react with metals, which are, comparatively, soft acids. Most of the metal–polymer interactions can also be viewed as acid–base interactions. When metal films are formed on a polymer by evaporative deposition in vacuum, they do not have oxide films. When chromium is deposited onto pyromellitic dianhydride-oxydianiline polyimide (PMDA-ODA PI), there is evidence for some chemical interaction between the two. In this case chromium is a soft acid and PI is hard base, thus they should not interact strongly. However, as Ho et al. [64] pointed out, the reaction does not proceed by the complexation between a chromium atom and PMDA. A chromium atom donates an electron and forms a charge-transfer complex with PMDA. In this manner, PI acts as a soft acid by accepting the electron and Cr becomes a soft base by donating the electron. Other transition metals such as Ti also form a charge-transfer complex with PMDA and the adhesion takes place via acid–base interaction.

2.21. Electrical double layer formed by donor–acceptor bonding

When donor–acceptor interaction takes place, an electrical potential difference develops at the interface. This potential difference acts against any further flow of electrons. Formation of an electrical double layer decreases the free energy of the system. If different portions of the surface have a different charge density, the double layer may have a mosaic structure. But in general, most theoretical analyses of the double layer assume that the interface carries a homogeneous surface charge density.

Let us consider the following case as discussed by Deryaguin et al. [65]. One of the surfaces is considered to be saturated with donor molecules, whereas the other is considered to be saturated with acceptor molecules. Let the surface densities of donors and acceptors be N_d and N_a respectively (Fig. 11). The heat of donor acceptor reaction depends on the distances of the donor and acceptor sites from the interface and the permittivities (ϵ_1 and ϵ_2) of the two materials.

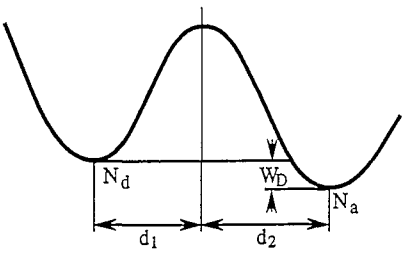

Fig. 11. Energy of electrons in donor and acceptor states. Adapted with permission from Plenum Publishing Corporation (Ref. [65]).

The electrostatic potential difference generated from the donor–acceptor interaction reduces the heat of reaction by an amount given by

$$\Delta H(n) = \Delta H_0 - e\Delta V(n) \tag{49}$$

If N is the maximum number of donor–acceptor pairs that can form at the interface in the absence of any electrostatic field, the number of actual pairs is obtained by minimizing the total free energy of the system (F) with respect to n.

$$F = F_0 + \Delta E - T\Delta S(n) \tag{50}$$

where ΔE is the change in the internal energy of the system which has the form:

$$\Delta E(n) = -n[\Delta H_0 - e\Delta V(n)] \tag{51}$$

The entropy term can be expressed as a combinatorial term of the form:

$$\Delta S(n) = k \ln \frac{N!}{(N-n)!n!} \tag{52}$$

Minimization of the free energy leads to a relation between n and the heat of reaction and potential difference as:

$$\frac{n}{(N-n)} = \exp\left[\frac{\Delta H_0 - e\Delta V(n) - en(\delta\Delta V(n)/\delta n)}{kT}\right] \tag{53}$$

In order to calculate n, one first needs a functional form for $\Delta V(n)$. In a simple parallel plate capacitor model $\Delta V(n)$ is expressed as:

$$\Delta V(n) = 4\pi en\left(\frac{d_1}{\epsilon_1} + \frac{d_2}{\epsilon_2}\right) \tag{54}$$

Deryaguin et al. calculated values of n for some real interfaces using Eqs. (53) and (54) and found that it can be ten to one hundred times smaller than N, the largest allowable pairs. The formation of an electric double layer at metal–semiconductor and polymer–semiconductor interfaces has been verified by the Russian group using various methods, some of which are discussed later.

The effect of the electrical double layer on the adhesion of polymers and semiconductor surfaces was studied using the field-effect technique. The surfaces of semiconductors, as was shown by Tamm, acquire energy states that are located in the forbidden gap, either due to defects or by the interruption of the periodicity. Surface states are readily created by the adsorption of foreign atoms or by defects in the form of vacancies and dislocations. The surface states are not totally localized at the surface thereby completely shielding the bulk semiconductor. The charge is distributed over a length from the surface. The adsorption of polymers on semiconductor surfaces modify the existing surface states or create new ones that are accessible by the measurement of surface conductance as a function of electric field applied normal to the interface. The surface conductance was determined in relation to the field-induced charge. Using this method, Deryaguin et al. determined the charging of a semiconductor-surface germanium in contact with various polymer films.

Polystyrene and polyvinyl alcohol decrease the magnitude of negative surface charge, whereas polyvinyl acetate and chlorinated polyvinyl chloride (PVC) reverse the sign of the germanium surface charge. These experiments suggest that these polymers behave as acceptors in comparison with germanium according to the following sequence:
Donor PS > PVA > PVAc > chlorinated PVC Acceptor which, with the exception of polystyrene, is in agreement with the donor–acceptor sequence of the most frequently encountered functional groups:

Table 9
Charging of germanium in contact with various polymers. Reprinted with permission from Plenum Publishing Corporation (Ref. [65])

Polymer	$Q_0 \times 10^9$ (C cm^{-2})
Germanium (free surface)	−2.5
Polystyrene (PS)	−0.6
Polyvinyl alcohol (PVA)	−0.1
Polyvinyl acetate (PVAc)	+0.15
Chlorinated PVC	+3.8

Donor $NH_2 > OH > OR > OCOR > CH_3 > C_6H_5 >$ halogens $> CO > CN$ Acceptor

These experimental results were obtained under vacuum; however, when measurements were carried out in air, surface conductance of the polymer film-coated germanium surface increased. This effect was attributed to the adsorption of water. Table 9 clearly shows that the electrophysical properties of the germanium surface is quite sensitive to the chemical properties of the polymers. In an experiment designed to determine how the concentration of polymer functional groups interacting with the germanium surface influences the electrophysical properties of the interface, copolymers of methyl methacrylate and methacrylic acid were used. The positive charge on the germanium surface increased systematically as the concentration of the acrylic acid increased.

2.22. *Electrical phenomena in breaking adhesive bonds*

This vast subject has been reviewed by Deryaguin et al. [65]. Most systematic studies in this area have been carried out again for polymer–semiconductor interfaces. Like the formation of adhesive bonds, breaking of adhesive bonds also changes the electrophysical properties of the surface. During the detachment of the polymer from a substrate, the surface charge density changes. The charge carriers are injected into or extracted from the germanium surface. The redistribution of the charge carriers between the bulk semiconductor and the space-charge region affects the concentration of the electrons and holes in the near-surface layer, thus a new equilibrium is achieved between the surface and bulk states. The work of peeling of gutta-percha from germanium exhibited a pronounced dependence on the environment. The work of adhesion was higher when peeling was done in vacuum compared with the peeling in air indicating that electrostatics play an important role in adhesion. The adhesive separation was accompanied with a strong emission of electrons. Furthermore, the change in surface conductance was observed without the application of an external field; it was influenced solely by the field existing in the gap between the polymer and the substrate.

Deryaguin et al. observed that the electroadhesion values increase with the increase of the rate of detachment; they also decrease with the increase of atmospheric pressure. Both of these effects are attributed to the electric discharge occurring in the gap of the crack leaflets. At slower speeds or high pressures, leakage of surface charge is possible and thus the adhesion values are low. The electroadhesion values decrease dramatically in a moist atmosphere due to a high degree of leakage.

These authors calculated theoretically the work of adhesion according to the following equation:

$$W = 2\pi\kappa^2 h/\epsilon \tag{55}$$

where κ is the double-layer charge density, h is the discharge gap and ϵ is the dielectric constant of the air. The experimentally observed adhesion values correlate with the theoretical values rather well (Table 10).

Table 10
Experimental and calculated values of the electrostatic work of adhesion of germanium to various polymers. Reprinted with permission from Plenum Publishing Corporation (Ref. [65])

Polymer	$W_{expt.}$ ($J\,m^{-2}$)	$W_{calc.}$ ($J\,m^{-2}$)
Benzylcellulose	2.0	2.0
Ethylcellulose	0.9	1.1
Cellulose nitrate	1.6	1.1
Cellulose acetate	2.3	0.8

These adhesion values are significantly higher than any estimates based on van der Waals or acid–base interactions and are subject to criticism because, despite the clear role of electrostatic forces in adhesion, the complete analysis of the adhesion values should at least consider such contributions as the bulk viscoelastic losses and the work required in bending and stretching of the polymer strips during peeling.

A direct experiment of the charge separation in adhesion has been carried out by Horn and Smith [66]. The authors measured the forces necessary to separate a glass lens from mica, using a cross-cylinder configuration. A pull-off force of 67 mN was recorded for the initial separation; however, a strong attractive force persisted over several micrometers. Using an electrometer, they recorded the charge accumulation after separation, which was 5–20 mC m^{-2}. The normalized force as a function of surface separation is shown in Fig. 12.

The integrated value of the force–distance curve gives a value of about 6.6–8.8 J m^{-2} for the total work necessary to separate the surfaces completely. These values are significantly larger than those required to separate two silica (0.08 J m^{-2}) or mica (0.11 J m^{-2}) surfaces. In another experiment, the authors measured the adhesion of glass to another aminosilane-treated glass and found a value of 3.3 J m^{-2} for the work of adhesion. The above values of the work of adhesion are significantly higher than the values expected from the van der Waals forces or acid–base interaction.

The effect of electrostatic double-layer forces has always been a puzzling issue in adhesion. If these values are indeed so high, why do they not show up explicitly in the fracture energies?

The relevant energies of crack initiation for these surfaces are much lower than the values obtained from the integration of the force–distance profile. For example, Horn and Smith reports that the initial pull-off force necessary to separate a cylindrical glass film of radius 20 mm from mica of the same

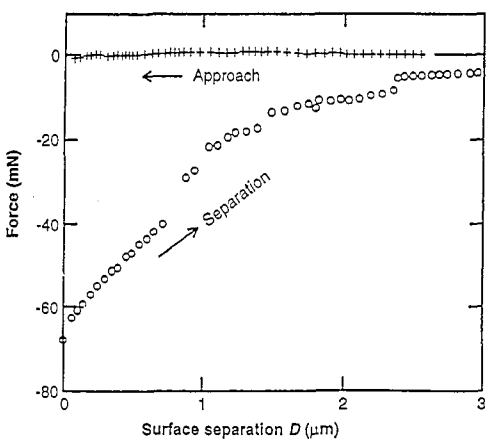

Fig. 12. Electrostatic force of interaction between silica and mica after the separation of interface. Reprinted with permission from R.G. Horn and D.T. Smith, *Science, 256* (1992) 362. © 1992 American Association for the Advancement of Science.

diameter is 67 mN. Using the above values of pull-off force, the work of adhesion calculated from the Johnson, Kendall and Roberts theory (see Section 3.1, Eq. (68)) is about 0.7 J m^{-2}. This value is a factor of 10 lower than that calculated from integrating the force–distance profile after separation. One may ask, is it the donor–acceptor interaction or the electrostatic interaction that controls adhesion? When an electron exchanges across an interface due to donor–acceptor interaction, Deryaguin's analysis shows that the electrical double layer actually prevents the flow of electrons from the donor to the acceptor surface, which reduces the total number of donor–acceptor bonds across an interface. According to Horn et al., one electronic charge is developed per 8–32 nm^2 after the separation of the two surfaces. The corresponding value is one electronic charge per 23 nm^2 for the interaction of silane-treated glass and untreated glass. The number of the ionizable surface groups is estimated to be about one per 0.5 nm^2—this means that only 2–7% of the ionizable groups are actually charged. These charged groups engage in electrostatic interactions whereas the uncharged surface groups simply engage in van der Waals and hydrogen-bonding interactions.

When the cross cylinders are separated, donor–acceptor bonds are broken and electrostatic charges separate onto the two surfaces, which gives rise to a long-range electrostatic attraction between the open surfaces of the crack. It is conceivable that the long-range electrostatic force present at the open surfaces of the crack acts to suppress the magnitude of the singularity of the tensile stress at the crack tip; the magnitude of the total force can be obtained by integrating it over a characteristic discharge gap, h. The puzzling fact however is that the integrated value of this force, expressed in terms of energy, is much higher than the values estimated by the donor–acceptor bonds and certainly higher than the value entering in the crack instability criterion. Although this discrepancy is not clearly understood, the view of this author is that the energy obtained by integrating the force–distance profile after the separation of the two surfaces has taken place tells only a partial story of fracture. While the phenomenon, described in Fig. 12, occurs within the open surfaces of the crack, one should bear in mind that the independent surfaces also become positively or negatively charged at the same time. Let us recall Dupré's equation of adhesion (Eq. (2)); if we add the contribution of the energy due to electrostatic attraction to Dupré's equation, the following equation is obtained:

$$W = \gamma_1 + \gamma_2 - \gamma_{12} + W_{el} \tag{56}$$

where γ_1, γ_2 and γ_{12} represent the interfacial tensions and W_{el} represents the extra electrostatic work necessary to overcome long-range attraction in the open gap. The relevant question is what values of the γ_1 and γ_2 one should use in Eq. (56); these are certainly not the values of uncharged surfaces, because they are modified due to the accumulation of surface charge. A charged surface has a lower surface tension than an uncharged surface, because the charges on the same surface repel each other. This negative component of the surface tension lowers the values of γ_1 and γ_2, which somewhat cancels the positive contribution of W_{el}. This fact was ignored in calculating the total attractive energy by integrating the force–distance profile. However, in a propagating crack, where a continuous flow of energy takes place from the interface to the fractured surfaces, the above factors are automatically accounted for in W. Thus, the effective value of W obtained from the fracture energies of a propagating crack should be used to correctly estimate the contribution of electrostatics to adhesion.

3. Direct measurement of the adhesion and surface energies from contact deformation

The methods of estimating the surface and interfacial energies of solids as discussed in the previous sections are indirect methods. Many of these methods are either cumbersome or flawed by the inexact theories of intermolecular interactions or misunderstanding of the mechanics of deformations near the

interfaces. The thermodynamic and statistical mechanical models of interfacial interactions have so far been tested only for liquid–liquid interfaces, because the surface and interfacial tensions can be measured directly for these systems. The only approximate method of estimating the surface free energies of low-energy solids is still based on contact angles. However, as Zisman [8] wrote in his classic review of 1964, the detailed description of γ_{sv} and γ_{sl} values obtained from contact angles remains incomplete unless an alternative method is found to estimate these quantities. Significant progress in estimating the surface thermodynamic quantities of solids have been made in recent years using the mechanics of contact deformations. The rest of this review will be dedicated to summarize these developments. The method to be described below is based on the mechanics of deformation of curved solid surfaces, which has its origin in Griffith's theory of fracture in brittle solids.

Inglis [67] and Griffith [68] realized that the great reduction of the strength in brittle solids is due to the small cracks and flaws present in the surface and bulk. These flaws act to magnify greatly the magnitude of the applied stress at the crack tip. Failure occurs when the stress at the crack tip exceeds the cohesive strength of the material. According to Inglis and Griffith, the stress at the tip of a long elliptical crack is given by the following formula:

$$\sigma = 2S(L/\rho)^{0.5} \tag{57}$$

where σ is the stress at the crack tip, S is the applied stress, L is the crack length and ρ is the radius of curvature of the crack tip. Failure occurs when σ exceeds the cohesive strength of the material. Eq. (57) is, however, of limited value because there is, in general, no simple way to measure the radius of curvature of the crack tip. A successful approach to materials failure was developed by Griffith using energy considerations. According to Griffith, the propagation of a crack in a solid results in the creation of two new surfaces with which are associated finite surface free energies. The energies of creating the fresh surfaces are derived from the elastic and potential energies from and around the crack tip. The criterion for failure, according to Griffith is given when the applied stress just exceeds the stress given by the following formula:

$$S = (4E\gamma/\pi L)^{0.5} \tag{58}$$

where E is the elastic modulus.

Many different crack problems have been solved using Eq. (58), and it is always found that the fracture stress depends on the square root of the surface free energy of the material.

Johnson, Kendall and Roberts (JKR) extended the Griffith criterion to describe the stability and instability of the contact of two spherical bodies as described in the next section.

3.1. Mechanics of deformation of curved solids

When a curved solid substrate comes into contact with another curved or flat substrate, the adhesion forces acting across the interface tend to deform the solids and thus increase their area of contact (Fig. 13). At equilibrium, the stored elastic energy due to deformation is balanced by the interfacial work of adhesion. The original theory of Johnson et al. [69] is a modification of the energy balancing method of predicting the contact deformation of curved solids developed by Hertz [70].

Hertz considered that the stresses produced at the interface between two curved solids under the action of an external load are compressive over the entire zone of contact, having zero values at the edges. This kind of stress distribution is valid when the two surfaces are non-interacting. Attractive interaction between solids introduces a tensile stress at and near the zone of contact, which is supported by the adhesive strength of the interface. According to Johnson et al., the stress at a position r from the center of contact is:

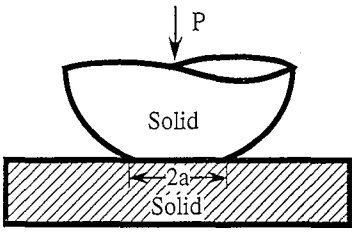

Fig. 13. Contact between a deformable semispherical solid with radius of curvature R and a deformable flat plate results in the formation of a circular region of radius a. The external medium might be air or a liquid. The deformation at the zone of contact results from the simultaneous effects of the surface and external forces (P). For clarity, the area of contact is exaggerated.

$$P(r) = (2E^*/\pi R)(a^2 - r^2)^{1/2} - C/(a^2 - r^2)^{1/2} \tag{59}$$

The first term of this equation is the Hertzian compressive stress. The second term is the Boussinesq [71] (tensile) stress distribution of a flat circular die resulting from adhesion. The value of the coefficient C is given by Eq. (65). Here E^* is given by

$$1/E^* = (1 - \nu_1^2)/E_1 + (1 - \nu_2^2)/E_2 \tag{60}$$

where ν is the Poisson's ratio, and E is the elastic modulus. R is defined as:

$$1/R = 1/R_1 + 1/R_2 \tag{61}$$

where R_1 and R_2 are the radii of curvatures of the two spheres.

According to Eq. 59, the tensile stress is infinity at the edge of contact, which predicts a sharp change of displacement at the contact edge. This scenario is similar to the original model of Griffith, which also assumed a blunt crack tip. Another model of contact deformation (DMT model) was derived by Deryaguin et al. [72]. In this model, the stress profile is considered to be Hertzian even when surface forces are present. The DMT model assumes that the crack surfaces open continuously similar to the scenario developed by Barenblatt. Even though the infinite stress at the edge of contact predicted by the JKR theory and the associated discontinuities in the displacement derivative are unphysical, stress must be tensile at the edge of contact in the presence of adhesive forces; its value is determined by the theoretical strength of the interface. Recently, Muller et al. [73] distinguished the behavior of the JKR and DMT contact by showing that the JKR approximation applies to strong adhesion and highly compliant materials, whereas the DMT approximation applies to low adhesion and non-compliant materials. Since, the majority of the contact deformation studies are carried out with soft elastic materials, the JKR approximation is more appropriate for our current discussion.

In the JKR theory, as reinterpreted by Greenwood and Johnson [74] and by Maugis et al. [75], the edge of contact of spherical bodies is considered as a crack tip with a stress intensity factor:

$$K_1 = (2\pi)^{0.5} \operatorname*{Lim}_{\xi \longrightarrow 0} (\sigma_z \sqrt{\xi}) \tag{62}$$

where ξ is the distance ahead of the crack tip and σ_z is the stress in the solid normal to the crack. The strain energy release rate is

$$G = K_1^2/2E^* \tag{63}$$

Equating $-P(r)$ to σ_z and $(a - r)$ to ξ respectively in Eq. (62), one obtains from Eqs. (59) and (62):

$$K_1 = C(\pi/a)^{1/2} \tag{64}$$

and from Eq. (63),

$$C = (2aE^*G/\pi)^{1/2} \tag{65}$$

Using the above value of C (Eq. (59)) can be integrated to obtain the total force P, which can be written in the following form:

$$G = (P - Ka^3/R)^2/6\pi Ka^3 \tag{66}$$

where $K = 4E^*/3$.

Using the Griffith criterion for stable crack growth or healing, G can be equated to the work of adhesion W. Therefore, Eq. (66) can be written in the familiar JKR form as follows:

$$a^3 = (R/K)\{P + 3\pi WR + [6\pi WRP + (3\pi WR)^2]^{0.5}\} \tag{67}$$

The crack is unstable when $\partial(G - W)/\partial a$ is greater than zero. Under fixed load P, this instability criterion gives rise to the value of the force, P, necessary to pull apart the spheres as:

$$P = 1.5\pi RW \tag{68}$$

The above equation applies when W is independent of a. There are cases when the above assumption is not valid; we will discuss this latter case in Section 3.16. In order to test Eq. (67), Johnson et al. pressed together two optically smooth rubber hemispheres and measured the area of contact as a function of applied loads. These measurements were carried out in air, under water, and under a dilute detergent solution. These data obeyed Eq. (67), from which the work of adhesion between solids could be determined. Johnson et al. estimated the values of γ_{sv} and γ_{sl} as 35 mJ m^{-2} and 3.4 mJ m^{-2} respectively. With these values, the predicted contact angle (64°) of water on rubber agreed well with the experimental value of 66°. This was the first experiment where all the variables of Young's equation were independently measured. There are other studies which provided further evidence for the validity of the JKR theory of contact mechanics [76–84]. Kendall conducted extensive studies in the adhesion of solids and developed appropriate energy-balancing methods to tackle the problems of the adhesion of parallel plates and peeling of elastomers from surfaces.

A problem, related to that worked out by Johnson et al., is the contact of two parallel cylinders which results in a rectangular deformation in the zone of contact. Using an energy-balance method, similar to that Johnson et al. used for spheres, an expression [85,86] relating the width of contact with the radii of the cylinders, external load and bulk modulii can be found as follows:

$$G = [(3\pi Ka^2l/8R) - P]^2/(6\pi Kal^2) \tag{69}$$

where G, K and R have the same meanings as used for spheres and where $G = W$ for crack growth or healing; a is the half width of deformation and l is the half length of the cylinder.

3.2. Comparison of surface free energies obtained from the deformations of spheres and cylinders

In order to verify either Eq. (66) or Eq. (69), it is necessary to conduct the measurements of deformations as a function of external loads, which allows determination of the elastic modulus and the work of adhesion simultaneously. Fig. 14 shows the schematics of an apparatus that allows convenient measurements of contact deformations as a function of load.

The apparatus shown in Fig. 14 was used to measure the deformations produced on contacting semispherical and semicylindrical lenses of elastomeric polydimethylsiloxane (PDMS) with flat PDMS sheets under both increasing and decreasing loads. These data were analyzed using the following forms of Eqs. (66) and (69):

Sphere on flat:

$$a^{3/2}/R = (1/K)(P/a^{3/2}) + (6\pi W/K)^{1/2} \tag{70}$$

Cylinder on flat:

$$(3\pi/8)a^{3/2}/R = (1/K)(P/la^{1/2}) + (6\pi W/K)^{1/2} \tag{71}$$

The intercepts and slopes of the lines obtained from the above equations are similar for spheres and cylinders, thus it provides a convenient comparison to be made of the data obtained for the two cases. Fig. 15 shows such plots. The average values of W obtained from the loading and the unloading experiments are about 40 mJ m^{-2} and 50 mJ m^{-2}, respectively. Since the surface free energy is half of the work of cohesion, the surface free energy of the polymer is estimated to be 20–25 mJ m^{-2},

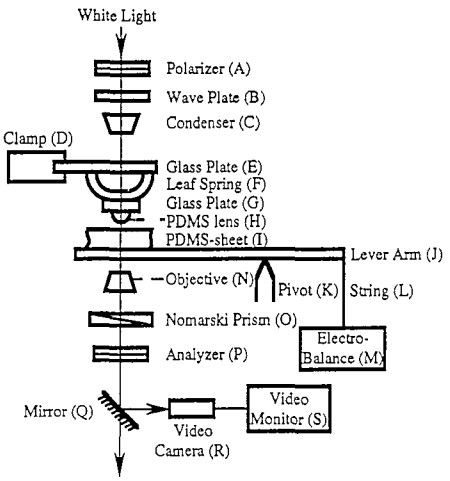

Fig. 14. Apparatus used to measure contact deformation. The flat sheet (I) is placed on one end of the lever arm (J) whose other end is connected to an electrobalance (M). The leaf spring (F) is a semicircular strip of transparent adhesive tape. The glass plate (G) is mounted with the leaf spring simply by pressing it against the adhesive layer. The elastomeric lens (H) adheres sufficiently with the glass plate without any adhesive. The lens (H) can be translated up, down or sideways. When the lens comes into contact with the flat sheet (I), any extra load is registered on the electrobalance. The corresponding contact deformation is recorded in the video system. Reprinted with permission from *Langmuir* (Ref. [82]). © 1991 American Chemistry Society.

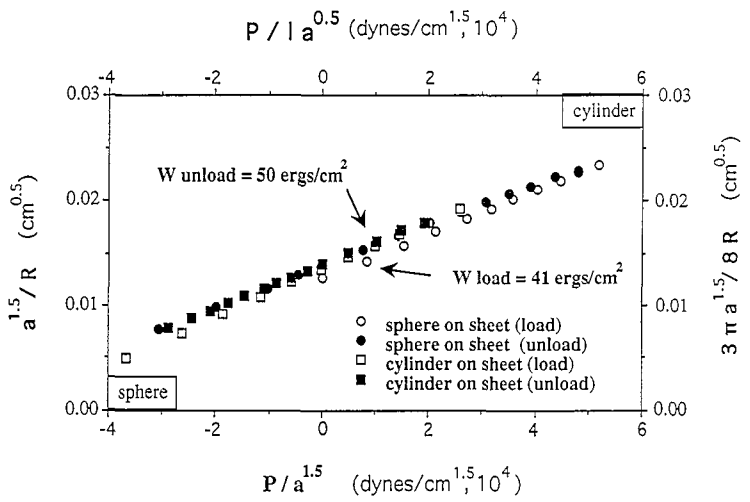

Fig. 15. Normalized plots of contact deformations obtained for spheres and cylinders of PDMS on PDMS flat sheets [86].

which is very close to the value of the surface tension of polydimethylsiloxane. For surfaces that exhibit negligible hysteresis, the surface free energy of PDMS is found to be about 22 ergs cm^{-2}. (Here, 1 erg $cm^{-2} = 1$ mJ m^{-2} and 100 dynes $cm^{1.5} = 1$ N $m^{-1.5}$. Note that the functions $P/a^{1.5}$ and $P/la^{0.5}$ have the same units of stress intensity factor, K_1 (see Eq. (62)).)

It is important to note that the surface energies of the polymer obtained from loading, in both cases, are not the same as those obtained from unloading—there exists a finite hysteresis in adhesion. This issue of adhesion hysteresis, implying the existence of metastable surface states, will be discussed in the later sections of this review, but before that we discuss how the JKR method can be used to carry out some interfacial studies of adhesion at solid–solid and solid–liquid interfaces.

3.3. Interaction under liquid media: verification of Young's equation

Verification of Young's equation of wettability requires that all the functions of Young's equation, γ_{lv}, γ_{sv}, γ_{sl} and θ, be measured independently. While γ_{lv} and θ can be directly measured, the surface and interfacial tensions at the solid–vapor or solid–liquid interfaces cannot, in general, be measured independently. There are, however, a few reported cases where all four functions of Young's equation could be measured independently. As mentioned earlier, Johnson et al. [69] were the first to measure the surface free energies of rubber at solid–air and solid–liquid interfaces which permitted them to verify directly Young's equation. Following Johnson et al., Pashley and Israelachvili [87] estimated the values of γ_{sv} (27 mJ m^{-2}) of an organic monolayer-coated mica and the γ_{sl} (11 mJ m^{-2}) at the interface between this surface and a dilute surfactant solution ($\gamma_{sl} = 40$ mJ m^{-2}) using the surface force apparatus. The experimental contact angle (64°) of the surfactant solution on the monolayer-coated mica agreed with the prediction (66°) based on Young's equation. Chaudhury and Whitesides [82] measured the contact deformations of a semispherical PDMS rubber on a flat PDMS sheet as a function of their surface properties in air and under liquids (mixtures of water and methanol), and estimated values of γ_{sv} and γ_{sl} using the JKR equation. The surface energy of PDMS (22 mJ m^{-2}) estimated from the contact deformations in air agreed well with the values estimated from contact angles (ca. 22 mJ m^{-2}). The force necessary to pull off the PDMS semispheres from the flat plates varied linearly with the radius of curvature of the lens (Fig. 16); the surface energy (22.6 mJ m^{-2}) calculated from the slope ($3\pi\gamma$ (Eq. (68))) of this line also agreed well with the JKR prediction. The measurements under water–methanol mixtures yielded values of γ_{sl}. Since all the values of Young's equation γ_{sv}, γ_{sl}, γ_{lv} and θ were independently measured, Young's equation could be verified. The authors plotted $\gamma_{lv} \cos\theta$ as a function of γ_{sl}, which yielded a straight line of slope very close to 1 (Fig. 17). The intercept in the $\gamma_{lv} \cos\theta$ axis yielded a value of γ_{sv} (21.1 mJ m^{-2}) which agreed well with the value (22 mJ m^{-2}) estimated from the JKR measurements made in air.

3.4. Adsorption of surfactant at the solid–liquid interface studied by the JKR method

Thermodynamic analysis of the adsorption of surfactant at the liquid–air interface can be performed using Gibbs adsorption equation:

$$\Gamma = -(C/RT)(\partial\gamma_{lv}/\partial C) \tag{72}$$

where Γ is the surface excess of the adsorbed surfactant, C is the concentration of the surfactant in the solution, and γ_{lv} is the surface tension of the solution.

By contrast, estimation of the surface excess quantities at the solid–liquid interface is not straightforward because its interfacial tension is not readily measurable. The relevant surface excess quantities, in this case, are obtained by indirect methods. There is one recent study where the JKR method has

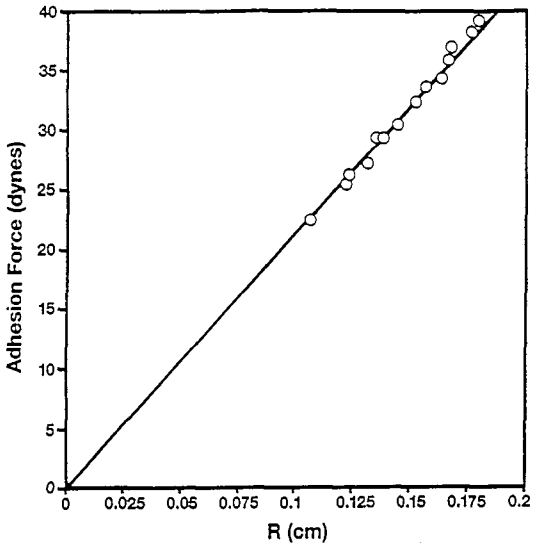

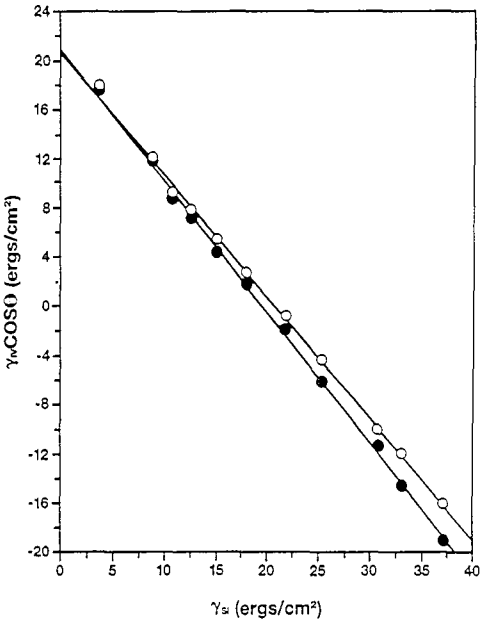

Fig. 16. Pull-off forces of semispherical PDMS from flat PDMS sheets.

Fig. 17. A plot of $\gamma_{lv}\cos\theta$ vs. γ_{sl} for PDMS semispheres interacting with PDMS sheets under the mixtures of water and methanol. The open and closed circles correspond to the data obtained from receding and advancing angles respectively. Figs. 16 and 17 are reprinted with permission from *Langmuir* (Ref. [82]). © 1991 American Chemical Society.

been used to measure the interfacial tension of the solid–liquid interface in the presence of surfactants. Haidara et al. recently used a self-assembled monolayer of decyltrichlorosilane supported on elastomeric polydimethylsiloxane as a model system to study the adsorption of a non-ionic surfactant $[H(CH_2)_{12}(OCH_2CH_2)_7OH]$ at the PDMS–water interface [88]. A semispherical lens of surface-modified PDMS was brought into contact with another flat sheet of the same material under water and then the surfactant was injected into the water. The contact area decreased with time and reached finally a stable value. The final area of contact varied systematically with the equilibrium concentration of the surfactant. Since these experiments were conducted at zero load, the interfacial tension was determined from the radius of contact according to the following equation:

$$\gamma_{sl} = Ka^3/12\pi R^2 \tag{73}$$

Since the values of the interfacial tensions were measured at different surfactant concentrations (C_b), a Gibbs plot of γ_{sl} versus $\ln C_b$ could be constructed. Fig. 18 shows such a plot where the Gibbs plot at the solid–liquid interface is compared with that at the liquid–vapor interface.

From the critical micellar concentrations (cmc), the molecular surface area of the adsorbed surfactant at the solid–liquid interface is found to be 53 Å^2, which is close to the area of 61 Å^2 at the liquid–vapor interface. The behavior of the adsorption pattern is, however, somewhat different at concentrations below the cmc. While the constancy of the slope of γ_{lv} versus $\ln C_b$ indicates a constant area per molecule at the air–liquid interface, the gradual change of slope of the curve for the solid–liquid interface indicates a continual change of the average area of the adsorbed surfactant, until the cmc is reached. This difference of behavior is inferred to be due to the differences in the free-energy changes in the self-assembly processes at the liquid–air and liquid–solid interfaces.

3.5. Adhesion energy and surface constitution

Chaudhury and coworkers [82–85] studied the adhesion energy of chemically modified PDMS surfaces as a function of their compositions. The chemical modification of the polymer was performed

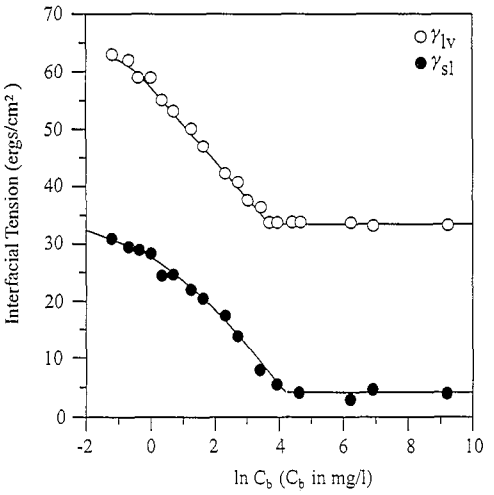

Fig. 18. Gibbs plot of surfactant adsorption at solid/liquid and air/liquid interfaces. (Here, 1 erg cm^{-2} = 1 mJ m^{-2}.) Reprinted with permission from *J. Phys. Chem.* (Ref. [88]). © 1995 American Chemical Society.

in two stages. In the first step, the polymer was oxidized in an oxygen plasma to generate a thin superficial oxide layer, which was further derivatized by reacting it with alkyltrichlorosilanes. The silanes adsorbed onto the polymer and formed self-assembled monolayer films. The chemical compositions of the monolayers were varied by altering the chemical functionalites of the tailgroup region. The monolayer films exhibited liquid-like phase states and thus both the adhesion and contact-angle hysteresis were low on these surfaces, making them suitable for systematic studies into the relationships between surface energy and surface constitution. These surfaces were subjected to contact angle and JKR tests, which yielded the necessary surface free energy values (see Tables 11a and 11b).

The surface free energies of these surfaces obtained from contact mechanics were comparable with the dispersion component of the surface free energies obtained from contact angles. If the surface free energy is decomposed into components arising from dispersion and polar forces, it overestimates the surface free energies [84].

Table 11a
Surface free energies (mJ m^{-2}) of DMS as a function of surface chemical compositions (geometric mean)

System	γ_{sv}^{JKR}	γ_{sv}^{d}	$\gamma_{sv}^{p}{}_{w}$	γ_{sv}^{tot}
$-CF_3$	16.0	15.0	0.8	15.8
$-CH_3$	20.8	20.6	.09	20.7
$-OCH_3$	26.8	30.8	6.4	37.2
$-CO_2CH_3$	33.0	36.0	6.4	42.4
-Br	36.8	37.9	1.7	39.6

Table 11b
Surface free energies (mJ m^{-2}) of PDMS as a function of surface chemical compositions (harmonic mean)

System	γ_{sv}^{JKR}	γ_{sv}^{d}	$\gamma_{sv}^{p}{}_{w}$	γ_{sv}^{tot}
CF_3	16.0	15.2	3.6	18.8
$-CH_3$	20.8	23.5	.4	23.9
$-OCH_3$	26.8	32.2	10.9	43.1
$-CO_2CH_3$	33.0	36.7	11.5	48.2
-Br	36.8	38.4	5.6	44.1

These observations are consistent with the acid–base concepts of interfacial interactions as discussed in Section 2.12. The polar surfaces examined here (ether and ester) are both bases and hence interact with its kind only via dispersion forces. These surfaces interact with water by forming hydrogen bonds; but, no hydrogen bonding is possible in the cohesive interactions of these surfaces. Hence the polar component of the surface tensions of these surfaces as obtained from the contact angle of water is fictitious, which has nothing in common with the forces that constitute the cohesive interactions of these surfaces.

There are several other details about these measurements that deserve some comment. From the direct adhesion measurement, the surface energy of the methyl ether surface was found to be about 26 mJ m^{-2}, which agrees reasonably well with the surface energy calculated from the contact angle of hexadecane. The surface energy obtained from the contact angle of di-iodomethane was significantly higher than the directly measured value. This observation is another example of the principle of independent surface action. The average orientation of the methyl ether group is perhaps such that its outermost functionality is predominantly methyl group. Thus when two methyl surfaces interact, the interaction is mainly influenced by the methyl functionality. This is also the case with the contact angle of hexadecane. However methylene iodide, which has a lower molar volume than hexadecane, penetrates more into the subsurface layer and recognizes the ether functionality. Bain and Whitesides [89] made similar remarks on the wettabilities of several liquids on ether functional surfaces. In these experiments, the self-assembled films of ether functional alkyl thiols were formed onto the surface of gold. The position of the ether group was varied systematically by placing it at progressively longer distances from the terminal methyl groups. It was found that the wettabilities of these surfaces were influenced by the positions of the ether groups. If the ether group is close to the surface, that surface is more hydrophillic than the surface where the ether group is buried deep in the monolayer.

Timmons and Zisman [90] observed a similar effect on contact-angle hysteresis. In their studies, the contact-angle hysteresis is negligible when the average diameter of the liquid molecule is larger than the average pore size of the monolayer films. For the fluorocarbon surface, the contact-angle hysteresis of di-iodomethane is about 23°, whereas the contact angle hysteresis of hexadecane was about 1°. The authors proposed that di-iodomethane penetrates into the fluorocarbon monolayer more than hexadecane giving rise to higher contact-angle hysteresis.

Another observation of Chaudhury and Whitesides [82,84] is that the surface energy of a fluorocarbon surface as estimated from the contact angle of a fluorocarbon liquid agrees well with the directly measured adhesion values. The hydrocarbon contact angle underestimates its surface energy. The situation is reversed for the surfaces composed of hydrocarbon group. Similar anomalies in the surface energy values of fluorocarbon and hydrocarbon surfaces have also been observed earlier by Fowkes [91]. Non-ideal interaction between hydrocarbon and fluorocarbon is also well known in their solubility properties. Good [16] and Fowkes [91] suggested that the origin of this anomaly is most likely due to the differences in the sizes of the molecules as well as their ionization potentials. This point is illustrated below with an example of the wetting behavior of a fluorocarbon liquid, perfluorodecalin on a CH_3-terminated self-assembled monolayer surface [84]. Perfluorodecalin forms a finite contact angle (38°) on a methyl surface even though its surface tension (18.2 mJ m^{-2}) is lower than that of the methyl surface (20 mJ m^{-2}), and, in all likelihood, they interact with each other via dispersion forces. Using the respective values of the surface tensions and contact angles, the Good–Girifalco interaction parameter between perfluorodecalin and the CH_3 surface is estimated as 0.85. Good calculated the interaction parameter between fluorocarbon and hydrocarbon using their ionization potentials as a surrogate for the natural frequency of electronic excitation and found its value to be:

$$\Phi_{FC-HC} = 2(I_{FC}I_{HC})^{0.5}/(I_{FC}+I_{HC}) = 0.91 \quad (74)$$

This calculated value is close to that which would be required to explain the discrepancy of the contact angle of perfluorodecalin on a methyl surface. Furthermore, the fluorocarbon groups are larger than the hydrocarbon groups, which may be another source of the non-ideal interaction of fluorocarbon and hydrocarbon.

3.6. Study of H-bonding interaction in model systems

Prediction of the H-bonding component of the surface energy and adhesion from contact angles is complicated by the fact that the models used to estimate the H-bonding interaction are approximate at best. There are, however, some special cases where an approximate estimation of surface free energy from contact angle may be possible. This is possible if the interfacial tension between the liquid and solid is close to zero or negligible in comparison with the surface free energy of the solid. If the interfacial tension γ_{sl} can be neglected, the surface free energy of the solid can be written approximately as:

$$\gamma_{sv} \approx \gamma_{lv} \cos \theta \tag{75}$$

Situations where the above equation applies are rare, but in some cases, where the nature of forces constituting the cohesive and adhesive forces are nearly the same, Eq. (75) should be approximately valid. For example, the contact angle of hexadecane on a methyl surface is typically 42–46°. From these values of contact angles and the surface tension of hexadecane (27.7 mJ m^{-2}), the surface free energy of a methyl surface is predicted to be (Eq. (75)) 19.2–20.5 mJ m^{-2}, which agrees well with the estimates based on the geometric mean combining rule of Good–Girifalco and Fowkes. The success of Eq. (75) in predicting the correct surface free energy of the methyl surface is due to the fact that the interfacial tension between hexadecane and the methyl surface is very much smaller than γ_s. Hydrogen-bonding surfaces, composed of high-density hydroxyl groups, may also satisfy the above criterion of nearly zero interfacial tension against water (and perhaps with other H-bonding liquids, such as glycerol, as well). In order to test this hypothesis, we have examined the surface free energy of a hydroxyl functional PDMS surface. This surface was prepared by reacting the oxidized PDMS with $Cl_3Si(CH_2)_9CH{=}CH_2$ to form an olefin functional monolayer film, which was further reacted with mercaptoethanol ($HS(CH_2)_2OH$) using a free-radical process [92].

$$PDMS_{ox}\text{–}O_3Si(CH_2)_9CH{=}CH_2 + HS(CH_2)_2OH \xrightarrow{\text{Benzophenone + UV light}} PDMS^{ox}\text{–}O_3Si(CH_2)_{11}S(CH_2)_2OH$$

The alcohol-functional monolayer surface was quite hydrophillic as evidenced by the contact angle of water ($\theta_a = 39$–$43°$, $\theta_r = 23$–$26°$), but exhibited significant hysteresis. There was some variability in the wettabilities of these surface and so was there some variability in their loading–unloading behavior in the JKR measurements [93]. The adhesion energy obtained from the loading experiments varied from 92 to 112 mJ m^{-2} from sample to sample, whereas the adhesion energies obtained from the unloading experiments varied from 162 to 228 mJ m^{-2}. This variability was partly due to the adsorption of moisture on these surfaces. The other significant source of this variability is due to the fact that the thiol addition reaction to a double bond is not quantitative and thus is a source of irreproducibility of the surface properties.

Ignoring the interfacial tension, the surface free energies of this surface prepared at five different times are calculated using the advancing contact angle values of water, glycerol and formamide. The results are tabulated in Table 12. In the last column of this table are also included the surface energy values obtained from the load-deformation experiments.

Table 12
Surface free energies (in mJ m^{-2}) of PDMS–OH obtained from contact angles (Eq. (75)) and JKR methods

Sample no.	Water	Glycerol	Formamide	JKR
1	54.9	53.9	53.4	56.8
2	56.6	54.3	55.3	52.2
3	53.2	52.4	53.8	45.6
4	53.7	52.1	–	47.0
5	55.7	55.9	–	49.3

Note that the surface energies of a given sample, as determined from water, glycerol and formamide, are very similar, indicating that the condition of negligible interfacial tension is nearly satisfied in these cases. The surface free energy values obtained from the JKR method are also similar to the values obtained from contact angles.

The surface free energies, γ_{sl}, obtained from the decompressive loads varied significantly from experiment to experiment and therefore they were not suitable for the analysis of surface energetics. However, these values of surface free energies are significantly higher than that would be expected from the receding contact angles of water, glycerol and formamide (the receding contact angles of glycerol and formamide are nearly zero). At this point it should be mentioned that a discrepancy in the surface energy values estimated from contact angle and contact deformations is to be expected on hysteretic surfaces because of the following reason. For the liquid–vapor interface, the contact line can escape the metastable states partially because the thermal ripplons provide the necessary energy to do so [94], whereas for the solid–solid contact ripplons are more suppressed and the hysteretic effects should be more pronounced.

3.7. Interaction between an amine and a carboxylic acid surface

In another effort to study the acid–base interaction across an interface, the olefin-terminated alkylsilane monolayers on PDMS were reacted with $HSCH_2CH_2NH_2$ and $HSCH_2CH_2CO_2H$ to form $PDMS^{ox}$–$O_3Si(CH_2)_{11}S(CH_2)_2NH_2$ and $PDMS^{ox}$–$O_3Si(CH_2)_{11}S(CH_2)_2CO_2H$ respectively. If an amine surface is contacted with a carboxylic acid surface, interfacial proton transfer is expected to occur according to the following scheme:

$$-CO_2H + H_2N- \longrightarrow -CO_2^{-}H_3^{+}N-$$

However, when the amine surface (amine surfaces become contaminated in air by complexing with carbon dioxide; therefore the surfaces should be used quickly after they are formed) contacted the carboxylic acid surface, the adhesion energy obtained from the compressive load-deformation experiments was found to be about 120 mJ m^{-2}, which is only slightly higher than the value (≈ 100 mJ m^{-2}) obtained from contacting the amine surface with an alcohol surface ($PDMS^{ox}$–$O_3Si(CH_2)_{11}S(CH_2)_2OH$). Thus the experiment did not prove unequivocally whether the charge-transfer complex is formed across the amine and carboxylic acid surfaces. Since the magnitude of the adhesion energy is in the range of normal H-bonding interaction, it can be stipulated that the proton transfer is rather weak. This result is expected if, due to lateral H-bonding, both the amine and carboxylic acid groups are stabilized preventing them from engaging in significant charge-transfer complexation.

The other possibility is that the surfaces are covered with adsorbed water which screens donor–acceptor interaction. Recent AFM measurements under good vacuum provide evidence for strong acid–base interaction between CO_2H and NH_2 surfaces [94a].

3.8. Interaction between hydrogen bonding and van der Waals surfaces

According to the theory of surface tension components, the adhesion energy between a non-polar surface and a hydrogen-bonding surface is due to dispersion forces, and its magnitude should be much lower than the adhesive energies of two hydrogen-bonding surfaces (100 mJ m^{-2}). In order to test the theory of surface tension components, we have performed load-deformation experiments using surfaces modified with fluorocarbon and hydrocarbon monolayers. The adhesion energy between PDMS^{ox}–$O_3Si(CH_2)_{10}CH_3$ and PDMS^{ox}–$O_3Si(CH_2)_{11}S(CH_2)_2OH$ obtained from the compressive–decompressive loads are 41.5 ± 4.47 mJ m^{-2} and 52.5 ± 1.6 mJ m^{-2} respectively. Similarly, the adhesion energies between a fluorocarbon surface PDMS^{ox}–$O_3Si(CH_2)_2(CF_2)_7CF_3$ and PDMS^{ox}–$O_3Si(CH_2)_{11}S(CH_2)_2OH$ are 31.3 ± 5.8 mJ m^{-2} and 40.1 ± 3.6 mJ m^{-2} respectively. These values are similar to the adhesion energies of dispersive solids providing proof that the H-bonding surfaces interact with van der Waals surfaces by dispersion forces alone.

3.9. Direct measurement of the adhesion energies of polymer films

Tirrell [95] and his collaborators developed a novel method of studying adhesion energies of stretched polymer films using contact deformation. On one side of the film, silver was deposited and the silvered side was mounted against a cylindrical glass lens. When two such polymer-coated glass lenses were brought into contact in a cross-cylinder configuration, a circular contact area developed, which was viewed using interference optics. The adhesive energies between the polymers were determined by measuring the pull-off energies and using Eq. (68).

For polyethylene, the surface free energy obtained from the direct measurement was about 33.3 mJ m^{-2}, which agrees well with the surface free energies (25–35 mJ m^{-2}) obtained from contact angles and melt data. This value is also close to that of a disordered surface of hexadecylalkylsiloxane grafted onto oxidized PDMS, which exposes primarily its methylene functionalities. The surface free energy of a polyethyleneterephthalate (PET) film was about 61 mJ m^{-2}, which is significantly higher than the values (ca. 43 mJ m^{-2}) obtained from the contact angles. Although the estimation of the surface free energy of solids using any of the existing theories of contact angles lead to some uncertainty, it should be pointed out that the surface free energies of these surfaces obtained from the onset of the instability of the contact, is subjected to hysteretic effects, that may lead to another degree of uncertainty. The interfacial tension between PET and PE measured by these authors was about 17.1 mJ m^{-2}. If one assumes that the van der Waals forces are compensated at the interface, the above value is then primarily due to the cohesive component of the surface tension of PET arising from specific interactions. This means that the dispersive component of the surface tension of PET is about 44 $(=61-17)$ mJ m^{-2}. This value is nearly same as that obtained from the contact angles. The dispersive component of the interfacial tension of the PE–PET interface is about 0.8 mJ m^{-2} $(=33+44-2(44\times33)^{0.5})$, which is much smaller than the total interfacial tension (17.1 mJ m^{-2}).

3.10. Non-equilibrium work of adhesion

For the cases of rubber spheres pressed against glass, Dutrowski [81] and, independently, Kendall [76] observed that the contact deformations obtained from loading and unloading do not always follow reversible paths—there exists a finite hysteresis. Dutrowski viewed that the initial deformation as a function of increasing load follows the Hertzian mechanics. The whole area is under a compressive stress. The second stage of deformation as a function of decreasing load was viewed to be due to adhesion, where Boussinesq's tensile stress distribution of a flat circular die is superimposed with the

Hertzian compressive stress at the center. According to the JKR theory, however, tensile stress always develops at the outer edge of adhesive contact, and the stress distribution should be invariant with respect to either increasing or decreasing the loads. Therefore other explanations of adhesion hysteresis should be sought.

Kendall's studies included examination of the rate and temperature on adhesion. The loading experiment was performed after the sphere made contact with the glass plate. The unloading experiment was performed after compressing the sphere to a certain load and then reducing the load to zero. When the sphere came into contact with glass, the contact diameter initially increased with time and then reached a nearly constant value. But this change of diameter with time was less pronounced than that seen in the unloading case (Fig. 19). This time-dependent evolution of contact area clearly indicates that they are due to viscoelastic processes operating at or near the crack tip. Nevertheless, the finite differences in the contact diameters at zero load and zero crack velocity is indicative of true interfacial adhesive hysteresis. Kendall compared this adhesion hysteresis with the hysteresis of contact angles. Horn et al. [80] used the surface force apparatus to study the contact deformation of solids. A conventional surface force apparatus (SFA) consists of two thin films of molecularly smooth mica surfaces glued onto curved glass discs. When two such curved mica surfaces are brought into contact with their axes perpendicular to each other, a circular deformation is developed in the zone of contact, which is amenable to the same JKR treatment as it applies to a sphere on a flat. Horn et al. carried out the load-deformation experiments using the SFA and found that the data did not behave according to the JKR prediction. The pull-out force obtained from the decompressive load-deformation branch deviated from the JKR prediction but agreed with the DMT prediction.

The authors concluded that while the general nature of the JKR theory predicting the mechanics of contact deformation is essentially correct, DMT theory should be used to predict the pull-off force. Horn et al. proposed that the glue holding the mica and glass together undergoes a plastic deformation as a result of large tensile stresses near the contact edge, which was the origin of contact-deformation hysteresis in the SFA measurements.

The studies carried out by Chaudhury and collaborators [82–85] indicate that the adhesion hysteresis arises from the surface effects of the types that are encountered in contact-angle hysteresis, thus providing direct evidence supporting Kendall's view that the adhesive hysteresis is linked to the metastable processes occurring at the surface and not in the bulk. The work of adhesion is expected to be rate dependent for systems where the separation occurs irreversibly, i.e. for systems where the initial and final states are separated by energy barriers (Fig. 20). For reversible process of adhesion and separation, where the potential energy of interaction can be described by a Lennard–Jones potential, W should be independent of the rate of separation. In this case, the concept of equilibrium work of adhesion applies. The non-equilibrium nature of the work of adhesion was recognized by Tomlinson [96] as well as by Kendall [97]. Kendall proposed that the rate processes occurring at the interface of two solids make the work of adhesion intrinsically non-equilibrium. Kendall imagined a scenario where the crack tip is under thermal fluctuation, undergoing a stick-slip forward and backward movement.

The applied stress favors the crack to propagate in a preferred direction. This scenario is related to that developed by Blake and Haynes [98] explaining the movement of the three-phase contact line of the liquid–solid–vapor interface, or that used by Schallamach [99] as well as Bartenev [100] in developing the theory of rubber friction. The molecular theory of rubber friction considers adhesion to be a thermally activated molecular stick–slip process. Unlike a hard material, rubber molecules are in a constant state of thermal agitation. When a rubber slides across a hard surface, the rubber molecules adhere to the base and an instant later these bonds are broken by the sliding action. Other bonds are formed at a microscopic distance ahead of the previous position, so that the elastomer molecules jump

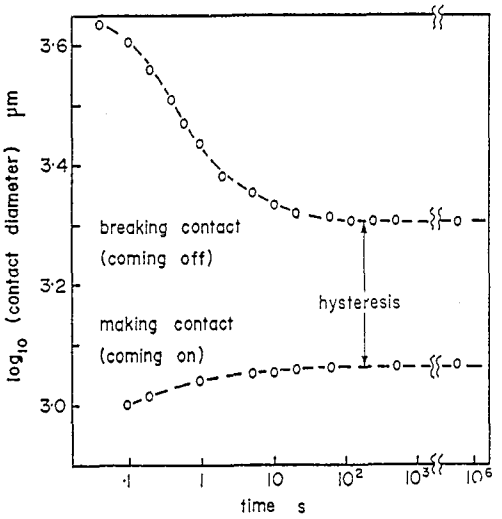

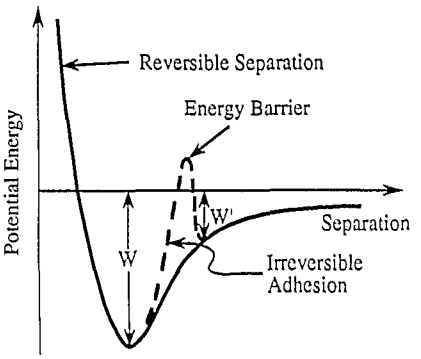

Fig. 19. Adhesion hysteresis of the rubber–glass interface. Reprinted with permission from *J. Adhesion* (Ref. [76]). © 1975 Gordon and Breach Publishers.

Fig. 20. Reversible and irreversible adhesion results from the absence or presence of an energy barrier. Adapted from Ref. [97].

a distance λ into their new position. The time from the breaking of a bond to the formation of a new bond is called the "unsettled life", τ, which can be expressed in terms of an Arrhenius equation $\tau = \tau_0 \exp(E_a/kT)$, where E_a is the activation energy or energy barrier and T is the absolute temperature. If a constant force (F) is applied at the interface, the effective activation energy is modified by a factor proportional to the force and one obtains $E_a^* = E_a - cF$. The sliding speed may be written as follows $V = \lambda/\tau$. Considering τ to follow an Arrhenius law, the speed of sliding can be written as:

$$V = V_0 \exp[-(E_a - F)/kT] \tag{76}$$

Eq. 76 explained the rubber friction results of Schallamach quite well.

The same basic idea was utilized by Blake and Hanes [98] to describe the motion of the wetting line of a liquid on a solid surface. Their results may be expressed in terms of an interfacial viscous force F_v where,

$$F_v/b = A \sinh^{-1} BV \tag{77}$$

where b is the length of the three-phase boundary, A and B are temperature-dependent constants and V is the velocity of the boundary.

Kendall [97] assumed that the separation of a rubber from a flat surface involves a shear component and used the Blake–Hanes method of a thermally activated molecular stick–slip process to derive an expression for the peel strength of rubber as:

$$F/b = W + A \sinh^{-1} BV \tag{78}$$

This equation was used by Kendall to explain the peel adhesion results.

The theory of the activated process led to the modern thermo-fluctuation theory of fracture. Valishin and Kartashov [101] reviewed this subject, according to which there are two states to fracture process. In the first stage, the rupture of an interfacial bond proceeds via fluctuation of the thermal motion activated by the enhanced stress of the crack tip. The elastic energy released at the slow stage is not sufficient to rupture the bonds. Rupture occurs when a thermal fluctuation begins with sufficient

energy to effect the elementary act of fracture. When crack accelerates gradually, the crack grows to a critical size; it enters a stationary stage and fracture proceeds at a constant velocity.

It is worth considering the possible mechanisms that give rise to the energy barriers to fracture of low-energy surfaces. One obvious case is the formation of hydrogen bonds or other types of specific acid–base bond at the interface involving charge transfer. Interdigitation is a second cause. A third cause is the contortion of a contact line due to surface imperfections. Consider the case of a liquid drop on a solid substrate that has some imperfections. The segment of the contact line which is in contact with the higher energy patches may be considered pinned in comparison with the segments that are in contact with the low-energy patches. The contortion of the contact line for a given drop volume can exhibit multiple energy states separated by energy barriers. This scenario of contact-angle hysteresis, relating metastable surface states, was proposed by Good [102], according to whom, depending upon the previous history of the system, the contact line corresponding to a specific drop volume may be locked into a specific state, and may not escape in the time frame of any experiment. Most later discussions on the contact-angle hysteresis on non-ideal surfaces focus on the calculations on these metastable states. Johnson and Dettre [103] computed these metastable states for liquid drops on ideally roughened surfaces which are chemically homogeneous. Neumann and Good [104] carried out such computations for ideally patterned heterogeneous surfaces. These computations showed that the contact angle on a non-ideal surface is not single valued but has multitude of non-equilibrium values, each state being separated from the next by a finite energy barrier. It has been conjectured that if the energy barrier separating the metastable states is very much larger than the characteristic vibration energy of the drop, the contact line may actually be frozen in a particular state with no noticeable relaxation within any observable experimental time frame. If the energy barriers separating the metastable states are comparable with the vibration energy of the drop, a real-time relaxation of the contact angle may occur. Thus, in a given experiment, static or dynamic hysteresis may be observed depending upon the magnitude of the energy barriers separating the metastable states. No systematic study correlating hysteresis and metastable states has, however, been reported. See Ref. [105] for a discussion of the more recent advances in the theory of contact angle hysteresis. Smith and Lindberg [106] found a decrease of hysteresis of contact angle when the liquid drop was coupled to a acoustic vibration of a loud speaker. Garoff [107] found that the contact angle responds to the vibration but exhibits a very slow relaxation indicating the presence of deep metastable states. Chaudhury [108] agitated liquid drops on a low-hysteresis Teflon–FEP surface by generating capillary waves on the liquid surface, where the angles reached a global value starting either from the advancing or receding mode.

The idea, which was central to Good's explanation of contact-angle hysteresis was now revisited in the context of the non-equilibrium dynamics of polymer chains on surfaces. Chakraborty et al. [109] carried out numerical simulations of the dynamics of polymer chains on surfaces and found the existence of multiple metastable states. When the energy barrier separating the metastable states is much larger than the thermal energy, the polymer chains are locked into a non-equilibrium configuration.

Good's view of contact-angle hysteresis may also be relevant to the adhesion hysteresis of solid surfaces. Existence of both the static and kinetic adhesion hysteresis can be found in many of the JKR adhesion studies, which will be discussed in later sections.

3.11. Adhesion hysteresis and surface constitution

Chaudhury and coworkers [82,83] modified the surface of PDMS using self-assembled monolayers and studied adhesion as a function of surface composition. The adhesion energies obtained from the compressive and decompressive loads depend significantly on the surface chemical composition.

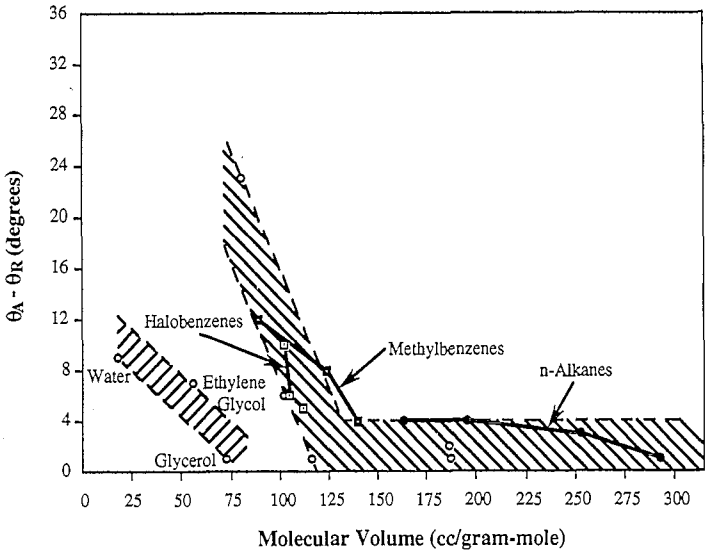

Fig. 21. Contact-angle hysteresis of liquids on fluorocarbon monolayers as a function of the size of probe liquids. Adapted with permission from Academic Press (Ref. [90]).

Large hysteresis is found on surfaces that contain the fluoroalkyl groups; hysteresis is negligible on the hydrocarbon surfaces. The higher adhesion hysteresis of the fluorocarbon monolayer is consistent with the higher contact-angle hysteresis observed for these systems, which is in conformity with the earlier findings of Timmons and Zisman [90]. Timmons and Zisman found the hysteresis of contact angles of liquids on a fluorocarbon surface is significantly higher than that of the hydrocarbon surface, which were thought to arise due to the penetration of the liquid molecules into the porous fluorocarbon films. This hypothesis of molecular penetration is supported by the fact that contact angle hysteresis increases with the decrease in the size of probe molecules (Fig. 21).

Based on the above scenario, the higher adhesion hysteresis of the fluorocarbon monolayers observed in the JKR measurements may be linked to the interdigitation of the fluoroalkyl chains. In terms of adhesion kinetics, the fluorocarbon–hydrocarbon interface exhibits characteristics that are remarkably different from those observed for two fluorocarbon or two hydrocarbon surfaces. For this unlike pair, the contact area during unloading exhibits a pronounced dependence on time, indicating that the hydrocarbon chains, which interdigitate the fluorocarbon chains, are not in a frozen state but relax slowly with time. However, this is not the case for two fluorocarbon surfaces where the chains are locked into deep metastable states, which do not relax within the experimental time frame.

The adhesion hysteresis for both the hydrocarbon and fluorocarbon monolayers can be decreased by making the monolayers more disordered or liquid-like. For example, a disordered fluorocarbon monolayer deposited on $PDMS^{ox}$ exhibits a lower adhesion hysteresis than a fully covered monolayer [84,85]. It is proposed that the disordered monolayer is free of defects of the types that freeze the motion of contact line. The studies of adhesion versus surface constitution, which are discussed in Section 3.5, were based on monolayer films that were in liquid-like states and thus were free of hysteresis. The subject of the dependence of hysteresis on the phase states of the monolayer films are discussed in the subsequent sections.

3.12. Adhesion hysteresis and interchain digitation

Briscoe et al. [110] speculated that the interdigitation of hydrocarbon chains is possible when they are in close contact. These authors transferred stearic acid monolayers on mica by the Langmuir–

Blodgett technique and studied their friction using a cross-cylinder geometry. The stearic acid was transferred either as a pure acid or a pure soap. When two such monolayers were sheared against each other, the acidic monolayer showed a smooth friction force at low and high velocities. The saponified monolayer exhibited a stick–slip behavior. Since the shear plane is where only the hydrocarbon groups (i.e. the terminal methyl groups) are exposed, the acidic or saponified anchoring sites should have no effect in the friction process. The authors thus speculated that the difference in the friction is due to the differences in the structure of the two films and that the stick–slip behavior results from a partial interdigitation of the hydrocarbon chains.

Israelachvilî et al. [111] recently carried out detailed experiments of adhesion hysteresis of Langmuir–Blodgett (LB) monolayers transferred onto mica. In these studies, the phase states of the monolayers on mica were controlled by transferring them as LB films at different surface pressures. Neither the crystalline monolayer nor the monolayer in the liquid state exhibits any noticeable adhesion hysteresis, whereas the monolayers in the glassy amorphous state exhibit significant adhesion hysteresis. In order to explain these results, the authors suggested that alkyl chains in the crystalline state do not interdigitate thus exhibiting no adhesion hysteresis. Even though the alkyl chains interdigitate while they are in the liquid-like state, the chains can relax easily without giving rise to hysteresis. However, when the molecules interdigitate in the glassy amorphous state, their motions are frozen, which gives rise to a pronounced adhesion hysteresis. Chaudhury and Owen [83] also found that the adhesion hysteresis depends on the phase state of the monolayer films (Fig. 22). The monolayer films of hexadecyltrichlorosilanes were produced by adsorbing them onto oxidized PDMS from the vapor phase. The adsorbed amount was controlled by the time of adsorption and the concentration of the silane in the gas phase. The phase states of the monolayers were characterized by infrared spectroscopy.

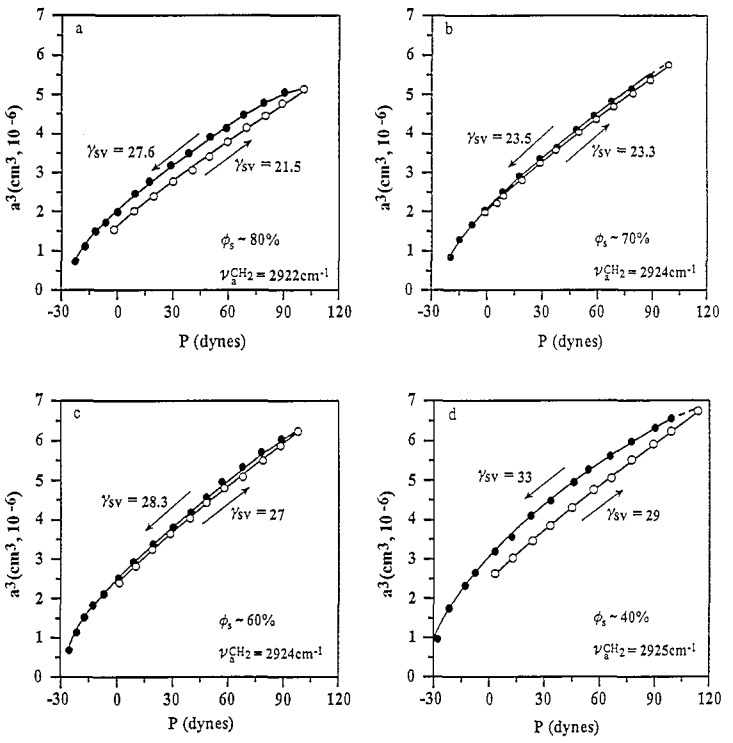

Fig. 22. Adhesion hysteresis of alkylsiloxane monolayers supported on PDMS. All surface free energies are expressed in ergs cm^{-2} (or mJ m^{-2}). Reprinted with permission from *J. Phys. Chem.* (Ref. [83]). © 1993 American Chemical Society.

Significant hysteresis is found for monolayers that are in the crystalline state. Hysteresis becomes negligible for monolayers that are in a liquid-like state, which is consistent with the finding of Israelachvili et al. Hysteresis increases again at the other end with sub-monolayer coverage. The hysteresis of surfaces covered with a very small amount of alkylsiloxane chains ($\Phi = 40\%$) is most likely due to the recognition of the bare silica patches by the two opposing surfaces. When such a surface is reacted with shorter chain alkanes (C_8), the bare sites are occupied and the hysteresis disappears almost completely (Fig. 23).

These results clearly indicate that the hysteresis of contact deformation is closely related to the surface chemical properties of the surfaces. In order to characterize the wettabilities of the surfaces, two liquids were chosen: an unstructured liquid, hexadecane and a structured liquid, water. Hexadecane exhibited negligible hysteresis with all the surfaces, but the hysteresis of the contact angle of water depends on the monolayer phase states significantly (Table 13).

It was proposed that the hysteresis of adhesion at the solid–solid interface is related to the same kinds of factors which give rise to contact-angle hysteresis, namely the pinning of a contact line due to surface structural defects. Hexadecane, being a non-polar unstructured liquid, is rather insensitive to surface structural defects.

The defects in the crystalline monolayer might arise due to kinetic co-existence of amorphous and crystalline domains, which results from the artifacts of self-assembly. The final stages of self-assembly are highly kinetically constrained, which may lead to the formation of kinetically co-existing amorphous and crystalline domains. These domains may differ in surface energy leading to the hysteresis in adhesion.

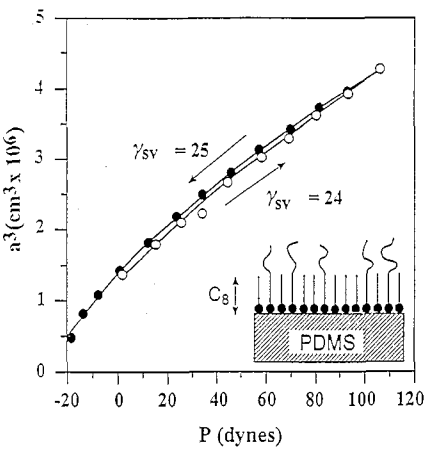

Fig. 23. Adhesion hysteresis with a mixed monolayer. Surface free energies are in ergs cm^{-2} (or mJ m^{-2}).

Table 13
Surface energies and phase state of monolayer. Reprinted with permission from *J. Phys. Chem.* (Ref. [83]). © 1993 American Chemical Society

Surface coverage	Phase state	γ_{sv}^a (mJ m^{-2})	γ_{sv}^r (mJ m^{-2})	$\Delta\gamma_{sv}$ (mJ m^{-2})	ΔW_{H_2O} (mJ m^{-2})	ΔW_{HD} (mJ m^{-2})
100	Solid	16.2	24.8	8.6	20	0
80	Sol/liq	21.5	27.6	6.1	18	0
70	liq.	23.3	23.5	0.2	8	0
60	liq.	27	28.3	1.3	12	0
40	liq.	28.5	32.8	4.3	20	0

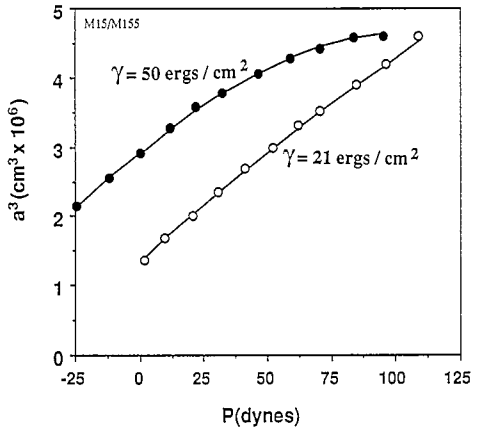

Fig. 24. Adhesion hysteresis of a methyl ether functional monolayer. (Here 1 erg $cm^{-2} = 1$ mJ m^{-2}.)

Another model of adhesion hysteresis is as follows. Even though the overall molecule is in the crystalline state, the tailgroup region may be in a glassy amorphous state. When two surfaces are brought into contact, partial interdigitation may occur in the tailgroup region. Since the relaxation of molecules in a glassy state, as speculated by Israelachvili et al., is normally slow, no noticeable relaxation may be observed within any normal experimental time frame, giving rise to adhesion hysteresis. It has not been possible to discern whether the hysteresis is due to contact line pinning or to interdigitation. It [112] has been observed that the structure of the tailgroup of a monolayer has a profound influence on adhesion hysteresis. For example, an ether functional monolayer exhibits a significantly higher hysteresis (Fig. 24) than a methyl functional monolayer, even though the main chain is in a pseudo-crystalline state. This observation suggests that the molecular processes occurring within the first few-angstrom region of the monolayer surface is quite sufficient to give rise to significant adhesion hysteresis.

Recently, Reiter et al. [113] investigated the instabilities of adhesion in self-assembled monolayers of octadecylsiloxane on mica under shear. At zero shear, the adhesion energy is about 22 mJ m^{-2} from the pull-off force measurements; but its value decreases by about 40% beyond a critical shear. The authors speculated that the endgroups of the molecules forming the surface of the monolayer are situated in some kind of potential well formed by the surrounding molecule of the opposing monolayer. At this equilibrium situation, the two monolayers are in closest contact. Up to a critical shear stress, the endgroups do not leave these potential wells; but beyond the critical shear stress, the endgroups are pulled out of their potential wells and slide across each other for some distance. This means that the surfaces are not in closest contact and the adhesion energy decreases. The experiments of the type described by Reiter et al. may be extended to other surfaces where the endgroups are other than methyl and thus the relationship between adhesion and interlocking of headgroup functionalities could be explored.

3.13. Stress-induced H-bonding at interfaces

Recent studies of Silberzan et al. [114] in Kramer's laboratory showed that polydimethylsiloxane, if its sol fraction is extracted, exhibits a pronounced adhesion hysteresis. While the compressive branch of the load-deformation cycle follows the JKR theory perfectly, the decompressive branch deviates significantly from the JKR prediction. In order to force the unloading data to fit the JKR theory, an unusually high elastic modulus was needed. It was proposed that the deviation of the observed behavior from the JKR prediction is possibly due to a stress-induced hydrogen-bond formation at the interface.

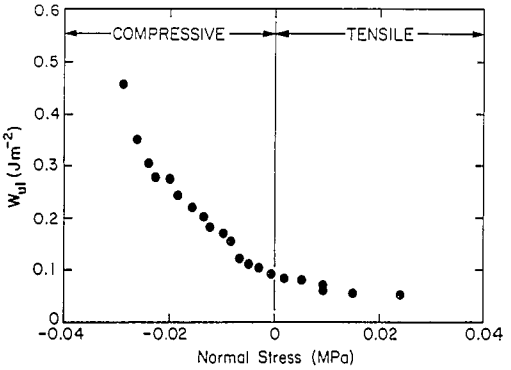

Fig. 25. Effect of stress on interfacial adhesion. Reprinted with permission from *Langmuir* (Ref. [114]). © 1994 American Chemical Society.

The PDMS used in these studies had excess cross-linking agents (SiH) which could be converted to silanol groups upon oxidation. It was thought that these silanol groups form hydrogen bonds across the interface; the rate of bond formation being a function of the normal stresses in analogy to the pressure-induced chemical reaction in bulk liquids. Instead of forcing the data to fit JKR theory, the authors analyzed the unloading data using the value of K obtained from the loading experiments. When the work of adhesion obtained this way was plotted against the normal stress (Eq. (59)), it was observed that the work of adhesion is low and does not vary too much in the region where the stresses are tensile (i.e. near the edges), but increases significantly towards the center where the stress becomes progressively more compressive (Fig. 25).

What gives rise to this pressure-induced hydrogen bonding at the interface? One hypothesis is that the normal stress promotes the collision of the H-bonding groups and thus drives the equilibrium of the interface towards the H-bonded state. If indeed the above scenario is valid, the rate of stress-induced H-bond formation should be related to the flexibility of the interface. In order to test the possible connection between this phenomenon and interfacial flexibility, let us examine the following two systems: the first system is comprised of a plasma-oxidized layer of PDMS interacting with mica and the second system is comprised of two PDMS, whose surfaces have been modified with CH_2OH functional alkyl siloxane monolayers [115].

A plasma-oxidized PDMS surface develops a superficial oxide layer, which is more rigid than the unmodified PDMS. Such an oxidized PDMS lens was brought into contact with mica and the contact deformations were measured as a function of compressive and decompressive loads. The elastic moduli (K) obtained from the compressive and decompressive loads are found to be 10^6 N m^{-2} and 1.1×10^6 N m^{-2} respectively, i.e. they are indistinguishable. The work of adhesion obtained from the loading and unloading experiments are 162(+6) mJ m^{-2} and 233(+39) mJ m^{-2} respectively. Thus, even though the surfaces exhibit significant hysteresis in adhesion, both the loading and unloading data follow the JKR theory exactly. For the $-CH_2OH$-modified PDMS surfaces, the value of K obtained from the loading data ranges from (4.4 to 4.8) $\times 10^5$ N m^{-2}, whereas the value of K obtained from the unloading data is in the range (5.3–6) $\times 10^5$ N m^{-2}.

Although the deviation of the apparent value of K obtained from force fitting the data to the JKR theory is an indication of its departure from the true JKR behavior, a better way to analyze these data, as was done by Silberzan et al., is to consider K as fixed, and estimate the value of W either as a function of the position from the edge of contact or the interfacial normal stress.

In Fig. 26 the values of W_{un} obtained for the above two systems are plotted against the normal stress. The work of adhesion for the PDMS^{ox}–mica interface shows no significant dependence on normal stress. The work of adhesion for the PDMS–OH/PDMS–OH interface, is weakly dependent

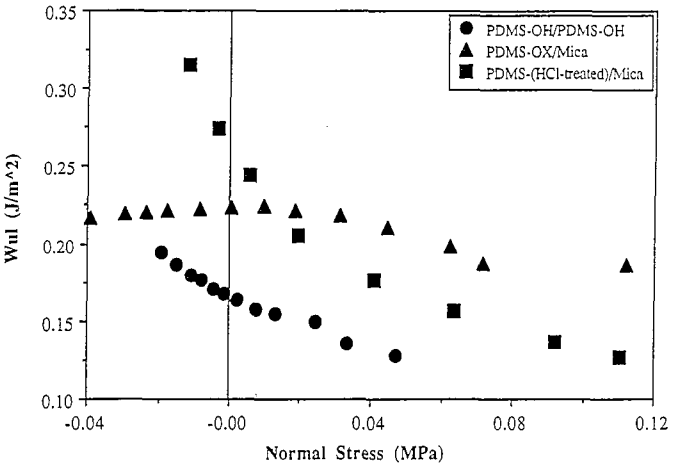

Fig. 26. Stress-induced interfacial hydrogen bonding depends upon interfacial flexibility.

on normal stress. Also included in this figure are the results obtained from the interaction of a hydrochloric acid-treated PDMS network and mica. HCl-treated PDMS develops some hydroxyl groups on its surface, which can form hydrogen bonds with the surface oxygens of mica. The work of adhesion for this interface, in contrast to the $PDMS^{ox}$–mica interface, exhibits a pronounced dependence on normal stress. These data indicate that H-bonding at the rigid interfaces is less sensitive to the normal stress than the flexible interfaces. The hydrocarbon part of $PDMS^{ox}$–$O_3Si(CH_2)_{11}S(CH_2)_2OH$ has some limited mobility and thus its adhesion shows a weak dependence on normal stress.

What is interesting to note in these studies is the fact that the work of adhesion between the HCl-treated PDMS and mica in the region of compressive stress is higher than the values obtained for the other two surfaces, which can engage in stronger H-bonding interactions. One explanation of this trend may be found in what is known as the Lake–Thomas effect [116]. During unloading, polymer chains are, to some extent, stretched in the immediate vicinity of the interface. The extra energy due to stretching and subsequent relaxation increases the effective work of adhesion more than the value of Dupré's work of adhesion. Shanahan and Michel [117] proposed a similar scenario earlier in order to explain the results of adhesion hysteresis involving polyisoprene of different cross-linking density and glass. This subject is reviewed in the next section.

3.14. Effect of cross-link density of rubber on adhesion hysteresis

Shanahan and Michel [117] used the JKR methodology to measure the adhesion energies of polyisoprene and glass as a function of the cross-link density of the rubber. The cross-linking density of polyisoprene was controlled by varying the concentration of the cross-linking agent, dicumylperoxide. The adhesion experiments were carried out by bringing a glass slide into contact with the rubber hemisphere and noting the change of the contact area as a function of time. No extra load was applied to the system, except the weight of the glass cover itself. In another experiment, the slide was pressed against the rubber with a known weight for about 5 min and the evolution of the contact area was monitored after the removal of the load. Similar to the earlier observation of Kendall, the contact area obtained from the "coming-on" experiments changed very little with time. However, the contact area obtained from the "coming-off" experiments showed a pronounced dependence with time, although it reached finally to a stable value. The analysis of the contact deformation obtained from the coming-on experiments yielded a value of the work of adhesion of 115 ± 30 mJ m^{-2}, which was almost independent of the cross-link density of the elastomer. However, the quasi-equilibrium adhesion energy

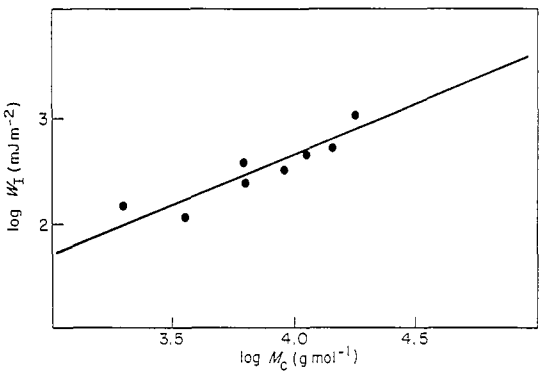

Fig. 27. Log W_I vs. log M_c for various degrees of cross-linking [117]. Reprinted with permission from Butterworth–Heinemann.

obtained from the coming-off experiments showed a pronounced dependence on the cross-link density. Fig. 27 summarizes these data, which plots the work of adhesion as a function of the average inter-cross-link molecular weight (M_c). The authors proposed three possible explanations for this effect. One explanation is based on the viscoelastic behavior of the elastomers. Elastomers of higher cross-link density is more elastic than the one of lower cross-linking. Thus, the lower cross-linked elastomer exhibits a faster relaxation and thus it evolves towards equilibrium much faster than the elastomer of lower cross-linking. This explanation implies that the differences of hysteresis are due to the differences in the total time taken by the system to reach true equilibrium.

A second explanation is based on the reptation model as introduced by de Gennes [118]. In this model, the total failure energy corresponds to the sum of that required to cause interfacial separation and that dissipated as friction during the extraction of chains from the bulk. This model assumes that a single primary-bond scission takes place somewhere along the chain enabling separation of the chain from the network. During extraction, the energy dissipation is proportional to M_c.

A third explanation is analogous to the theory of Lake and Thomas [116]. Shanahan and Michel (Fig. 28) used a model of hypothetical "magnetic spaghetti" to explain the effect of M_c on the adhesion hysteresis. If an electromagnet is placed close to the mass of an imaginary ferromagnetic "spaghetti" and turned on, magnetic attraction will cause the whole mass to stick to the electromagnet without any energy dissipation. This corresponds to the coming-on adhesion experiment. However, if one now tries to pull the mass of spaghetti away from the magnet, internal movement, disentanglement, stretching and relaxation of the spaghetti will lead to higher energy expenditure.

As Lake and Thomas showed, the expended energy during stretching is proportional to the molecular weight, and thus the coming-off adhesion energy is expected to be proportional to M_c. According to Shanahan and Michel, it is difficult to opt preferentially for one or other of the above explanations of adhesion hysteresis.

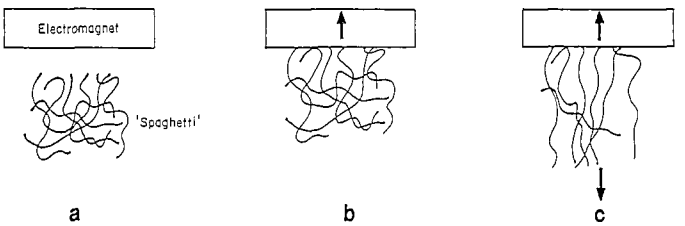

Fig. 28. Analogy of rubber/glass failure with behavior of ferromagnetic "spaghetti" and an electromagnet: (a) electromagnet without current; (b) attraction with electromagnet switched on; and (c) disentanglement and orientation of "spaghetti" during separation [117]. Reprinted with permission from Butterworth–Heinemann.

The reptation model used to explain the high adhesion hysteresis requires the chain scission and its subsequent pull-out from the network. However, for this to happen, the interfacial interaction does have to be stronger than the energy of bond cleavage. Polyisoprene interacts with glass primarily by van der Waals interaction. There is however the possibility that part of the surface of the polymer is oxidized, and some hydrogen bonding exists between the rubber and glass. The magnitude of the adhesion energy (≈ 115 mJ m^{-2}) from coming-on experiments indicates that some hydrogen bonding occurs between rubber and glass. However, the Van der Waals or hydrogen-bond component of the adhesion energies are much lower than the energy needed to cleave the carbon–carbon bonds. It is easier for the hydrogen bonds to break at the interface during separation than cleavage of carbon bonds. In experiments where covalent bonds are formed between the two surfaces, cohesive failure occurs in the polymer. Such an observation was made by us in the adhesion of semispherical polydimethylsiloxanes and a glass substrate, where the glass was coated with a self-assembled monolayer containing terminal olefin groups. Since PDMS has some residual SiH groups, it reacts with the olefins, catalyzed by the trace platinum catalyst (used to vulcanize the rubber). This causes the polymer to adhere so strongly to glass that it fractures cohesively when an attempt is made to separate the two.

If viscoelastic relaxation is the cause of adhesion hysteresis, then it should be dependent on the rate of separation. Although no such data was presented by Shanahan and Michel, in a related quasi-static experiment with extracted PDMS networks Silberzan et al. [114] observed no significant dependency of the adhesion hysteresis on the rate of separation. This lack of rate dependency in the quasi-static situations decribed here precludes the viscoelastic relaxation as a possible cause of adhesion hysteresis for the PDMS networks. It is most likely that the high adhesion hysteresis stems from the extension and relaxation of polymer chains.

3.15. Study of adhesion hysteresis between PDMS and surface-modified silica

Large hysteresis seen in the adhesion of a PDMS lens and plasma-oxidized PDMS sheet is due to H-bonding [119] (or perhaps formation of siloxane bridges across interface). However, when the plasma-oxidized PDMS is modified with silanes of different chain lengths (C_8–C_{14}), the adhesion hysteresis decreases dramatically but it does not disappear completely. Quite possibly, these self-assembled monolayers have defects and the dangling chains of the polymer are able to sense the underneath silica through these defects. As expected, the polymer chains can more easily sense the defects through a thinner monolayer film than a thicker one. In all cases, the adhesion hysteresis increases towards the central part of the contact region, probably because the polymer chains, aided by the compressive stress, can push aside the adsorbed hydrocarbons and interact with the underneath silica. Fig. 29 shows that the stress-induced adhesion decreases as the length of the grafted chains on silica increases. The adhesion hysteresis becomes negligible when the chain length is about C_{14}.

3.16. Modification of JKR theory: gradient of the work of adhesion

When W is a function of position, Kramer [114] pointed out that the gradient of the work of adhesion acts to prevent the propagation of crack; consequently the instability criterion of JKR needs modification. For position-dependent work of adhesion, $W(a)$, the instability criterion becomes:

$$\partial(G-W)/\partial a=0 \tag{79}$$

Eqs. (66) and (79) yield the instability condition of contact for any arbitrary spherical curvatures of two surfaces:

$$P_{po}=-[(a^6K^2/R^2)-2\pi Ka^4(\partial W/\partial a)]^{1/2} \text{ at } a=a_{min} \tag{80}$$

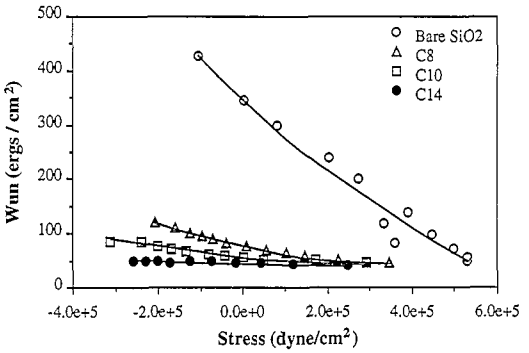

Fig. 29. Interaction between PDMS and surface-modified silica. W_{un} decreases as the length of the silane monolayer increases. (Here, 1 erg $cm^{-2} = 1$ mJ m^{-2}; 1 dyne $cm^{-2} = 0.1$ N/m^{-2}.)

Kramer et al. showed that the additional term, proportional to the gradient of work of adhesion, is a significant contributor to the pull-off force. For the case of extracted PDMS network, the corrective second term is found to be almost a factor of 10 higher than the normal JKR term.

3.17. Adhesion studied by atomic force microscopy

A new tool to study the interaction between surfaces at a nanoscopic level was pioneered by Binnig et al. [120]. In these measurements, a small cantilever is used to measure the force between a tip attached to the cantilever and the surface of interest. The force is measured from the deflection of a calibrated cantilever. Measuring the cantilever deflection as a function of its position generates a force map or image of the surface. Because of its primary use to image an insulating surface, the technique is known as atomic force microscopy (AFM). A vast literature exists in the use of AFM to the study of various surface-related phenomena e.g. adhesion, friction and mechanical properties of surfaces. Normally, the tip used to measure force is made up of silicon, silicon nitride or tungsten. Pashley et al. [121] added a useful feature to this method by attaching small colloidal-size polymer spheres at the tip of the microscope. Rutland and Senden [122] used this method to verify the DLVO theory of colloidal interactions. Apart from imaging the surfaces, AFM has also been very useful in studying the mechanical properties of surfaces. Burnham et al. [123] studied adhesion between a tungsten tip and such surfaces as alumina, mica, graphite, teflon and monolayer-coated alumina. These experiments exhibited adhesion hysteresis; the origin of this hysteresis, to some extent, is mechanical in origin, as explained by Israelachvili et al. [111]. Consider that two surfaces, separated by a finite distance, interact with each other via a finite attractive potential (Fig. 30). D_0 is the final equilibrium distance. One of the surfaces is connected to a spring of spring constant K_s. When the surfaces are brought towards each other, a mechanical instability occurs at a distance D_A, where the spring constant of the van der Waals spring becomes higher than K_s.

The surfaces thus jumps into contact at D_A. On separation from adhesive contact, the surfaces spontaneously jump from D_0 to D_R. Separation jumps are generally greater than the approaching jumps and this is the origin of mechanical adhesion hysteresis as is seen not only in the AFM studies but also in other macroscopic adhesion studies. The mechanical adhesion hysteresis is eliminated if the external spring constant is much greater than the effective van der Waals spring constant (dF/dD). The nature of the hysteresis observed in many AFM measurements is qualitatively different from the chemical adhesion hysteresis described in Sections 3.10–3.16. A measure of adhesion hysteresis in AFM studies is sometimes reported in terms of the indentation depth as a function of load—these measurements are based on stable crack growth or healing and thus are reliable for studying interfacial adhesion hysteresis.

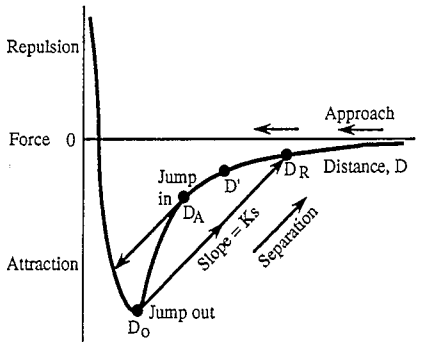

Fig. 30. Origin of mechanical adhesion hysteresis. Reproduced with permission from *J. Phys. Chem.* (Ref. [111]). © 1991 American Chemical Society.

Burnham and Colton [124] used nano-indentation method to study the mechanical properties of surfaces. The penetration depth versus load exhibited a hysteresis during the compression–decompression cycle, which was attributed to the plastic deformation of the surface. This hysteresis due to plastic deformation has also been observed in the adhesion of polymer spheres. Rimai et al. [125] studied the adhesion of polymeric particles to various solid substrates by measuring the contact area using electron microscopy. Some of their adhesion data departed from the JKR prediction, which were attributed to the plastic deformation or non-linear elastic effects. In some spectacular cases, the particles were totally engulfed by the deforming solid substrate.

Joyce et al. [126] studied the adhesion between a tungsten tip and monolayer-coated gold substrates using a modified version of an atomic force microscope. Although the large hysteresis of adhesion, normally observed with tungsten and gold, is diminished significantly by the alkyl thiol monolayer, it was significant for a crystalline hexadecyl mercaptan film, but almost negligible for a nonanethiol monolayer [127]. The authors ascribed the adhesion hysteresis to the anelastic deformation of the monolayer films under compressive stress, resulting in the entanglement of the hydrocarbon chains. It was suggested that the short-chain alkane thiols have a faster relaxation time than the longer-chain alkanes. Further studies are required to establish the proper scaling relationship between adhesion hysteresis and alkyl chain length.

Siepman and McDonald [128] recently carried out Monte Carlo simulation of self-assembled monolayers that are under the influence of compressive stress and found that the monolayers relax almost elastically after the stress is removed. This calculation was carried out for compressive stress only. In real cases, shear stress as well as a gradient of normal stress is present along the interface. Perhaps these stress gradients need to be considered to account for the hysteresis observed in the studies of Joyce et al.

Let us now return to the studies of Coulton et al. and compare their adhesion results with those predicted by the theories of surface energetics. The work of adhesion, according to the Good–Girifalco–Fowkes theory, should scale with the square root of the surface free energy of the substrate. Burnham et al. found that the adhesion pull-off forces obtained from the AFM studies are proportional to $(\gamma_s)^{0.5}$ for three high-energy surfaces (mica, graphite and alumina). The pull-off forces of the organic surfaces, however, deviated from this prediction. The authors speculated that this deviation is possibly related to their mechanical properties such as lower modulus or viscoelastic behavior. It should, however, be pointed out that the organic surfaces may interact with the AFM tip only via dispersion forces, whereas the other inorganic surfaces are likely to engage in H-bonding interactions. In order to check the square-root dependence of the surface energy, the dispersion and the non-dispersion components of the surface free energy need to be separately estimated. The authors used Zisman's γ_c as a surrogate

for γ_s to test the hypothesis of $\gamma_s^{1/2}$ dependence. Even though the observed trend is remarkable, in more refined treatments of these types of data detailed estimates of the different forces that contribute to adhesion should be considered.

The monolayers used to modify the surfaces of alumina in the experiments of Burnham et al. were $CF_3(CH_2)_{16}CO_2H$ and $CH_3(CH_2)_{16}CO_2H$ deposited by the LB technique. Alteration of only the outermost group from CH_3 to CF_3 resulted in the decrease of adhesion force by about 75%, which is another demonstration of the principle of independent surface action. The adhesion energy of Teflon was, however, significantly lower than that of the CF_3 surface. Based on the fact that the critical surface tension of wetting of the CF_2 surface is higher than that of the CF_3 surface, the adhesion energy of the perfluoromethylene surface should be higher than that of the perfluoromethane surface. This discrepancy may arise due to the fact that the CF_3 group has an uncompensated dipole of about 1 Debye and thus it interacts with the AFM tip via forces in addition to the dispersion forces. The other cause for this discrepancy may reside in the hysteresis of adhesion, which for the CF_3 surface is significantly higher than that of the teflon surface.

Recently, Wrighton et al. [129] modified the tip of an AFM microscope using self-assembled monolayers and studied adhesion of these modified tips to gold surfaces, which were also modified with scanning Auger microprobes. In this way, they studied adhesion between carboxylic acid, methyl groups and the cross interaction between carboxylic acid and methyl groups. These measurements were carried out in ethanol. The higher adhesion between the carboxylic acid surfaces indicate that the carboxylic acid groups have much higher affinity for each other than with ethanol. Very weak adhesion between the methyl surface and carboxylic acid surfaces indicate that the interaction between carboxylic acid and a methyl group is not strong enough to displace the bound ethanols to carboxylic acid groups. For similar studies using AFM for chemical imaging of surfaces see also Ref. [130].

4. Adhesion and friction

Briscoe et al. [110] measured shear forces between stearate monolayers transferred onto mica and found that the surfaces slid past each other either smoothly or in stick–slip fashion. They speculated that in the case of stick–slip motion, the hydrocarbon chains of the two surfaces interdigitate. This kind of interdigitation was also speculated by Timmons and Zisman [82] to be a cause of contact-angle hysteresis. These studies indicate that adhesion hysteresis and friction, two types of energy dissipative processes occurring at interfaces, are somehow related.

Kendall [131], Roberts and Thomas [132], Briggs and Briscoe [133] and Barquins and Courtel [134] conducted systematic studies in the rolling as well as sliding motion using rubber and glass and found the connection between friction and adhesion hysteresis.

Kendall [131] determined the adhesion hysteresis for glass and a soft rubber by means of a peeling experiment. The fracture energy was determined from the peeling of the rubber. The energy of adhesion was determined from the healing of the crack between rubber and glass. From the differences of the two energies, Kendall estimated the adhesion hysteresis. Kendall also measured the frictional force for a glass cylinder rolling over a rubber as a function of the rolling velocity. Kendall found a good correlation between friction forces and adhesion hysteresis.

Roberts and Thomas [132] also performed similar rolling experiments using glass cylinders and rubber. The adhesion hysteresis was estimated as the difference between the adhesion energies of trailing and leading edges according to following equation:

$$\Delta W = m_g \sin \theta / l \tag{81}$$

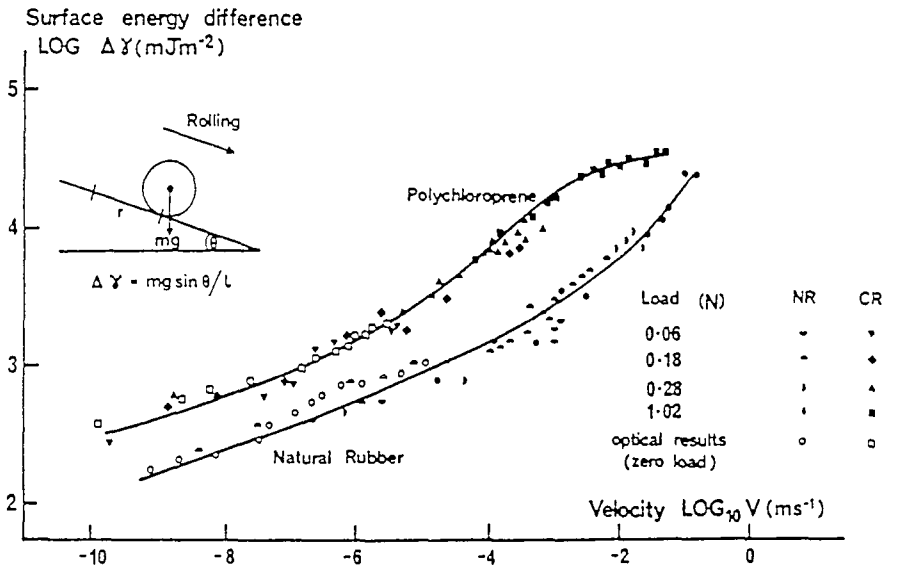

Fig. 31. Rolling of friction of glass cylinders on smooth-plane rubber tracks correlated with adhesion hysteresis [132]. Reprinted with permission from *Rubber Chemistry and Technology*, American Chemical Society.

where m_g is the weight of the cylinder, l is the length and θ is the angle of inclination.

The velocity of rolling, which is a measure of rolling friction, decreased, in proportion to the increase of ΔW. These results are summarized in Fig. 31.

Roberts and Thomas [132] as well as Briggs and Briscoe [133] measured the shear forces by sliding rubber spheres on flat glass surfaces. In this case Schallamach waves were observed traversing the contact area of the rubber–glass interface. The mechanism of the formation of Schallamach waves has been investigated by Barquins et al. [135]. Schallamach waves are formed as a result of elastic instability of the rubber due to lateral compressive forces. The lateral compressive force causes a buckling of the rubber, which traverses the contact area as waves but is damped for lossy viscous media (Fig. 32). Roberts attributed the energy loss in sliding motion to the energy associated with the peeling of Schallamach waves. Using an energy criterion, Briggs and Briscoe as well as Roberts and Thomas showed that the tangential stress can be related to the adhesion hysteresis (ΔW), wavelength of the Schallamach wave (λ) and the wave velocity (w) as follows:

$$F = \Delta W w / \lambda V \tag{82}$$

where V is the speed of sliding.

When the energy gained in the wake of a wave (W_a) is small compared with the energy of peeling (W_p), W can be approximated as equal to W_p. In order to test Eq. (82), Roberts conducted experiments with a range of spherical rubber vulcanizates sliding against optically smooth glass. Eq. (82) tallied with the experimental results for four decades of sliding speeds (Fig. 33). The theory however broke down at very high velocities. The Roberts–Thomas model of friction essentially considers the sliding as a collection of microscopic peeling of Schallamach waves. The model does not invoke the possibility of true relative sliding of the two surfaces. While at low sliding speeds, the sliding is mediated by the propagation of Schallamach waves, it is plausible that at high speeds, true slippage at the interface might occur, thus increasing the frictional dissipation. The sliding behavior at high speeds may therefore be a combination of peeling of Schallamach waves and interfacial slippage. The relationship between interfacial slippage and frictional dissipation is not yet a well understood subject, nor is the relationship between friction and interfacial adhesion.

Fig. 32. An example of compressive instability formed by sliding an elasomeric lens of polydimethylsiloxane on an adhesive tape (sliding direction of the lens is from left to right). The ridges thus formed do not propagate because of viscous damping. The ridge pattern is visible on the tape even after the lens is removed. In the cases of cross-linked rubber, the ridges propagate in the direction opposite to sliding forming Schallamach waves.

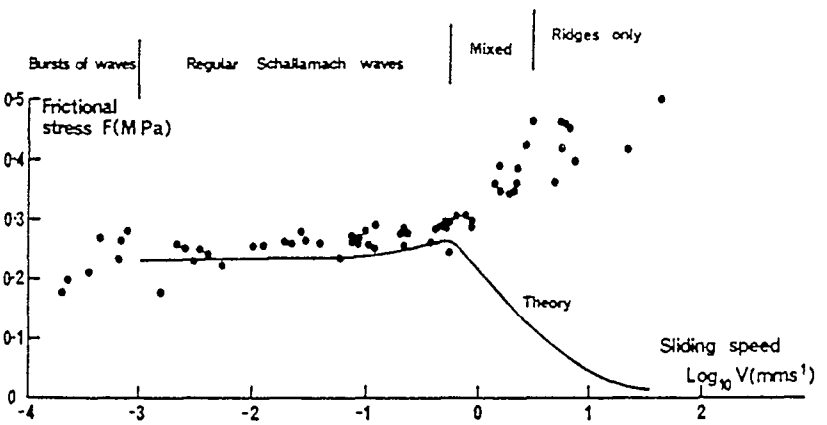

Fig. 33. Variation in sliding friction stress with speed for a rubber sphere ($R = 18.5$ mm) on glass at room temperature. The visual appearance of waves is indicated. ○, experiment; solid line, theory [132]. Reprinted with permission from *Rubber Chemistry and Technology*, American Chemical Society.

In the tribological studies of polymer on polymer and metal on polymer, there is a general trend for a solid of higher surface energy to have higher friction than one of lower surface free energy [136]. There are however exceptions. Surface force experiments [137] of Briscoe and Evans show that a hydrocarbon film has a lower interfacial shear strength than a fluorocarbon film. Recently, DePalma and Tillman [138] carried out friction measurements on hydrocarbons and fluorocarbons containing self-assembled monolayers of trichlorosilanes adsorbed onto silicon, and found that the hydrocarbon monolayers are better lubricants than the fluorocarbon monolayers. Overney et al. [139] used a friction

force microscope to image the fluorocarbon and hydrocarbon monolayers and found that the friction of a fluorocarbon monolayer is higher than the hydrocarbon monolayer. This difference in their frictional properties allowed these authors to image a mixed monolayer of hydrocarbon and fluorocarbon, where fluorocarbons formed phase-separated domains in the sea of a hydrocarbon monolayer. The authors proposed that the differences in their frictional properties arise due to the differences in the rigidity of the monolayers. This line of reasoning is consistent with the recent finding of Brown [140] who observed that surface mobility has a dramatic effect on interfacial sliding. Brown modified surfaces of polystyrene with block copolymers of polystyrene and polydimethylsiloxane. The friction stress on the rigid polystyrene was significantly higher than that of the polymer covered with a highly mobile PDMS film.

Chaudhury and Owen [141] measured friction between a PDMS elastomer and self-assembled films of hydrocarbon and fluorocarbons on mica at a low sliding speed. They found that the friction of a fluorocarbon surface is significantly higher than that of a hydrocarbon surface. Under an optical microscope they found no evidence of the formation of a Schallamach wave and the sliding appeared to follow by uniform slippage. They ascribed the difference in the friction behavior to adhesion hysteresis. The fluorocarbon surface exhibited higher hysteresis in both adhesion and contact angle than the hydrocarbon surface. The authors proposed that for both the dissipative processes, adhesion hysteresis and friction, partial interdigitation between the polymer chains and the fluorocarbon monolayers are responsible. This line of reasoning is similar to the model of Timmons and Zisman [90], who proposed earlier that the high contact-angle hysteresis of the fluorocarbon monolayer is due to intercalation of the probe liquids in the monolayer films. These authors measured the contact angles of a number of probe liquids on the fluorocarbon surface and found that the contact-angle hysteresis increases systematically with the decrease in the size of the liquid molecules. For example, di-iodomethane, whose molecular volume is about 80 cm^{-3} mol^{-1} exhibits a hysteresis of about 23° on a fluorocarbon monolayer; whereas the hysteresis of hexadecane (whose molecular volume is 292 cm^{-3}) is only about 1°.

Chaudhury and Owen also observed that the contact angle hysteresis of di-iodomethane (35°) on the fluorocarbon monolayer is significantly higher than that (1°) observed on the hydrocarbon monolayer. Similarly a PDMS liquid exhibits a contact-angle hysteresis of about 12° on the fluorocarbon monolayer, whereas the hysteresis on the hydrocarbon monolayer is only about 1°.

Israelachvili et al. [142] invoked a model of adhesion hysteresis to explain the frictional stresses of LB films transferred onto mica. LB monolayers, which initially showed high adhesion hysteresis and high friction, exhibited lower hysteresis and lower friction when the monolayer was exposed to the vapor of decane. It was postulated that decane intercalates in the monolayer and fluidizes it, which decreases hysteresis and thus friction. They also found that friction is related to the phase states of the monolayer films. The friction was high for the hydrocarbon molecules in a glassy amorphous state. Low friction was observed for monolayers that were in a crystalline or liquid-like state. It was postulated that the crystalline hydrocarbon monolayers do not interdigitate, thus those monolayers exhibit low friction. Even though the molecules interdigitate in the liquid-like state, they also relax easily and thus both the adhesion hysteresis and friction stresses are low. However, when the molecules interdigitate in the glassy amorphous state, they do not relax without dissipating some energy. The authors explained the results assuming that the entire area of contact undergoes subsequent processes of adhesion and separation of interfaces. Thus the energy loss during the compression–decompression JKR cycles should be relevant to the friction energy dissipation during sliding. The authors proposed an equation of friction stress as follows:

$$S = \Delta W / \delta \tag{83}$$

where δ is a characteristic molecular length defined by the length of interdigitation and ΔW is the adhesion hysteresis. This equation is a limiting case of the equation proposed by Briggs and Briscoe as well as Roberts and Thomas, where $w = V$ and λ is the characteristic length scale of molecular dimension. Thus, extending the Roberts–Thomas model, sliding of two smooth surfaces may be viewed as the propagation of a large number of microscopic or molecular Schallamach waves; based on this picture the correlation between friction with adhesion hysteresis becomes obvious. The propagation of the ultimate molecular Schallamach wave between surfaces corresponds to the nucleation and propagation of dislocations in crystalline solids [143]. Earlier, Gittus [144] viewed Schallamach waves as the propagation of Volterra dislocations (which he called interfaceons) through non-crystal solids. Eq. (83) was used by Israelachvili et al. to interpret the frictional stresses of monolayer-coated mica. Using δ to be of the order of molecular dimension, a reasonable correlation between calculated and theoretical frictional stresses was obtained. However, if the same equation is used to predict the frictional stresses of silicon rubber against monolayer-coated mica (see Ref. [141]) a large value of δ (ca. 0.15 μm) is needed. The discrepancy is not understood. However, the elasticity of rubber is significantly lower than mica. It is quite possible that Eq. (83) needs to be modified by the elasticities of the sliders, as it determines the critical stress necessary for dislocation propagation.

From the above discussion, it seems clear that at least two fundamental properties of interfaces control friction: interfacial rigidity and adhesion hysteresis. When we speak about interfacial rigidity we have not yet specified on what length scale this rigidity is important. It is possible that the flexibility of only the outermost headgroup is quite sufficient to give rise to pronounced effects. In fact, the large difference in the frictional behavior of CH_3- and CF_3-containing surfaces, apart from the difference in adhesion hysteresis, may also be due to the fact that CH_3 group is locally more mobile than the CF_3 group.

5. Summary and general comments

Although the theories of intermolecular forces, based on electrodynamic fluctuation and interfacial electron transfer, describe interactions between condensed phases adequately, several aspects of these theories need further improvements. Macroscopic theories describe the general global behavior of interfaces well but ignore the roles played by the fine structures of surfaces and interfaces. The scope of the microscopic theories is restricted because of the lack of detailed knowledge of the structures of surfaces or due to the complications resulting from many-body interactions. Recent studies [145] of sum-frequency vibration spectroscopy, a non-linear optical technique, show that the structure of a surface is clearly perturbed when it interacts strongly with another condensed phase, alerting us that the structural perturbations need to be considered seriously in understanding interactions between surfaces.

The problem is even more severe for surfaces that engage in donor–acceptor or hydrogen-bonding interactions. The single molecular donor–acceptor properties, which are obtained from heat of mixing in dilute solutions, may not be highly relevant when the molecules on a surface undergo partial Lewis neutralization due to lateral interactions. When a Lewis-neutralized surface interacts with another, lateral donor–acceptor bonds need to be broken before new bonds are formed across the interface—thus part of the energy gained by forming a new surface is compensated by the energy lost by the break up of lateral bonds. This issue of subtle reconstruction of strongly interacting surfaces has not been seriously dealt with in the current theories of adhesion and fracture.

One puzzling issue about the donor–acceptor interaction is its connection to electrical double layers. On the theoretical level, the study of Deryaguin et al. is probably the only one that presents a

unified view of the two phenomena. There exist many calculations of donor–acceptor interactions involving a detailed quantum-mechanical formalism, but they are generally silent about the effects produced by the electrostatic fields resulting from the concomitant formation of an electrical double layer. Part of the confusion about the effects produced by the electrostatic double layer and charge separation arises from the way they are experimentally measured. Estimation of the electrostatic work of adhesion from peel experiments is often based on the simplistic assumption that all the energy of fracture goes into separating the surfaces. The mechanics of stretching and bending of the adhesive as well as the possible viscoelastic losses are not always clearly accounted for. The elegant and pioneering experiments of Deryaguin et al. clearly point out the role of electrostatics in adhesion, but as the authors indicated, its exact quantification would require direct in-situ measurements of the electrification phenomena, while the crack still propagates. The electrostatic energy obtained by integrating the force–distance profile after the separation of the two surfaces is not totally adequate for calculating the electrostatic adhesion energy. A self-consistent theory, delineating the energy flow from the unfractured to the fractured surfaces resulting from the charge rearrangement at the crack tip and including the long-range electrostatic interaction within the open surfaces of the crack, is to be much desired in order to determine the proper roles of donor–acceptor and electrostatic interactions in adhesion and fracture.

Adhesive fracture energies of polymeric interfaces generally have a dissipative component. Gent and Schultz [146] expressed the total fracture energy as a product of two terms: one arising from the thermodynamic work of adhesion, and the other is attributed to bulk rheology. Within the last few years there has been a resurgence of interest in measuring adhesion energies of solid surfaces separately from the rheological effects. The method of contact mechanics, introduced by Johnson, Kendall and Roberts, has shown great promise in that respect. One fascinating part of these new studies is the discovery that many of the non-equilibrium phenomena associated with adhesion are related to the molecular-level processes occurring at surfaces. These non-equilibrium processes are not only relevant to understanding adhesion between surfaces but also to understanding friction.

Earlier, Kendall pointed out that the adhesion and fracture of the van der Waals surfaces, the interaction of which can be described by a potential of the Lennard–Jones type, can follow a non-hysteretic path. However, for other types of interactions accompanied by an intermediate energy barrier, adhesion and fracture of surfaces should follow a hysteretic path. The results of the direct measurement of adhesion are in general agreement with the view of Kendall. Van der Waals surfaces generally show much lower adhesion hysteresis than the hydrogen-bonding surfaces. The adhesion hysteresis seen for the van der Waals surfaces is related to the energy barriers produced by the interdigitation of surface functionalities or metastability produced by surface heterogeneity. A stress-induced reconstruction of the surfaces has also been thought to be another contributor to adhesion hysteresis. But none of the above models has been rigorously verified.

One issue about the JKR theory that often eludes us is the detailed balance of the forces at and near the crack tip. This issue has been addressed by Muller et al. [73], but these treatments start with the premise that the forces of interaction between the open surfaces of the crack are of the Lennard–Jones type. It is particularly important to readdress this issue; say, when specific interactions operate at the interface or when polymer chains are extended near the crack tip.

We will close this review with one final comment about the quantitative correlation between friction stress and adhesion hysteresis. The current studies indicate that friction and adhesion hysteresis are related qualitatively. A quantitative relation between the two processes may also be found, but this search may be delayed because of the following reason. The adhesion energy obtained from the unloading experiments of JKR can be significantly position dependent in the case where a stress-induced surface reconstruction takes place. Since the compressive stress is a maximum towards the

central part of the contact, stress-induced reconstruction is most significant in that part of the contact area. There is, however, no way of gaining any information of adhesion about that region from the conventional JKR experiments, because elastic instability takes over much earlier and the surfaces separate at a finite area of contact. Unless methods are developed to gain information of adhesion hysteresis of this central region, true quantitative correlation between friction and adhesion hysteresis cannot be developed. One possible way to achieve the above objective is to scan the entire region of contact by using a rolling motion of either a sphere or cylinder on a flat substrate. However a rolling motion involves application of a torque, which creates an asymmetric pressure distribution in the zone of contact for hysteretic surfaces. This problem of adhesive contact mechanics involving asymmetric pressure distribution requires a theoretical solution.

Acknowledgements

The author gratefully acknowledges Professor E.J. Kramer, Dr. H.R. Brown, Professor G.M. Whitesides and Dr. M.J. Owen for many valuable discussions during the course of these investigations and while writing this manuscript, and acknowledges Ms. Bimin Zhang Newby for drawing several figures for this review. This work was supported by the Dow Corning Corporation.

References

[1] I. Langmuir, *Collected Works*, Pergamon Press, New York, 1960.
[2] I. Langmuir, *J. Am. Chem. Soc., 38* (1916) 2221.
[3] I. Langmuir, *J. Franklin Inst., 218* (1934) 143.
[4] I. Langmuir, *Science, 87* (1938) 493.
[5] I. Langmuir, *Trans. Faraday Soc., 15*(3) (1920) 62.
[6] H.W. Fox, P.W. Taylor and W.A. Zisman, *Ind. Eng. Chem. 39* (1947) 1401; H.W.; Fox, W.A. Zisman, *J. Colloid Sci., 5* (1950) 514.
[7] H.W. Fox, E.F. Hare and W.A. Zisman, *J. Colloid Sci., 8* (1953) 194; *J. Phys. Chem., 59* (1955) 1097.
[8] W.A. Zisman, *Adv. Chem. Ser., 43* (1964) 1.
[9] T. Young, in G. Peacock (ed.), *Miscellaneous Works* Vol 1, J. Murray, London, 1855.
[10] M.K. Chaudhury and G.M. Whitesides, *Science, 256* (1992) 1539.
[11] N.K. Adam, *Adv. Chem. Ser., 43* (1964) 52.
[12] C.J. van Oss, R.F. Giese and R.J. Good, *Langmuir, 6* (1990) 1711.
[13] C.D. Bain, *Ph. D. Thesis*, Harvard University, 1988.
[14] N. Camilline, E.E.D. Chidsey, G-yu Liu, T.M. Putvinski and G. Scoles, *J. Chem. Phys., 94* (1991) 8493.
[15] B. deKoven, D. Fisher and M.K. Chaudhury, unpublished work, 1994.
[16] R.J. Good, in R.J. Good and R.R. Stromberg (eds.), *Surface and Colloid Science*, Plenum, 1979, Vol. 11, p. 1.
[17] L.A. Girifalco and R.J. Good, *J. Phys. Chem., 61* (1957) 904; *J. Phys. Chem., 64* (1960) 561.
[18] F.M. Fowkes, *Ind. Eng. Chem., 56* (1964) 40.
[19] D.K. Owens and R.C. Wendt, *J. Appl. Polym. Sci., 13* (1969) 1741.
[20] D.H. Kaelble, *J. Adhesion, 2* (1970) 66; D.H. Kaelble and K.C. Uy, *J. Adhesion, 2* (1970) 50.
[21] S. Wu, *Polymer Interface and Adhesion*, Marcel Dekker, New York, 1982.
[22] J.W. Gibbs, *Collected Works*, Vol. I, Longman Green, New York, 1926.
[23] A. Dupré, *Theorie Mechanique de la Chaleur* , Gauthier–Villars, Paris, 1869, p. 369.
[24] D. Berthelot, *Compt. Rend., 126* (1898) 1703.
[25] R.S. Bradley, *Philos. Mag., 13* (1932) 853
[26] J.H. de Boer, *Trans. Faraday Soc., 32* (1936) 10.
[27] H.C. Hamaker, *Physica, 4* (1937) 1058
[28] A.D. McLachlan, *Proc. Roy. Soc. London, A271* (1963) 387.
[29] J. Israelachvili, *Quart. Rev. Biophys., 6* (1974) 341.
[30] H.B.G. Casimir and D. Polder, *Phys. Rev., 73* (1948) 360; C.I. Sukenik, M.G. Boshier, D. Cho, V. Sandoghdar and E.A. Hinds, *Phys. Rev. Lett., 70*(5) (1993) 560.

[31] R.J. Good and C.J. Hope, *J. Chem. Phys., 55* (1971) 111.
[32] M.K. Chaudhury, *J. Colloid Interface Sci., 119* (1987) 174.
[33] E.M. Lifshitz, *Zh. Eksp. Tear. Fiz., 29* (1955) 94; I.E. Dzyalshinskii, E.M. Lifshitz and Pitaevskii, *Adv. Phys., 10* (1961) 165.
[34] J. Mahanty and B.W. Ninham, *J. Chem. Phys., 59* (1973) 6157.
[35] P. Silberzan and L. Leger, *Phys. Rev. Lett., 66* (1991) 185.
[36] D.H. Hough and L.R. White, *Adv. Colloid Interface Sci., 14* (1980) 3.
[37] C.J. van Oss, M.K. Chaudhury and R.J. Good, *Chem. Rev., 88* (1988) 927; *Adv. Colloid Interface Sci., 28* (1987) 35.
[38] M.K. Chaudhury, *Ph. D. Thesis*, State University of New York at Buffalo, 1984.
[39] B.W. Ninham and V.A. Parsegian, *Biophys. J., 10* (1970) 646.
[40] H. Krupp, *Adv. Colloid Interface Sci., 1* (1967) 111.
[41] F.M. Fowkes, in K.L. Mittal (ed.), *Physicochemical Aspects of Polymeric Surfaces*, Plenum, New York, 1983, Vol. 2, p. 583; in J.J. Burke (ed.), *Surfaces and Interfaces*, Syracuse University Press, New York, 1967, Vol. 1, p. 199; *J. Phys. Chem., 66* (1962) 382; *J. Adhesion Sci. Technol., 1* (1987) 7; W. Gutowski, in L.-H. Lee (ed.), *Fundamentals of Adhesion,* Plenum, New York, 1991, p. 87.
[42] J.D. Hoffman, G.T. Davis and J.I. Lauritzen, Jr., in N.B. Hannay (ed.), *Treatise on Solid State Chemistry*, Plenum, New York, 1975, Vol. 3, p. 497.
[43] F.M. Fowkes, *J. Colloid Interface Sci., 28* (1968) 493.
[44] E.B. Greenhill and S.R. McDonald, *Nature, 171* (1953) 37.
[45] E.J. Kramer and L.L. Berger, *Adv. Polym. Sci., 91/92* (1990) 1.
[46] C.J. van Oss, J. Visser, D.R. Absolom, S.N. Omenyi and A.W. Neumann, *Adv. Colloid Interface Sci. , 18* (1983) 133.
[47] E.I. Vargha-Butler, T.K. Zubovits, M.K. Weibel, D.R. Absolom and A.W. Neumann, *Colloids Surf., 15* (1985) 233; S.N. Omenyi, R.S. Snyder, D.R. Absolom, C.J. van Oss and A.W. Neumann, *J. Dispersion Sci. Technol., 3* (1982) 307.; A.W. Neumann, J. Visser, R.P. Smith, S.N. Omenyi, D.W. Francis, J.K. Spelt, E.B. Vargha-Butler, W. Zingg, C.J. van Oss and D.R. Absolom, *Powder Technol., 37* (1984) 229.
[48] S.N. Omenyi and A.W. Neumann, *J. Applied Phys., 47* (1976) 3956; S.N. Omenyi, R.P. Smith and A.W. Neumann, *J. Colloid Interface Sci., 75* (1980) 117; S.K. Li, R.P. Smith and A.W. Neumann, *J. Adhesion, 16* (1984) 105.
[49] J.C. Bolger and A.S. Michaels, in P. Weiss and D. Cheevers (eds.), *Interface Conversion*, Chapter 1, Elsevier, New York, 1969; J.C. Bolger, in K.L. Mittal (ed.), *Adhesion Aspects of Polymeric Coatings*, Plenum Press, New York, 1983, p. 3.
[50] R.S. Drago, G.C. Vogel and T.E. Needham, *J. Am. Chem. Soc., 93* (1971) 6014.
[51] S. Ohki and C.B. Ohki, *J. Theoretical Biol., 62* (1976) 389.
[52] F.M. Fowkes, *J. Adhesion Sci. Technol., 1* (1987) 7.
[53] W.B. Jensen, *The Lewis Acid–Base Concept*, Wiley Interscience, New York, 1980.
[54] P.A. Small, *J. Appl. Chem., 3* (1953) 71.
[55] S.R. Wasserman, Y.-T. Tao and G.M. Whitesides, *Langmuir, 5* (1989) 1074.
[56] E.B. Troughton, C.D. Bain, G.M. Whitesides, R.G. Nuzzo, D.L. Allara and M.D. Porter, *Langmuir, 4* (1988) 365.
[57] R.I. Carey, J.P. Folkers and G.M. Whitesides, *Langmuir, 10* (1994) 2228.
[58] S.R. Holmes-Farley, R.H. Reamey, T.J. McCarthy, J. Deutch and G.M. Whitesides, *Langmuir, 1* (1985) 725.
[59] R.J. Good, M.K. Chaudhury and C.J. van Oss, in L.H. Lee (ed.), *Fundamentals of Adhesion*, Plenum Press, New York, 1991, p. 153; *Adv. Colloid Interface Sci., 28* (1985) 35; *Chem. Rev., 88* (1988) 927.
[60] L.H. Lee, in L.H. Lee (ed.), *Fundamental of Adhesion*, Plenum Press, New York, 1991, pp. 1, 349.
[61] R.G. Pearson, *J. Am. Chem. Soc., 85* (1963) 3533.
[62] G.; Klopman and R.F. Hudson, *Theor. Chim. Acta , 8* (1967) 165.
[63] S.R. Cain, L.J. Matienzo and F. Emmi, *J. Phys. Chem. Solids., 50*(1) (1989) 87.
[64] P.S. Ho, R. Haight, R.C. Silverman, B.D. White and F. Faupel, in L.H. Lee (ed.), *Fundamental of Adhesion*, Plenum Press, New York, 1991, p. 383.
[65] B.V. Deryagin, N.A. Krotova and V.P. Smilga, *Adhesion of Solids*, Nauka, Moscow, 1973, and references cited therein (in Russian); V.P. Smilga, *Research in Surface Forces*, Vol. 1, Izd. Akad. Nauk, SSSR 1961, p. 76 (English translation, New York, Consultants Bureau, 1963, p. 58).
[66] R.G. Horn and D.T. Smith, *Science, 256* (1992) 362; R.G. Horn, D.T. Smith and A. Grabbe, *Nature, 366* (1993) 442.
[67] C.E. Inglis, *Trans. Naval Arch., 69* (1913) 219.
[68] A.A. Griffith, *Philos. Trans. R. Soc. London, 221A* (1920) 163.
[69] K.L. Johnson, K. Kendall and A.D. Roberts, *Proc. R. Soc. London, A324* (1971) 301.
[70] H. Hertz, in D.E. Jones (ed.), *Miscellaneous Papers*, London, Macmillan, 1896.
[71] J. Boussinesq, *Application des Potentials à l'etude de l'équilibre et du mouvement des solides élastiques*, Gauthier–Villars, Paris, 1885.
[72] B.V. Deryaguin, V.M. Muller and Yu.P. Toporov, *J. Colloid Interface Sci., 53* (1975) 314; B.V. Deryaguin, *Kolloid Z., 69* (1934) 155.
[73] V.M. Muller, V.S. Yushchenko and B.V. Deryaguin, *J. Colloid Interface Sci., 77* (1977) 91.
[74] J.A. Greenwood and K.L. Johnson, *Philos. Mag., 43* (1981) 697; D. Maugis and M. Barquins, *J. Appl. Phys. D, 11* (1978) 1989.
[75] D. Maugis and M. Barquins, in L.H. Lee (ed.), *Adhesion and Adsorption of Polymers: Polymer Science and Technology*, Plenum Press, New York, 1980, Vol. 12A, p. 203; M.. Barquins and R. Courtel, *Wear, 32* (1975) 133.

[76] K. Kendall, *J. Phys., D: Appl. Phys., 5* (1973) 1782; *8* (1975) 1449; *Proc. R. Soc. London, A341* (1975) 409; *A344* (1975) 287; *J. Adhesion, 7* (1975) 137; *J. Mater. Sci., 11* (1976) 638, 1263, 1267; *10* (1975) 1011.
[77] A.D. Roberts and A.B.'Othman, *Wear, 42* (1977) 119.
[78] D. Tabor, *J. Colloid Interface Sci., 58* (1977) 2.
[79] A.E. Lee, *J. Colloid Interface Sci., 64* (1978) 577.
[80] R.G. Horn, J.N. Israelachvili and F. Pribac, *J. Colloid Interface Sci., 115* (1987) 480.
[81] R.C. Dutrowski, *Trans ASME,* (1969) 732.
[82] M.K. Chaudhury and G.M. Whitesides, *Langmuir, 7* (1991) 1013.
[83] M.K. Chaudhury and M.J. Owen, *J. Phys. Chem., 97* (1993) 5722.
[84] M.K. Chaudhury and G.M. Whitesides, *Science, 255* (1992) 1230; M.K. Chaudhury, *J. Adhesion Sci. Technol., 7* (1993) 669.
[85] M. Barquiris, *J. Adhesion, 26* (1988) 1.
[86] M.K. Chaudhury, T. Weaver, C.Y. Hui and E.J. Kramer, unpublished work, 1995, presented at the American Physical Society Conference, Condensed Matter Physics, 1995, submitted for publication.
[87] R.M. Pashley and J.N. Israelachvili, *Colloids Surf., 2* (1981) 169.
[88] H. Haidara, M.K. Chaudhury and M.J. Owen, *J. Phys. Chem., 99* (1995) 8681.
[89] C.D. Bain and G.M. Whitesides, *J. Am. Chem. Soc., 110* (1988) 334.
[90] C.O. Timmons and W.A. Zisman, *J. Colloid Interface Sci., 22* (1966) 165.
[91] F.M. Fowkes, *J. Phys. Chem., 67* (1963) 2538.
[92] M.K. Chaudhury, *Biosensors,* in press.
[93] M.K. Chaudhury, unpublished work, 1990.
[94] L.W. Schwartz and S. Garoff, *Langmuir, 1* (1985) 219.
[94a] R.C. Thomas, J.E. Houston, R.M. Crooks, T. Kim and T.A. Michalske, *J. Am. Chem. Soc., 117* (1995) 3830.
[95] V. Mangipudi, M. Tirrell and A.V. Pocius, *J. Adhesion Sci. Technol., 8* (1994) 1251; W.W. Merrill, A.V. Pocius, M. Tirrell and Thakkar, *Langmuir, 7* (1991) 1975.
[96] G.A. Tomlinson, *Philos. Mag., 7* (1929) 905.
[97] K. Kendall, *J. Adhesion, 5* (1973) 179.
[98] T.D. Blake and J.M. Haynes, *J. Colloid Interface Sci., 30* (1969) 421.
[99] A. Schallamach, *Proc. Phys. Soc., London, B66* (1953) 386.
[100] G.M. Bartenev, *Dokl. Akad. Nauk SSSR, 96* (1954) 1161; RARPA Translation 925, *Proc. 3rd All-Union Conference on Friction and Wear,* Moscow, 1960, Vol. 2, p. 7.
[101] A.A. Valishin and E.M. Kartashov, *Polym. Sci., 35* (1993) 35.
[102] R.J. Good, *J. Phys. Chem. Am. Chem. Soc., 75* (1952) 5041.
[103] R.E. Johnson and R.H. Dettre, *Surf. Colloid Sci., 2* (1969) 85.
[104] A.W. Neumann and R.J. Good, *J. Colloid Interface Sci., 38* (1972) 341; R.E. Johnson and R.H. Dettre, *J. Phys. Chem., 68* (1964) 1744.
[105] J.F. Joanny and P.G. de Gennes, *J. Chem. Phys., 81*(1) (1984) 552.
[106] T. Smith and G. Lindberg, *J. Colloid Interface Sci., 66* (1978) 263.
[107] S. Garoff, personal communication, 1994.
[108] M.K. Chaudhury, unpublished work, 1994.
[109] A.K. Chakraborty and P.M. Adriani, *Macromolecules, 25* (1992) 2470; A.K. Chakraborty, J.S. Shaffer and P.M. Adriani, *Macromolecules, 24* (1990) 5226.
[110] B.J. Briscoe, D.C.B. Evans and D. Tabor, *J. Colloid Interface Sci., 61* (1977) 9.
[111] Y.L. Chen, C.A. Helm and J.N. Israelachvili, *J. Phys. Chem., 95* (1991) 10737.
[112] M.K., Chaudhury, unpublished work, 1993.
[113] G.; Reiter, J.S.; Peanasky; L.; Cai, A.L.; Demirel, S., Granick, *Polym. Preprints, 34* (1993) 284; *J. Chem. Phys., 101* (1994) 2606.
[114] P. Silberzan, S. Perutz, E.J. Kramer, and M.K. Chaudhury, *Langmuir, 10* (1994) 2466.
[115] M.K. Chaudhury, *Polym. Preprints, 34* (1993) 281.
[116] G.J. Lake and A.G. Thomas, *Proc. R. Soc. London, A300* (1967) 108; A. Carre and J. Schultz, *J. Adhesion, 17* (1984) 135.
[117] M.E.R. Shanahan and J. Michel, *Int. J. Adhesives, 11* (1991) 170; M.F. Vallat, P. Ziegler, P. Vondracek and J. Schultz, *J. Adhesion, 35* (1991) 95.
[118] P.G. de Gennes, *J. Chem. Phys., 55* (1971) 572; in J.M. Georges (ed.), *Macroscopic Aspects of Adhesion and Lubrication,* Elsevier, Amsterdam, 1982, p. 355.
[119] M.K. Chaudhury, unpublished work, 1992.
[120] G. Binnig, C.F. Quate and C. Gerber, *Phys. Rev. Lett., 56* (1986) 930.
[121] W.A. Ducker, T.J. Senden and R.M. Pashley, *Langmuir, 8* (1992) 1831.
[122] M.W. Rutland and T.J. Senden, *Langmuir, 9* (1993) 412.
[123] N.A. Burnham, D.D. Dominguez, R.L. Mowery and R. Colton, *J. Phys. Rev. Lett., 64* (1990) 1931.
[124] N.A. Burnham and R.J. Colton, *J. Vac. Sci. Technol., A7* (1989) 2906.
[125] D.S. Rimai, L.P. DeMejo and R.C. Bowen, *J. Appl. Phys., 68* (1990) 6234; *J. Adhesion Sci. Technol., 3* (1989) 623; *J. Adhesion Sci. Technol., 2* (1988) 331; *5* (1991) 959.
[126] S.A. Joyce, R.C. Thomas, J.E. Houston, T.A. Michalske and R.M. Crooks, *Phys. Rev. Lett., 68* (1992) 2790.

[127] G.S. Ferguson, M.K. Chaudhury, G.B. Sigal and G.M. Whitesides, *Science, 253* (1991) 776.
[128] J.I. Siepmann and I.R. McDonald *Phys. Rev. Lett., 70* (1993) 453.
[129] C.D. Frisbie, L.F. Rozsnyai, A. Noy, M.S. Wrighton and C.M. Lieber, *Science, 265* (1994) 2071.
[130] J.L. Wilbur, H.A. Biebuyck, J.C. MacDonald and G.M. Whitesides, *Langmuir, 11* (1995) 825.
[131] K. Kendall, *Wear, 33* (1975) 351.
[132] A.D. Roberts and A.G. Thomas, *Wear, 33* (1975) 45; A.D. Roberts, *Rubber Chem. Technol., 52* (1979) 23.
[133] G.A.D. Briggs and B.J. Briscoe, *Wear, 35* (1975) 357.
[134] M. Barquins and R. Courtel, *Wear, 32* (1975) 133.
[135] M. Barquins, R. Courtel and P. Thirion, *Wear, 27* (1974) 147.
[136] H. Czichos, in L.H. Lee (ed.) *Polymer Wear and Its Control*, ACS Symp. Series, Vol. 287, American Chemical Society, Washington, DC, 1985, p. 3; W.A. Zisman, *Rec. Chem. Prog., 26*(1) (1965) 13.
[137] B.J. Briscoe and D.C.B. Evans, *R. Proc. Soc. London, A380* (1981) 389.
[138] V. DePalma and N. Tillman *Langmuir, 5* (1989) 868.
[139] R.M. Overney, E. Meyer, J. Frommer, D. Brodbeck, R. Luthl, L. Howald, H.-J. Guntherodt, M. Fujihira, H. Takano and Y. Gotoh, *Nature, 359* (1992) 133.
[140] H.R. Brown, *Science, 263* (1994) 1411.
[141] M.K. Chaudhury and M.J. Owen, *Langmuir, 9* (1993) 29.
[142] H. Yoshizawa, Y.L. Chen and J. Israelachvili, *J. Phys. Chem., 97* (1993) 4128.
[143] E.J. Kramer, personal communication, 1995.
[144] J.H. Gittus, *Philos. Mag., 32* (1975) 133.
[145] T. Hui-Ong, R.N. Ward, P.B. Davies and C.D. Bain, *J. Am. Chem. Soc., 114* (1992) 6243.
[146] A. Gent and N.J. Schultz, *J. Adhesion, 3* (1972) 281.